University of South-Eastern Norway

www.usn.no

FMH606 Master's Thesis 2021

Process Technology

CFD-Simulations of inhomogeneous H_2-air explosions

Omid Aghaabbasi

Faculty of Technology, Natural sciences and Maritime Sciences
Campus Porsgrunn

University of South-Eastern Norway

www.usn.no

Course: FMH606 Master's Thesis, 2021

Title: CFD-Simulations of inhomogeneous H_2-air explosions

Number of pages: 81

Keywords: H_2-air explosions, homogeneous H_2-air mixture, inhomogeneous H_2-air mixture, Flame Acceleration, Deflagration-to-Detonation Transition, Detonation, CFD simulation, OpenFOAM, XiFoam.

Student: Omid Aghaabbasi

Supervisor: Prof. Dag Bjerketvedt, Prof. Knut Vaagsaether, Stip. Mathias Henriksen

External partner: MoZEES

University of South-Eastern Norway

www.usn.no

Summary:

Since demands for energy resources increase globally in recent years due to growth of application consumption, finding alternative resources for traditional fossil fuels raises. These current fuels are diminishing continuously and have huge pollutions and destructive environmental effects on creature and also human lives. Among renewable and green alternative fuels, hydrogen fuel is introduced as a promising and zero emission energy carrier which is accessible and clean that also known as future fuel. Due to low ignition energy required for hydrogen combustion, abrupt explosions are inevitable. So, safety study of H_2-air explosion has specific importance to reduce unexpected incidents. Based on various initial conditions, configuration and dimension of studied geometry, different explosion regimes can be observed. Also, inhomogeneous conditions for H_2-air mixture are more realistic in the world due to stratification of H_2 in air based on low density. So, inhomogeneous H_2-air mixture explosion is highly considered in research studies such as safety aspects.

In this project, in order to simulate flame acceleration of explosions in channel, openFOAM CFD toolbox has been employed as reliable numerical simulation method. For this reason, 6 simulation cases have been executed by XiFoam solver within a 1700*100 mm^2 2D channel and without presence of obstacles. It was applied a high enough aspect ratio of length to height to be sure of stronger explosion. Homogeneity and inhomogeneity effects in H_2-air explosions have been investigated in this work with further consideration of stoichiometric, lean, and rich fuel conditions by implementing different equivalence ratio. First homogeneous H_2-air mixture has been considered which implemented in whole domain of geometry. Then inhomogeneous H_2-air mixture has been investigated by making two homogeneous layers in channel as hydrogen-air flammable cloud in half top of channel and air as inert gas in half bottom of it.

In these explosion scenarios, flame acceleration in the channel has been investigated by considering some key parameters such as flame front position, flame speed and pressure.

Results of these parameters show that with more fuel concentration by increasing equivalence ratio and going from fuel-lean to fuel-rich condition, flame front goes faster with higher velocity and pressure. This behavior is similar for both homogeneous and inhomogeneous H_2-air mixtures. Furthermore, since there is more flammable H_2-air mixture in homogeneous case than inhomogeneous one and flame can freely stretch in this condition, flame elongates and consequently results to enlargement of flame surface area with higher reaction rates. So, flame exhibits higher acceleration, velocity, and pressure in this condition rather than inhomogeneous one.

Preface

This master thesis was performed in Department of Process, Energy and Environment Technology, Faculty of Technology, Natural Sciences and Maritime Sciences (TNM) at University of South-eastern Norway (USN) with cooperation of MoZEES, a Norwegian Research Center as external partner.

I would like to thank my supervisors Prof. Dag Bjerketvedt and Prof. Knut Vaagsaether who provided me with their guidance each time I encountered problems and difficulties and pushed me in the right direction. Their help was very consequential for me during this work. Furthermore, I would like to thank Mr. Mathias Henriksen whose experiences in openFOAM and Python were significantly effective and helpful for me during simulation process.

Porsgrunn, 19.05.2021

Omid Aghaabbasi

Contents

Nomenclature

Abbreviations

CFD	Computational Fluid Dynamics
CJ	Chapman-Jouguet
DDT	Deflagration to Detonation Transition
DNS	Direct numerical simulation
FA	Flame Acceleration
LES	Large eddy simulation
MIE	Minimum Ignition Energy
openFOAM	open source Filed Operation And Manipulation
RANS	Reynolds-average Navier-stokes
RM	Richtmyer-Meshkov instability
SGS	sub-grid scales
VN	post-shock or Von Neumann state
ZND	Zel'dovich Von Neumann Döring model

Symbol	Description	Unit
A_c	Channel cross section area	$[m^2]$
A_f,$A_{f,T}$,$A_{f,L}$	Flame surface area, Turbulent flame surface area, Laminar flame surface area	$[m^2]$
A_s	Sutherland coefficient	$[Pa.s/K^{1/2}]$
a	Thermal diffusivity	$[m^2/s]$
b	Regress variable	$[-]$
C_b,C_u	Concentration of burned and unburned mixtures	$[kmol/m^3]$

C_k	Molar concentration of species k	$[kmol/m^3]$
c_p	Heat capacity at constant pressure	$[J/K]$
C_v	Heat capacity at constant volume	$[J/K]$
Co	Courant number	$[-]$
c	Progress variable	$[-]$
c_i	molar fraction of species i	$[-]$
D, D_k	Mass diffusivity, Diffusion coefficient of species k	$[m^2/s]$
D_{CJ}	Detonation Chapman-Jouguet velocity	$[m/s]$
E_a	Activation energy	$[kJ/kmol]$
F_i	Body force	$[m/s^2]$
ft	Fuel mass fraction	$[-]$
H	Height of channel	$[m]$
h, h_k, h_s	Enthalpy, specific enthalpy of species k, sensible enthalpy	$[kJ/kg]$
h_f^i	Heat of formation of species i	$[kJ/kg]$
K	Thermal conductivity	$[W/mK]$
K_a	Karlovitz number of laminar flame thickness	$[-]$
$K_{a\delta}$	Karlovitz number of reaction zone flame thickness	$[-]$
k	Karlovitz stretch factor	$[-]$
L	Characteristic length scale of mean flow	$[m]$
L_e	Lewis number	$[-]$
L_M	Markstein length	$[m]$
M_a	Markstein dimensionless number	$[-]$
MW_k	Molecular weight of species k	$[kg/kmol]$

$\dot{m}$	Mass flow rate	$[kg/s]$
P, P_u	Pressure, Pressure of unburned mixture	$[atm, kpa]$
$\dot{q}_k$	Total reaction rate of species k	$[kmol/m^3.s]$
R	Universal molar gas constant	$[kJ/kmol.K]$
$\mathcal{R}_e$, $\mathcal{R}_{e_\eta}$, $\mathcal{R}_{e_\ell}$	Reynolds number, Reynolds number of smallest eddies, Reynolds number of integral length scale	$[-]$
S_{c_k}	Schmidt number	$[-]$
S_L, $S_{L,S}$, S_{L0}, S_T	Unstretched laminar burning velocity, Stretched laminar burning velocity, Laminar flame speed in room condition, Turbulent burning velocity	$[m/s]$
T, T_b, T_u	Temperature, Temperature of burned and unburned mixture	$[K]$
T_s	Sutherland temperature	$[K]$
t_d	Diffusion time	$[s]$
U	Characteristic velocity scale of mean flow	$[m/s]$
U_s	Surface-filtered velocity of flame	$[m/s]$
u_i, $\bar{u}$, u'	Velocity in i direction, Time- averaged flow velocity, Velocity fluctuation	$[m/s]$
W	Constant of fuel in Gülder laminar flame speed correlation	$[-]$
Xi	Flame wrinkling	$[-]$
Y_k	Mass fraction of species k	$[-]$
Z	Constant in Gülder laminar flame speed correlation	$[-]$
α, β	Mixture strength- dependent constants in power law	$[-]$
Γ, Γ_k	Diffusion coefficient	$[m^2/s]$
δ_{ij}	Kronecker delta	$[-]$
δ_L, δ_R	Laminar flame thickness, Thickness of reaction zone	$[m]$

ε	Dissipation rate of turbulent kinetic energy	$[m^2/s^3]$
ξ, η	Constants of fuel in Gülder laminar flame speed correlation	$[-]$
ℓ_T, ℓ_η	Characteristic length scale of large (integral)eddies, Characteristic length scale of smallest eddies	$[m]$
κ	Turbulent kinetic energy	$[m^2/s^2]$
λ	Detonation cell width	$[m]$
μ, μ_t	Dynamic viscosity, Turbulence dynamic viscosity	$[N.s/m^2]$
ν	Kinematic viscosity of flow	$[m^2/s]$
Ξ, Ξ^*_{eq}	Sub-grid flame wrinkling, Equilibrium wrinkling at Kolmogrov turbulence length scale	$[-]$
$\rho, \rho_{re}, \rho_{pr}$	Density, Reactant density, Product density	$[kg/m^3]$
σ	Expansion ratio	$[-]$
$\sigma_h, \sigma_\kappa, \sigma_\varepsilon$	Prandtl number, Turbulent Prandtl number of turbulent kinetic energy, Turbulent Prandtl number of dissipation rate	$[-]$
σ_s, σ_t	Surface-filtered resolved strain rates	$[s^{-1}]$
τ_{ij}	Viscous stress	$[N/m^2]$
$\tau_L, \tau_T, \tau_\eta$	Laminar flame time scale, Large (integral)eddies time scale, Smallest eddies (Kolmogorov) time scale	$[s]$
ϑ, υ	Characteristic velocity scale of large eddies, Characteristic velocity scale of smallest eddies	$[m/s]$
ϕ	Equivalence ratio	$[-]$
$\varphi, \bar{\varphi}, \varphi', \tilde{\varphi}, \varphi''$	Scalar property of fluid, time- averaged of scalar property of fluid, fluctuation of scalar property of fluid, mean value in favre averaging of scalar property of fluid, fluctuation in favre averaging of scalar property of fluid	
$\dot{\omega}_k$	Reaction rate source (or sink)	$[kg/m^3.s]$

1 Introduction

Combustion is an exothermic process when a considerable amount of heat and energy releases during reaction of fuel and oxidizer (mostly air) and consequently has some products. Requirements for this process are a flammable cloud and an ignition source to combust it. Gaseous combustion is chemical reaction between fuel and oxidant that both are in gas phase. Two main categories of gaseous combustion are premixed and non-premixed flames. Premixed flames take place when fuel and oxidant are mixed at molecular level prior to combustion and then source of ignition causes to explode the mixture. There are many examples of premixed flames, like what happen in internal combustion engine or gas turbine. In contrast, non-premixed ones are that reactants initially separated, and reaction take places at interfaces of fuel and oxidizer. For instance, fuel can be as a flame jet which enters air and burns there afterwards. These flames are also known as diffusion flames since fuel and oxygen come separately to combustion zone and due to diffusion, they mix up and react[1, 2].

Gas explosion is a combustion process of premixed gas cloud that results to high pressure and this pressure depends on how fast flame propagates and how it expands from gas cloud[3].

Explosion of a flammable cloud mixture can be easily occurred by even small ignition source such as spark, electrical shock, friction, etc. and may have catastrophic consequences such as loss of human lives, damage to building or properties and so on. There are many gas explosions examples with huge catastrophic consequences in the world like what happens in coal mines explosions by natural gases, in oil and gas production such as Piper Alpha accident in North Sea in U.K in 1988 or nuclear accidents like Three-mile island in USA in 1979 or Fukushima Daiichi disaster in Japan in 2011.

Experiencing different explosion regimes, flame speed, strength and other impacts of explosions depend on diverse conditions of flammable mixture such as type of fuel, inhomogeneity, and congestion, in addition to presence of confinement, aspect ratio (length to diameter/ height) of tube or channel and existence of turbulence in flow[4].

Hydrogen as a fuel can make a flammable cloud due to mixing with air and because of low density, stratify in air, and results spatial concentration gradients[4]. This observation of inhomogeneity exists for H_2 -air mixtures and mostly governs in real world situations instead of homogeneous condition. So, consideration of inhomogeneous mixture for H_2-air cloud is highly important for study and research aspects such as safety and transition by means of lab-scale experiments or numerical simulation by computer software. Explosion of homogeneous fuel-air cloud were studied widely both in experiments and numerical simulation before while in contrast, inhomogeneous conditions of flammable cloud got less attention in experiments.

1.1 Objective of project

In this project, a literature study of flame propagation in inhomogeneous fuel-air clouds have been reviewed with focus on inhomogeneous H_2-air cloud by evaluating different regimes of flame acceleration from start of ignition, then transition to detonation and finally detonation propagation in this mixture. Afterward, CFD simulations have been performed to investigate and make comparison of flame acceleration between homogeneous and inhomogeneous H_2-air

explosions with further consideration of stoichiometric and non-stoichiometric conditions to observe their effects on flame propagation and other related variables.

1.2 Method

In order to assess different parameters of gas explosions and investigate the results, laboratory scale experiment and observation of results there, are most reliable method that can imitate real conditions. It is considered in many works and projects with a highly enough approximation to predict, observe, and assess results and effects of gas explosions. But laboratory equipment and tools also have limitations. They are not always accessible for any conditions. Besides, setting up experimental condition may have high cost for different initial parameters and in many cases, results take much time and energy.

Alternatively, numerical simulation by computer tools can be a proper alternative solution for prediction and assessment of data which is much faster in preparation with ease of setting up and low cost of running in comparison with laboratory scale experiments. There are many software toolboxes that represents various compliance with experimental data. Since the present work is an example of fluid interaction, a Computational Fluid Dynamics (CFD) toolbox has been chosen to evaluate the behavior of explosions.

For this purpose, OpenFOAM (open-source Field Operation And Manipulation) software has been selected as CFD toolbox. Here, XiFoam solver has been applied since it is suitable for premixed and partial premixed combustion with turbulence flows. In this solver, combustion and turbulence are modeled with flame wrinkling combustion model by using a reacting progress variable along with chosen turbulence model. In present simulations, Gülder correlation is selected as a suitable model for laminar flame speed. Study geometry is a 1700*100 mm^2 2D channel which is totally close at left, top and bottom walls and fully open at right end wall without presence of obstacles. Ignition source is located near top of channel at end left wall.

1.3 Report structure

This report is outlined in following chapters. Chapter 2 reviews literature study on flame propagation of inhomogeneous fuel-air clouds with specific focus on H_2-air mixture. In this chapter, effect of inhomogeneity in fuel-air cloud and different flame propagation regimes with considering inhomogeneous hydrogen-air mixture are discussed. Chapter 3 describes finite volume method with governing equations in this process. Also, models of turbulence and combustion along with case study simulation setup are explained in this chapter. Chapter 4 introduces simulation cases and illustrates their results by showing flame propagation in channel with further observation of front position, velocity, and pressure for each one. Chapter 5 discusses simulation cases and make comparison among them based on results obtained from simulations and finally chapter 6 makes conclusion of this work with further work suggestions.

2 Flame propagation of fuel-air clouds

In industrial gas explosion accidents, flammable clouds form due to fuel release, mix with air as oxidizer and finally explode by any ignition sources. Two modes of explosions are deflagration and detonation. Deflagration mode is a self-sustaining propagation of localized combustion zone propagates into unburned gas at subsonic velocities, while detonation wave is a shock wave explosion-driven that propagates into unburned gas at supersonic velocities [1]. Explosion of H_2-air in initial conditions of ambient temperature and pressure, can be easily reached since required ignition energy to explode hydrogen is extremely low rather than other flammable fuels [5].

There are two ignition mechanism that depend on ignition energy. First one is mild or weak ignition where flame starts from ignition point and propagates as deflagration mode in this mechanism through fresh mixture. So, diffusion of heat and species is important and dominates flame propagation. Minimum ignition energy (MIE) for hydrogen-air mixture at standard condition depends on hydrogen concentration and for stoichiometric conditions is near 0.017 mJ [5] while MIE for other combustible gases are around 0.2-0.3 mJ [6]. Therefore, ignition of hydrogen can be easily reached by even small spark, mechanical friction etc. and is highly possible to occur. Second one is strong ignition mechanism that needs high ignition energy and happens if reflecting shock is strong enough to lead rapid auto-ignition. This makes direct explosion at reflecting wall. Blast wave produces and explosion shapes direct detonation mode. In P-T diagram for $H_2 - O_2$ systems as shown in figure 2.1, extended second explosion limit crosses region of obtained temperature and pressure for ability of detonation limit, between 12 and 70 vol% of hydrogen. It discriminates weak ignition on left side from strong ignition on right side [7]. This crossed region shows critical conditions for strong ignition and consequently onset of detonation in H_2-air mixture. As obtained from detonation experiments, required ignition energy for strong ignition and direct detonation is significantly high. This energy per surface area for stoichiometric H_2-air mixture is 0.7 MJ/m^2 while for propane is 3.1 MJ/m^2 and for methane is 10 MJ/m^2 [8]. Hence, direct detonation in real industrial explosions is impossible and a Deflagration to Detonation Transition (DDT) process is required for detonation. Explosion of flammable H_2-air cloud is classified in premixed gas explosion since hydrogen and air are mixed prior to combustion. Therefore, behavior of premixed gas explosion is studied for H_2-air explosion.

Previously, experiments and study works were performed widely on homogeneous and stoichiometric fuel-air clouds. For instance, effects of shapes and distribution of obstructions were investigated on produced explosion pressure in natural gases for methane-air by Moen et al. [9] or propane-air by Eckhoff et al.[10] and Hjertager et al.[11]. Also, different fuel concentration of homogeneous clouds was discussed by Hjertager et al.[12] and they observed maximum pressure and flame speed occurred in slightly fuel rich concentration in methane-air and propane-air. But these experiments were considered as idealized situation of scenarios since in reality inhomogeneous conditions govern and fuels concentration are non-uniform in air.

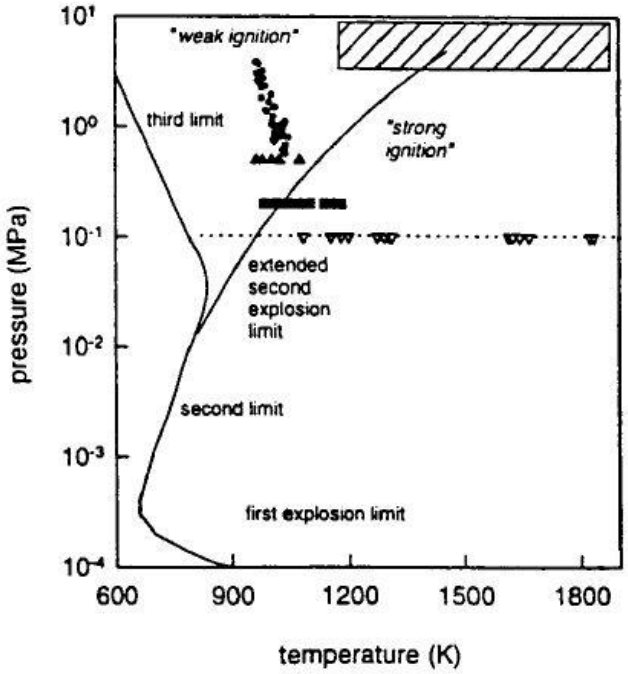

Figure 2.1. P-T diagram in $H_2 - O_2$ systems with extended second explosion limit observed by experiments[7].

2.1 Inhomogeneity effect in fuel-air cloud

In contrast to homogeneous condition of fuel-air cloud, some experimental studies were performed to consider inhomogeneity of fuel-air mixture. There is a simplification for study of inhomogeneity by reduction of concentration gradients compare to three-dimensional structure. It is classified in many projects works to parallel and vertical concentration gradients due to direction of them relative to flame propagation direction. First category is parallel concentration gradients where they have same direction as flame propagation. This condition is highly relevant for nuclear reactors where steam is in vertical tubes and gradients consider in same directions and interacts with gravitational effects. Second one is transverse or vertical concentration gradients. In this kind of concentration gradients, they have direction perpendicular to flame propagation and was studied in many works and strong effect of gradients on Flame Acceleration (FA) process and possibility of DDT observed specifically in unobstructed configuration. In this section, observations of inhomogeneous fuel-air mixtures in previous studies are discussed.

Hjertager et al.[13] investigated methane-air clouds in a large-scale obstructed tube by simulating two types of leakage arrangement in pipes as axial and radial to generate inhomogeneous conditions. They showed that explosion pressure is highly dependent on leakage arrangement, mass of injected fuel and delay time of ignition. There was observed maximum explosion pressure occurred in axial leak arrangement with stoichiometric conditions and time delay less than 50 seconds while for radial leak arrangement it happened for under stoichiometric masses of methane. On specific conditions, inhomogeneous methane-air clouds produce high pressure as homogeneous cases and furthermore for small methane masses, inhomogeneous mixture may produce higher explosion pressure compared to homogeneous conditions. It was an important observation that shows inhomogeneity of

mixture may have worse effects in real world than homogeneous ideal conditions. C.Wang et al.[14] investigated effect of transverse concentration gradients in methane-air on flame propagation in horizontal duct and observed that time between leakage of methane in duct and ignition that defined as ignition delay, strongly affects flame shape and speed in stratified methane-air mixture. They showed stratified methane-air cannot be ignited at ignition delay less than 3 minutes. But by increasing delay time from 4 min. to 15 min., flame speed and overpressure increases monotonically, while after that time, they remain constant. Furthermore, overpressure in time of 15-25 min obtained nearly same as homogeneous condition of methane-air mixtures.

Since inhomogeneous conditions for H_2-air mixture have most probability to occur, they reveal with spatial or three-dimensional concentration gradients in reality. These conditions were investigated experimentally in project works like Vollmer et al.[15, 16], Kuznetsov et al. [17, 18] and Boeck et al. [19, 20] and compared results with homogeneous mixtures. Vollmer et al.[16] investigated vertical concentration gradients in hydrogen-air mixtures and showed they had major influence on flame acceleration (FA) by change in maximum velocity and pressure. Peak overpressure at end of tube can increase to two orders of amount compared to homogeneous mixtures. So, mixtures with vertical concentration gradients have higher dangerous effects than homogeneous ones of same hydrogen concentration. They showed also [15] depend on geometrical configuration, DDT can happen at considerably lower or higher fuel concentrations. Furthermore, they concluded that one-dimensional parameters like blockage ratio and characteristic length scales are not sufficient to describe DDT in hydrogen-air mixture with concentration gradients. Kuznetsov et al. [17, 18] investigated flame propagation regimes and maximum pressure loads by considering effect of hydrogen concentration gradients, layer thickness, presence of obstruction and average and maximum hydrogen concentration. They observed three different regimes for horizontal flame propagation as slow (subsonic) flame, sonic deflagration, and detonation. Higher flame propagation velocity leads to higher pressure loads and highest mixture reactivity and ratio of distance between obstacles to layer thickness are governing parameters in propagation regimes.

Sommersel [21] studied hydrogen dispersion and effect of inhomogeneous hydrogen explosions in long channels. Hydrogen leakage in partially confined spaces was investigated based on ammonia plant explosion incident in Porsgrunn in 1985. In that work, effect of explosion overpressure was discussed by changing mass flow rate, jet direction, time of ignition and level of obstruction. It was observed that hydrogen-air cloud behaves as gravity current, and dispersion of hydrogen is highly sensitive to considered geometry. Here, Froude scaling is a useful tool to analyze effect of hydrogen explosion in geometries. Furthermore, obstructed geometry significantly increases overpressure in system while unobstructed geometries reveal less pressures. Finally, it was concluded that two key parameters of dispersion effect and degree of obstructions, influence strength of hydrogen explosion. Besides, shock wave propagates faster in horizontal channel than in vertical one.

Also, Ettner et al. [22] performed some numerical simulation for inhomogeneous mixtures by means of density-based codes and validation of them for inhomogeneous H_2-air was observed in OpenFOAM CFD toolbox [23, 24].

In following sections, different flame propagation regimes are described in detail as flame acceleration, onset of detonation and detonation in addition to investigation of inhomogeneity effect in H_2-air mixture on them.

2.2 Flame acceleration

Flame acceleration process includes sequences of four main phases. In this section, these phases are presented respectively after ignition of flammable mixture.

2.2.1 Laminar deflagration

After ignition, flame front propagates laminarly into mixture and causes flame surface area to enlarge. Enlargement of flame surface area leads to increase in reaction rate, which is integral of local burning velocity over the flame surface area. So, by enlargement of flame surface area, flame accelerates. The propagation mechanism governs here is through diffusion of heat and species and known as deflagration. Figure 2.2 shows distribution of temperature, reaction rate and mixture concentration through a one dimensional of stationary, laminar premixed deflagration wave.

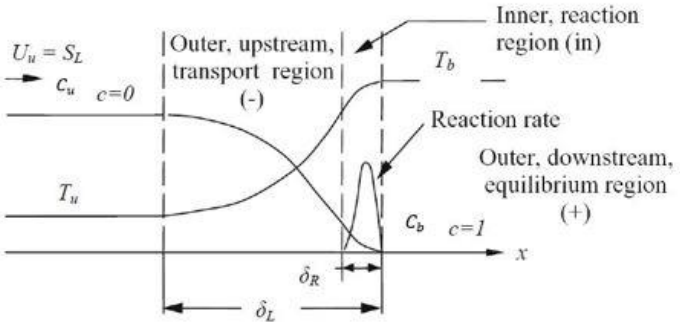

Figure 2.2. 1D illustration of internal structure of laminar, premixed, stationary flame [25].

In figure 2.2 unburned gas velocity U_u is equal to laminar burning velocity S_L which is characteristic velocity scale in laminar premixed combustion. Temperature T_u and concentration C_u of fresh or unburned mixture change across flame thickness δ_L and results to T_b and C_b respectively in burned region. In premixed combustion, definition of progress variable c is useful where $c = 0$ in reactants and $c = 1$ in products. Heat from chemical reaction released mainly from small region within flame named as reaction zone and has a characteristic thickness δ_R. Laminar burning velocity S_L and laminar flame thickness δ_L are thermochemical quantities that are independent of geometry or local flow conditions.

A simple 2D illustration of laminar deflagration in closed channel can be seen in figure 2.3.

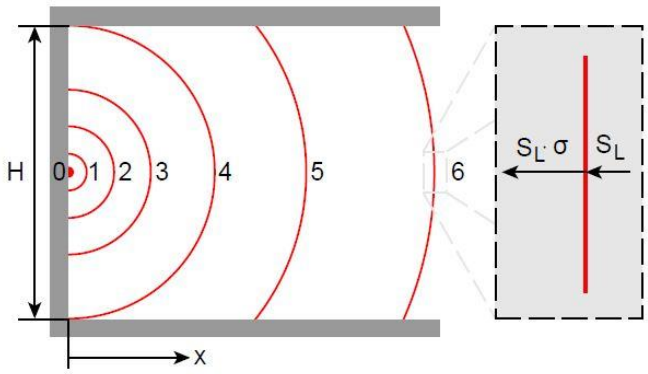

Figure 2.3. simple 2D illustration of laminar flame propagation (Left) and laminar flame front detail (Right) [4]

In figure 2.3, unstretched laminar burning velocity S_L is flame propagation velocity of mixture ahead of flame which is unburned mixture. In other hand, product velocity behind flame is $S_L\sigma$ where σ is expansion ratio and is ratio of reactant density to product density.

$$\sigma = \frac{\rho_{re}}{\rho_{pr}} \tag{2.1}$$

By an external observer, relationship between flame speed $S_L\sigma$ and laminar burning velocity is:

$$S_L\sigma = u + S_L \tag{2.2}$$

Where u is velocity of flow ahead of flame. This equation can be shown by flame surface area A_f and channel cross section A_c as below [4].

$$S_L\sigma A_f = uA_c + S_L A_f \tag{2.3}$$

It shows that enlargement of flame surface area results to increase the visible flame speed.

In previous years, there were many analytical correlations for simulation of laminar flame speed as a function of equivalence ratio, pressure, and temperature [26, 27]. Among these correlations the most widely used and simplest form is fully empirical known as power law form that applied in many investigations [28-31] and expressed in equation (2.4).

$$S_L(\phi, T_u, P_u) = S_{L0}(\frac{T_u}{T_0})^{\alpha}(\frac{P_u}{P_0})^{\beta} \tag{2.4}$$

Where S_{L0} is velocity for an equivalence ratio ϕ calculated in room conditions by considering $T_u = T_0$ and $P_u = P_0$. α and β are mixture strength- dependent constants.

Gülder [27] suggested an empirical correlation to express laminar flame speed S_{L0} as below.

$$S_{L0} = ZW\phi^{\eta}\exp\left[-\xi(\phi - 1.075)^2\right] \tag{2.5}$$

Where W, η and ξ are constants for given fuel and $Z = 1$ for single constituent fuels.

So, by substitution Gülder correlation for S_{L0} in equation (2.4), it results the following correlation that have been empoyed in this work as a suitable correlation for modeling of laminar flame speed.

$$S_L = W\phi^{\eta}\exp\left[-\xi(\phi - 1.075)^2\right](\frac{T}{T_0})^{\alpha}(\frac{P}{P_0})^{\beta} \tag{2.6}$$

Characteristic length scale or thickness of laminar flame δ_L and chemical time scale τ_L of laminar flame can be obtained from laminar flame speed S_L [25]:

$$\delta_L = \frac{\nu}{S_L} \quad ; \quad \tau_L = \frac{\nu}{{S_L}^2} \tag{2.7}$$

Where, ν is kinematic viscosity of flow. Here, it is assumed that viscosity and diffusivity are approximately equal or change similar to each other.

In case of hydrogen, Konnov [32] also introduced a correlation for unstretched laminar burning velocity S_L as a function of molar concentration of H_2 as a 6th order polynomial.

So, explosion of fuel-air cloud starts with Laminar deflagration regime which flame front is undistort and smooth. But after a short time, flame front is distorted, and instabilities are produced highly. Therefore, laminar deflagration regime is short, and it can be neglected compared to total duration of explosion process.

2.2.2 Cellular flame propagation

As mentioned in previous section, shortly after ignition, fuel-air flames tend to be unstable and distorted. By rising instabilities and distortion of flame front, flame surface area increases, and this behavior known as cellular flames. Here, flow still remains laminar. Hence, cellular flames classified in laminar flame. This instability situation happens in H_2-air explosion especially in lean conditions. This regime has been observed in experiments [4] and explained as dynamic process in many works [33-35]. Instabilities lead to strengthen overall reaction rate and accelerate the flame. Cellular length-scale after ignition has initially decreased and known as wavelength [36, 37]. In lean mixtures it can be seen separated flames with local quenching, while in stoichiometric and rich mixture flames are symmetric and there is no local quenching [4]. So, by increasing concentration of fuel, wavelength of cellularity grows and stability of flame front increases.

Instabilities and distortion are due two main mechanism. Hydrodynamic (Landau-Darrieus) instability[38, 39] that describes flame wrinkling is based on local acceleration and deceleration of flame in two different section. These sections are produced as result of convergence or divergence of streamlines and expansion across the flame that shapes convex and concave, respectively. Diffusive-thermal instability [6] is another mechanism that acts along with hydrodynamics instability and strengthen or weaken flame wrinkling. Here, diffusion of heat interacts with species diffusion. If diffusion of species leads to increase concentration of components in convex section, it results to higher reaction rates. Also, locally increasing temperature depends on thermal diffusion. In low thermal diffusivity condition, enhanced species concentration combine with weak heat flux and causes a high temperature region. So, burning velocity is increased in convex and decreased in concave section that leads to strengthen the flame wrinkling. In other hand, in high thermal diffusivity, high heat flux leads to balancing of burning velocities between convex and concave sections and consequently reduced flame wrinkling. By having Lewis number L_e as equation (2.8), effect of diffusivity instability on flame wrinkling can be described.

$$L_e = \frac{a}{D} \tag{2.8}$$

Lewis number expressed by ratio of thermal diffusivity a to mass diffusivity D of limiting species in the mixture (fuel). Figure 2.4 shows stability and instability effect of Lewis number on regions of flame curvature. If Lewis number is less than unity, it strengthens the flame wrinkling and result to flame instability while Lewis number more than unity weaken it and make the flame stable. In, H_2-air mixture due to high diffusivity of H_2 there is a high tendency to have cellular flame propagation.

Also in H_2-air mixture, Lewis number can be shown experimentally as a function of equivalence ratio [40] and exhibits transition from stability to instability close to stoichiometric conditions.

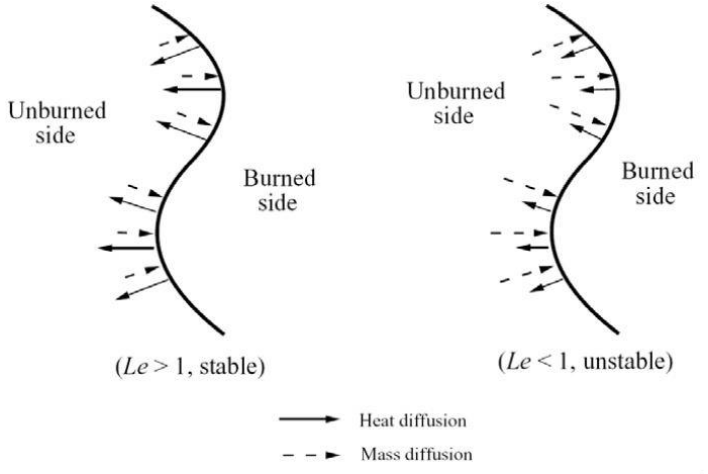

Figure 2.4. Effect of Lewis number on flame stability [25].

Markstein investigated cellular flame propagation [41] by introducing Markstein length L_M that defines effect of flame stretch rate on local burning velocity and can be expressed as follow.

$$S_L - S_{L,S} = L_M k \tag{2.9}$$

Here $S_{L,S}$ is stretched flame burning velocity and Karlovitz stretch factor k describes normalized rate of flame surface area change [42] and it can be obtained as equation below.

$$k = \frac{1}{A_f}\frac{dA_f}{dt} \tag{2.10}$$

Markstein length L_M in H_2-air mixture can be determined experimentally as a function of equivalence ratio [43, 44] as shown in figure 2.5. In this figure it can be observed that below stoichiometry of H_2-air mixture, Markstein length L_M is negative and above it, L_M is positive. Flame instability is strengthened in negative L_M , since positive (negative) stretch rate increases (decrease) local flame velocity as described in equation (2.9). In other hand, flame instability is weakened in positive L_M.

Markstein dimensionless number M_a expressed in equation (2.11) can also describes effect of flame curvature and strain [41].

$$M_a = \frac{L_M}{\delta_L} \tag{2.11}$$

Finally, it can be concluded that for $L_e < 1$ and $M_a < 0$ instability increases and flame wrinkling enhanced, while for $L_e > 1$ and $M_a > 0$ there is less instability and flame wrinkling damped.

Experimental sequences [4] in figure 2.6 shows that for homogeneous H_2-air mixture, by increasing H_2 concentration from 15 to 40 vol%, Markstein length L_M developed from negative to positive amount. For lean mixtures up to 20 vol%, it can be seen separated flame islands with quenching but for higher amount of concentration, there is no local quenching and flame front get more stability.

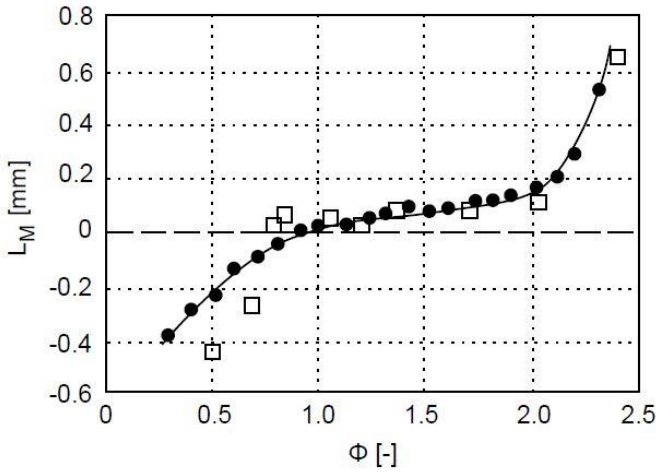

Figure 2.5. experimental values of Markstein length L_M in H_2-air as a function of equivalence ratio. Sources: Black dots [43] and White squares [44].

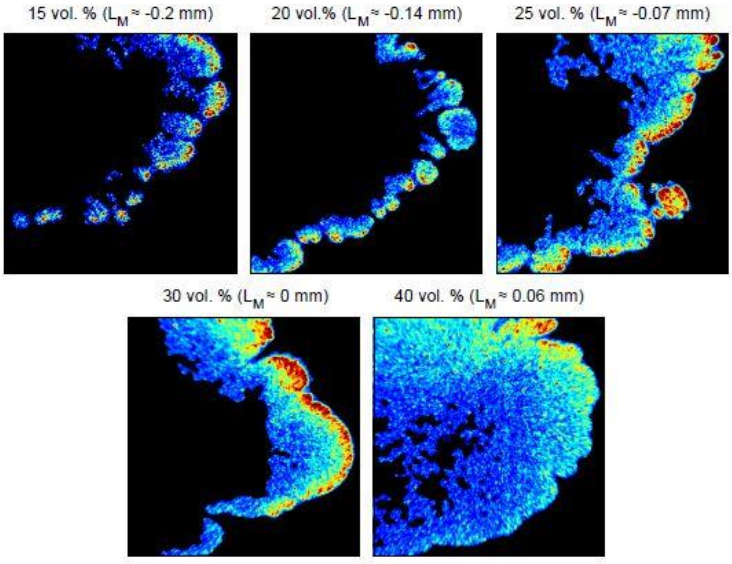

Figure 2.6. Sequences of cellular flames of homogeneous H_2-air mixture by increasing H_2 concentration with correspond Markstien length L_M [4].

So, by flame front distortion and cellular flame propagation, overall reaction rate increases, and it supports FA process.

2.2.3 Slow turbulent deflagration

In closed channels, by having end wall ignition, flame acts like a piston that pushes the fresh mixture ahead of flame in flame propagation direction. It leads to high flow velocity and further high Reynolds number ahead of flame that result in forming and strengthening chaotic condition known as turbulence. This mostly happened in wall boundary layers and near existing obstruction in geometry. In slow regime, flame propagating encounters different flow behavior rather than laminar but still is in deflagration mode and it is almost controlled by subsonic fluid mechanic processes.

Reynolds dimensionless number measures relative of inertia forces and viscous forces and defines based on characteristic velocity scale U, characteristic length scale L of mean flow and kinematic viscosity ν of flow.

$$\mathcal{R}_e = \frac{UL}{\nu} \tag{2.12}$$

In turbulence, there are spatial velocity fluctuation and Reynolds describes local flow velocity u by time- averaged flow velocity $\bar{u}$ and velocity fluctuation u' [45].

$$u = \bar{u} + u' \tag{2.13}$$

Turbulent flows reveal shape of rotational flow structures, named as turbulent eddies with a wide range of length scales [2]. Mean size of large eddies is known as integral scale. In these flows, it can be seen that characteristic velocity scale ϑ and characteristic length scale ℓ_T of large eddies, are of the same order as velocity U and length scales L of mean flows. Large eddies (integral) length scale ℓ_T and time scale τ_T can be defined as in equation (2.14).

$$\ell_T = \frac{u'^3}{\varepsilon} \quad ; \quad \tau_T = \frac{\ell_T}{u'} \tag{2.14}$$

Where, ε is dissipation rate of turbulent kinetic energy and u' is characteristic velocity fluctuation in integral length scale.

Therefore, Reynolds number obtained by large eddies scales are close in value to Reynolds number by mean values. It shows that large eddies are dominated by inertia effects and viscous effects have less importance [2].

The largest eddies elicit energy from mean flow by stretching process where mean flow velocity gradients distort turbulent eddies. Furthermore, smaller eddies are also stretched highly by larger eddies and at lower level by mean flow. So turbulent kinetic energy is transferred from large eddies to smaller and smaller ones at a viscous dissipation rate. The total process of transferring turbulent kinetic energy from mean flow to large eddies and further to smaller eddies is known as kinetic energy cascade. These smallest eddies in turbulent flows are dominated by viscous effects and have smallest length scales of 0.1 to 0.01 mm. Reynolds number of smallest eddies based on characteristic velocity υ and length scales ℓ_η equals to 1 [2].

$$\mathcal{R}_{e_\eta} = \frac{\upsilon \ell_\eta}{\nu} = 1 \tag{2.15}$$

It means for smallest eddies in turbulent flows, viscous effects and inertia effects have same strength. Smallest scales are named Kolmogorov microscales [46, 47]. In these microscales, viscous stresses are mostly considered, and energy associated with them is dissipated and converted to thermal internal energy. This dissipation causes increased loss of energy in turbulent flows. Kolmogorov microscales of length scale ℓ_η , velocity scale υ and time scale τ_η are expressed in term of energy dissipation rate ε of turbulent flow and fluid kinematic viscosity ν.

$$\ell_\eta \approx \left(\frac{\nu^3}{\varepsilon}\right)^{\frac{1}{4}}; \quad \upsilon \approx (\nu\varepsilon)^{\frac{1}{4}} \quad ; \quad \tau_\eta \approx \left(\frac{\nu}{\varepsilon}\right)^{\frac{1}{2}} \tag{2.16}$$

In high flow velocity, dissipation rate ε increases and consequently micro length scale ℓ_η decreases. Therefore, high flow velocity shows lower smallest eddy size than low flow velocity.

Finally, ratio of small scales to large scales characteristic can be expressed based on Reynolds number $\mathcal{R}_{e_\ell}$of integral length scale as follows [48].

Length scale ratio: $\frac{\ell_\eta}{\ell_T} = \mathcal{R}_{e_\ell}{}^{-\frac{3}{4}}$ (2.17a)

Time scale ratio: $\frac{\tau_\eta}{\tau_T} = \mathcal{R}_{e_\ell}{}^{-\frac{1}{2}}$ (2.17b)

Velocity scale ratio: $\frac{\upsilon}{\vartheta} = \mathcal{R}_{e_\ell}{}^{-\frac{1}{4}}$ (2.17c)

Typical values for $\mathcal{R}_{e_\ell}$ can be $10^3 - 10^6$ [2].

In turbulent premixed flame, turbulent propagation speed or turbulent burning velocity S_T is not only related to characteristic of flow, but also depends on properties of fuel-oxidizer mixture. Many correlations were proposed for relating turbulent burning velocity to laminar flame speed corresponding to different regimes of turbulent premixed flames. At first, Damköhler [49] theoretically introduced turbulent burning velocity based on two different regimes and due to magnitude of turbulence scale in comparison with laminar flame thickness. He assumed that for turbulence scales larger than laminar flame thickness, interaction of wrinkled flame front with turbulent field is independent of length scales and purely kinematic. It corresponds to corrugated flamelet regime as shown in figure 2.7. Also, he expressed mass rate $\dot{m}$ in term of laminar and turbulent velocities as below.

$$\dot{m} = \rho_u S_L A_{f,T} = \rho_u S_T A_{f,L} \tag{2.18}$$

Where ρ_u is unburned mixture density and $A_{f,T}$ and $A_{f,L}$ are turbulent and laminar flame surface areas, respectively.

So, ratio of turbulent to laminar burning velocity would be:

$$\frac{S_T}{S_L} = \frac{A_{f,T}}{A_{f,L}} \tag{2.19}$$

For large scale and weak turbulence intensity, Damköhler expressed above ratio by using geometrical approximation with a Bunsen flame as follows.

$$\frac{A_{f,T}}{A_{f,L}} = \frac{S_L + u\prime}{S_L} \tag{2.20}$$

Finally:

$$\frac{S_T}{S_L} = 1 + \frac{u\prime}{S_L} \tag{2.21}$$

Where, u' is characteristic fluctuation velocity in unburned mixture.

For strong turbulence $\frac{u\prime}{S_L} >> 1$ so, equation (2.21) would be:

$$S_T \approx u' \tag{2.22}$$

There were many works that revised and updated Damköhler analysis like Calvin and Williams [50]or Pope and Anand [51]. Among them, Gülder [52] expressed turbulent to laminar flame velocity ratio based on smallest eddies which is employed in present work.

$$\frac{S_T}{S_L} = 1 + 0.62\sqrt{\frac{u'}{S_L}}\mathcal{R}_{e\eta} \tag{2.23}$$

To summarize turbulence-flame interaction, combustion regime diagram was introduced by Borghi [53] and revised by peters [54, 55] with length and velocity scales as shown in figure 2.7. Other definition for turbulent combustion regimes was proposed by Williams [56] that used Reynolds and Damköhler numbers.

Turbulent Reynolds number based on integral length scale expressed as:

$$\mathcal{R}_{e_\ell} = \frac{u'\ell_T}{\nu} = \frac{u'}{S_L}\frac{\ell_T}{\delta_L} \tag{2.24}$$

Also, to investigate interaction between turbulence and flame, Karlovitz [57] introduced two dimensionless numbers in turbulent deflagration.

$$K_a = \left(\frac{\delta_L}{\ell_\eta}\right)^2 \;;\; K_{a\delta} = \left(\frac{\delta_R}{\ell_\eta}\right)^2 \tag{2.25}$$

K_a and $K_{a\delta}$ are ratio of laminar flame thickness δ_L and thickness of heat released zone δ_R respectively to Kolmogrov length scale ℓ_η.

Turbulent combustion regime illustrated in figure 2.7 used these three above mentioned dimensionless numbers. Lines $\mathcal{R}_e = 1$, $K_a = 1$ and $K_{a\delta} = 1$ are transition boundaries specified between different turbulent combustion regimes.

By means of boundary line $\mathcal{R}_e = 1$, turbulent flame regimes are separated from laminar flame regime. Laminar flame regime is characterized by $\mathcal{R}_e < 1$, weak turbulence intensity and small turbulence scale and flame front propagates at speed of S_L.

In this figure, two wrinkled and corrugated flamelet regimes are characterized when large eddies dominate laminar flame thickness ($\ell_T > \delta_L$) and interact with flame front which results in macroscopic enlargement of flame surface area. Here, structure of flame front remains as laminar flame and local burning velocity of flame front still equals to laminar burning velocity. It shows local transport of heat and species is not changed by large eddies. Boundary line of $u' = S_L$ separates these two flamelet regimes from each other.

In wrinkled flamelet regime, flame thickness is much smaller than Kolmogorov length scale and flame maintains its laminar structure, turbulence just wrinkles the flamelet surface slightly. This regime is characterized by $\mathcal{R}_e > 1$, $K_a < 1$ and $\frac{u'}{S_L} < 1$.

Top side of dashed line $u' = S_L$, is corrugated regime and due to $K_a < 1$, flame maintains its laminar structure but because of larger fluctuations and consequently $\frac{u'}{S_L} > 1$, it leads to forms islands shapes of unburned and burned mixtures.

Above the boundary line $K_a = 1$, is reaction sheet regime and here transport of heat and species in flame front enhanced. So, local burning velocity is higher than laminar burning velocity. This regime is characterized by $\mathcal{R}_e > 1$, $K_a > 1$ and $K_{a\delta} < 1$. For lower boundary of K_a (equals to unity), which $\delta_L \approx \ell_\eta$, largest eddies flame behaves as flamelet eddies. While for

$K_a > 1$, which $\delta_L > \ell_\eta$, smallest eddies can penetrate into flame front structure and increase rate of heat and mass transfer which is only due to diffusion.

Above the boundary line $K_{a\delta} = 1$, is well-stirred reactor regime. Here, $\mathcal{R}_e > 1$ and $K_{a\delta} > 1$ and in this regime, heat release zone thickness is larger than smallest eddies that results strong effect of turbulence. Therefore, Kolmogorov eddies enter structure of reaction zone. This high diffusivity causes heat rate transfer from heat released zone to preheat zone and results to local flame extinction. Potential of turbulent eddies to penetrate the heat release zone of laminar flame is defined by $K_{a\delta}$. Here, for $K_{a\delta} > 1$, chemical reaction cannot be finished by one eddy circulation. Also, local flame quenching can happen due to mix of reacting gas with cold reactants. This shows upper boundary for turbulent burning velocity which in safety analysis considers 10 times of laminar burning velocity [58].

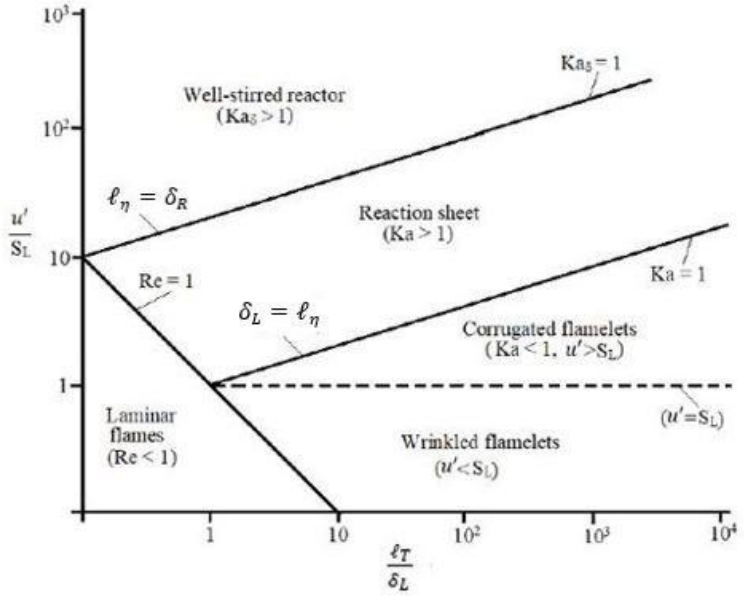

Figure 2.7. Different turbulent combustion regime diagram for premixed mixture [55].

Experimental sequences of slow deflagration for homogeneous H_2-air mixture was observed by Boeck [4]. It has been seen that in unobstructed configuration, turbulent in fresh mixture ahead of flame front were confined by wall boundaries and turbulent eddies lead to wrinkle the flame front and make it corrugated adjacent the walls while it was compact in the center of channel.

Turbulence and flame interaction increases burning velocity up to 10 times higher than laminar burning velocity. So, reaction rate increases significantly and in fresh mixture ahead of flame produces flow generation.

Finally, it can be concluded turbulence in premixed combustion flame wrinkles and stretches laminar flame structure, increases flame surface area and further, effective flame speed. Large turbulent eddies wrinkle and corrugate the flame and consequently, deformation raise the speed. In the other hand, small turbulent eddies may penetrate and change laminar flame structure if they are smaller than laminar flame thickness [27].

2.2.4 Fast turbulent deflagration

When flame speed reaches sound speed of reactants, fast turbulence regime occurs. In this regime flow compressibility gets more importance and also, constant acceleration can be seen. Here, flame propagation is mostly characterized by existence of gas dynamics discontinuities like shocks, precompression of fresh mixture and interaction with flame. Experiments shows with high amount of H_2 concentration, shock starts to form at flame speed of 300-400 m/s and transition from slow to fast deflagration and shock formation observed due to pressure waves reflecting [4]. So, total pressure wave propagates higher than sound speed in mixture. By presence of obstacle, shock formation occurs earlier due to pressure wave reflection compared to unobstructed configuration. Increasing fuel concentration, results to strengthening of reflected shocks that interacts with flame and this observation is important in FA process. Flame-shock interaction was discussed in many works [59, 60]. This interaction causes distortion and wrinkling of flame by Richtmyer-Meshkov (RM) instability [61]. RM instability appears since shock interacts with interface of reactants and products [62]. In experiments by Thomas et al. [63] it was observed that high shock-flame interaction leads to acceleration of flame. Khokhlov et al. [64] also showed it is essential to reach onset of detonation. Large scale RM instability is main mechanism in order to increase heat release rate with macroscopic enlargement of flame surface area during single shock-flame interaction, while small scale instability has less effect here since it fails rapidly [64]. Also, in FA process, shock-flame interaction occurs continuously.

So, propagating waves in fresh mixture during acceleration, gather and result to shock formation which compress and heat fresh mixture. Shock-flame interaction increase reaction rate. By increasing reaction rate due to this flow generation, along with shock and turbulence formation, flame accelerates to fast deflagration regime which also known as strong acceleration. In H_2-air explosion, fast deflagration causes velocities up to order of 1000 m/s along with overpressure up to about 10 bars while weak acceleration results in velocities of order 100 m/s [4]. Among this acceleration, flame front velocity relative to gas ahead of front remains subsonic and often maximum deflagration velocity close to reaction product sound speed can be seen.

2.2.5 Flame Acceleration in inhomogeneous condition of H_2-air mixture

Recently results from experiments [4] investigated explosion of inhomogeneous H_2-air mixture by considering vertical concentration gradients within the channel and compare them with homogeneous conditions. Inhomogeneous H_2-air mixture obtained by introducing diffusion time t_d as time between H_2 injection and mixture ignition. Here, $t_d = 60$ seconds represents homogeneous condition and diffusion times less than it like $t_d = 3{,}5{,}7.5{,}10$ seconds showed inhomogeneous conditions. Effect of inhomogeneity of hydrogen in FA process was investigated based on two phenomena in unobstructed and obstructed:

2.2.5.1 Flame shape and structure

a) Unobstructed channel: After ignition, it can be observed that for inhomogeneous mixture of H_2-air, flame front is inclined while for homogeneous mixture it has a symmetric (not totally, due to buoyancy effects) behavior with respect to channel centerline. Flame cannot propagate into mixture at the bottom of channel when local

H_2 concentration is less than a certain value. Also, in inhomogeneous mixture wavelength of flame front cellularity changes from large cell at top to smaller at bottom that is according to local Markstein length in concentration gradient profile. Lower flammability limit in inhomogeneous mixtures can be around 6-8 vol% for H_2 concentration up to 20 vol.% which is not in range of limits [65] for horizontal and downward flame propagation, therefore combustion is not complete. So, lower flame boundary in channel is straight and do not propagates further through the bottom. In this kind of configuration, inhomogeneous mixture has significantly higher flame acceleration compared to homogeneous mixture due to more elongation and further increase in flame surface area that leads to higher overall reaction rate. This surface area enlargement for homogeneous can be obtained by obstacles.

Flame shape highly depends on inhomogeneity and steepest gradients (lower diffusion time) have more flame elongation in constant H_2 concentration. This shows that inhomogeneity of mixture increases flame elongation. In similar inhomogeneous mixture condition, it can be observed that for low amount of H_2 concentration and lean mixture, flame front accelerates irregular and even oscillates that can prevent elongation. By increasing H_2 concentration, maximum local flame speed occurs in top of channel and flame propagates there faster.

Furthermore, flame speed $S_L\sigma$ has effect on flame elongation. In high local H_2 concentration regions, reactant density ρ_{re} is low. This leads mixture ahead of flames accelerates faster and flame elongation enhanced. Besides, by increasing H_2 concentration and increase in local reactant sound speed, at top of channel slow deflagration regime appears while at bottom of channel it shows fast deflagration regime. So, curved shocks and reflection of them are observed at bottom while they disappear at top of channel because of lower local shock Mach number.

So, for inhomogeneous H_2-air mixtures, in unobstructed configuration flame elongates significantly and FA is influenced by mixture properties and macroscopic flame shape.

b) Obstructed channel: In homogeneous mixture of H_2-air , flame is symmetric in upstream of channel with a slot in flame tip [66], while for inhomogeneous mixture, flame is inclined upstream of obstacle and reaches it at top earlier. After the obstacle, flame goes through bottom of channel which nearly shapes symmetric. In case of multi obstacles, by reaching upstream of last obstacle, flame fronts become almost similar for homogeneous and inhomogeneous mixtures. Also, by rising blockage ratio, flame elongation would be prevented considerably for both homogeneous and inhomogeneous mixtures and there is a similarity of flame shapes between them.

Therefore, obstructed configuration quenches the flame elongation significantly in comparison with unobstructed one. So, enlargement of flame surface area and high increase in reaction rate results to strong FA process that only take places in unobstructed configuration.

2.2.5.2 Flame velocity

a) Unobstructed channels: Inhomogeneous mixtures have stronger FA in all phases of process than homogeneous ones. So, they make faster FA to reach the critical condition of onset of detonation, while homogeneous ones have slow flame propagation without significant FA progress to reach DDT. Therefore, maximum local flame speed is much higher for inhomogeneous mixtures than homogeneous ones in same H_2 concentration.

b) Obstructed channels: For inhomogeneous mixtures it can be observed that after a specific H_2 concentration (24 vol%), FA retarded and have lower velocities rather than homogeneous mixtures. It shows that FA relates to mixture properties in obstructed configuration.

For describing FA process and also strong FA prediction in obstructed configuration, mixture property can be investigated by expansion ratio σ [67]. It can be shown that expansion ratio for inhomogeneous mixtures remains less than amount for homogeneous ones at same H_2 concentration. This parameter is calculated by integral approach over the channel height.

Laminar burning velocity S_L is another parameter to describe FA and calculated by integral approach over the height of channel. It can be observed for higher H_2 concentration of 24 vol%, burning velocity is lower for inhomogeneous mixtures than homogeneous ones. By contrast, in lower H_2 concentration of this value, burning velocity is higher for inhomogeneous mixtures.

So, combination of expansion ratio σ and laminar burning velocity S_L leads to flame speed $S_L\sigma$. It can be considered as integral approach combination of these two parameters.

Finally, for obstructed channel FA is related to laminar burning velocity in addition to expansion ratio. Therefore, integral approach is a key solution in FA process to consider effective flame speed for inhomogeneous H_2 -air mixture. FA is self-enforcing gas-dynamic and fluid-dynamic feedback cycle, hence flammable mixture reaction and further, overall reaction rate is driven force for FA in closed channel. Effect of turbulence and shock-flame interaction have similar behavior on inhomogeneous and homogeneous mixtures.

2.3 Onset of detonation

By reaching flame velocity mostly estimated by sound speed of reaction products, onset of detonation occurs. Local explosion takes place in this condition that leads to local overpressure and abrupt change in explosion front velocity. In order to appear DDT, some criteria need to be satisfied. Mixture and geometry variations have effects widely on DDT that causes different models for it. Mechanism for onset of detonation mainly divided in to two groups [58], first due to shock reflection and second due to instabilities and mixing processes like shock-flame interaction, quenched mixture island explosion, fluctuation of pressure and temperature in flow and boundary layers. In numerical simulation [68] was observed that all mechanism have same importance and detonation starts from a hot spot with further detonation wave distributed in mixture. Phenomenon of explosion in explosion firstly recognized by Urtiew and Oppenheim [69]. Boeck [4] presented change in geometrical configuration by obstacle spacing and blockage ratio, modifies major onset mechanism. But totally, location of hot spot formation as first step in onset of detonation is random and unpredictable. For example, in simulation of stoichiometric ethylene-air mixture experiment [68], location of ignition after solid wall shock reflection varies for different shock Mach numbers and due to fluctuation of temperature and pressure behind the reflecting shock, it is located randomly.

Numerical investigation for $H_2 - O_2$ [70] shows that wall boundary layer is consistently compressed by group of weak shocks between a leading shock and following flame, auto-ignition happens that results a flame travels to leading shock and a local explosion causes onset of detonation. So, for unobstructed configuration, a hot spot formation in wall boundary layers

and behind shock travelling, results to onset of detonation. This local explosion may happen between leading shock and turbulent flame or directly near the flame.

In obstructed configuration, onset of detonation is highly probable by shock reflection off an obstacle as investigated by Thomas [71], Kellenberg and Ciccarelli [72] and showed formation of hot spot after shock reflection at obstacle and detonation wave. Thomas [71] proposed a criterion for predicting onset of detonation based on speed of sound, height of obstacle and induction time (time between mixture being at specific temperature and pressure and ignition) behind reflected shock.

2.3.1 Onset of detonation in inhomogeneous condition of H_2-air mixture

By reaching critical condition of local overpressure and temperature, onset of detonation happens after FA process and this mechanism is same for homogeneous and inhomogeneous conditions. This phenomenon was also investigated in different channel configurations by considering vertical concentration gradients for inhomogeneous H_2-air mixtures [4].

a) Unobstructed channel: Onset of detonation here observed in channel walls adjacent to turbulent flame and depends highly to small scale phenomena like interaction of shocks and wall boundary layer. For homogeneous mixtures, DDT only take place at H_2 concentration of 35-40 vol%. This range is in a good agreement with FA occurrence range for this kind of mixture that shows FA leads to DDT. In contrast, DDT starts earlier for inhomogeneous mixture and can take place at lower amount of H_2 concentration. This observation is also in good agreement with FA behavior of inhomogeneous mixtures as it is due to flame elongation and increased effective flame speed $S_L\sigma$ for low H_2 concentration. But for higher amount of H_2 concentration, DDT cannot occur for inhomogeneous mixtures that shows an upper limit of DDT there. Lower DDT limit can be estimated for both of mixtures as proposed by Kuzntesov et al.[17] and Grune et al.[73] and is more relevant for industrial accidents like what happened in nuclear reactor. So, for inhomogeneous mixture, strong FA overcomes DDT in mixtures with high H_2 concentration.
b) Obstructed channel: In homogeneous mixture, onset of Detonation occurs at lower H_2 concentration in obstructed rather than unobstructed channel. A shock causes auto-ignition in wall boundary layers and reflected off the obstacles. Local explosions occur near obstacles as the first step of process. Then explosion converts to detonation after second hot spot generation at channel walls.

In inhomogeneous mixture, obstructed configuration hinders early DDT which is in contrast to unobstructed one. It can be observed onset of detonation may occur in slightly higher H_2 concentration close to required condition for homogeneous mixture. Onset mechanism is similar for both of mixtures as it starts with strong ignition in post reflected shock mixture and causes diffraction of waves near obstacles. Then Detonation occurs at channel walls due to reflection of the waves. But with this difference that inhomogeneity influences preferred location for first local explosion. In low rate of H_2 concentration in inhomogeneous mixtures, local explosion occurs only at upper obstacle after shock reflection and detonation can be also observed only at channel top wall downstream of obstacle. This similar observation can be seen by increasing H_2 concentration and blockage ratio. More H_2 concentration may cause to have local explosion at both top and bottom of channel but strength of explosion at top of channel is

higher due to higher propagation velocity and still detonation occurs at top of channel downstream of obstacle. By increasing H_2 concentration (30 vol%), local explosions have similar strength in both sides, but for higher concentration (35 vol%), strength of local explosion in bottom exceeds the top one.

From effective flame speed model that was discussed in FA section, it can be seen from specific amount of H_2 concentration (24 vol%), flame speed for homogeneous mixture increases by rising H_2 concentration and enforces FA, while effective flame speed for inhomogeneous mixture cannot increase significantly. It results lower FA tendency and consequently lower potential for DDT in comparison with homogeneous mixture.

Onset of detonation also can be analyzed by post reflected shock detailed chemical kinetics simulation. As shown in figure 2.1 by Lee and Hochgreb [7], extended second explosion limit determines boundary between mild and strong ignition. This helps to have a criterion for critical conditions of fast deflagration shock that results strong ignition after reflecting from obstacle. It shows that on left side of extended second explosion limit, post shock conditions behind incident shocks and reflected shocks results to mild ignition. On the right side, post reflected shock conditions result to strong ignition and local explosions at reflecting wall as first step of onset of detonation. Chemical kinetics simulation shows that strong ignition after shock reflection can be obtained if pressure ratio or Mach number of fast deflagration precursor shock reaches the critical conditions. Critical condition is measured by post-incident shock overpressure and is independent of H_2 concentration. This critical overpressure leads to local explosion and strong ignition after shock reflection as first and crucial step of onset of detonation and has range of 10-11 bar. From combination of chemical kinetics criterion with geometrical criterion it can be observed that even small obstacles may results to have onset of detonation for H_2 -air mixture at ambient conditions.

As discussed above, post incident shock overpressure is practical to determine critical condition for strong ignition and onset of detonation in both homogeneous and inhomogeneous conditions. Experimental values show that for a global flame Mach number, homogeneous mixture has higher overpressure than inhomogeneous mixture. It means that for inhomogeneous condition flame propagates faster to reach equal overpressure at same position. Furthermore, at higher flame Mach number than one, overpressure for obstructed configuration is more than for unobstructed one. Flame Mach number and reactant sound speed for inhomogeneous mixtures should be locally considered at location of pressure measurement, while for homogeneous mixture these values are identical everywhere. Correlation of overpressure and flame Mach number for unobstructed and obstructed configurations with further comparison of homogeneous and inhomogeneous mixtures was modeled by [4, 74]. At end, flame Mach number and flame speed are calculated from conservation of mass within flame front. It can be observed that in fast deflagration regime behind the shock, maximum overpressure occurs, and it can be considered as critical condition for onset of detonation. Expansion of flame leads to pressure reduction. So, relation of overpressure and flame Mach number is connected to model of strong ignition by overpressure as it is critical condition for onset of detonation. So, a critical local flame Mach number should be obtained to have strong ignition and consequently onset of detonation. From one dimensional model by Krok [74], critical flame Mach number is 2.6-2.7 to have peak overpressure of 10-11 bar, while for three dimensional model and experiment by Boeck [4] , it is lower at around 2.4-2.6. Main challenge here is to calculate speed of sound of reaction products.

So, inhomogeneous H_2-air mixture with transverse concentration gradients leads to higher DDT probability in unobstructed configuration, while for obstructed configuration, if flame elongation is possible, it may have the same mechanism for DDT in both homogeneous and inhomogeneous mixture.

2.4 Detonation

After onset of detonation, detonation wave propagates in fresh mixture and flame propagation due to diffusion of heat and species reduced. Detonation is supersonic and consists of three-dimensional shocks that lead to auto-ignition by compressing and heating the mixture. In this regime, flame propagation velocity of H_2-air rises up to 2000 m/s.

Chapman [75] and Jouguet [76] introduced CJ model as a simple one-dimensional detonation. In this model detonation is considered as single discontinuity and it discriminates fresh mixture and equilibrium state behind detonation. Minimum detonation velocity in this model equals to stable solution of a one-dimensional detonation without losses which is considered as CJ detonation. This point is characterized by sonic flow of products behind detonation wave.

To reach the CJ solution, conservation of mass, momentum, and energy [77, 78] across detonation front are employed as shown below. Here, state 0 considers as initial gas condition and state 1 is post-shock state.

Mass conservation: $$\rho_0 u_0 = \rho_1 u_1 \tag{2.26}$$

Momentum conservation: $$P_0 + \rho_0 u_0^2 = P_1 + \rho_1 u_1^2 \tag{2.27}$$

Energy conservation: $$h_0 + \frac{u_0^2}{2} + q = h_1 + \frac{u_1^2}{2} \tag{2.28}$$

By eliminating u_1 from mass and momentum equations, Rayleigh line is defined:

$$u_0^2\left(\frac{1}{\rho_0} - \frac{1}{\rho_1}\right) = \frac{P_1 - P_0}{\rho_0^2} \tag{2.29}$$

These equations make a diagram named Hugoniot curve in $(P - v)$ illustrated in figure 2.8 that comes from energy equation. In this diagram, CJ detonation solution can be obtained from combination of Rayleigh line and product Hugoniot and shown in this figure as upper CJ point. So, CJ solution can be obtained only by equilibrium states and independent of chemical kinetics and structure of detonation front. Detonation velocity from CJ model has a good agreement with velocity obtained from experiments of large tube with low wall roughness.

For reproduction of shock and reaction zone interaction, ZND model (Zel'dovich [79], Von Neumann [80], Döring [81]) was proposed that splits discontinuity of CJ model to a shock and following reaction zone. In Hugoniot diagram, post-shock state or Von Neumann (VN) state considers as intersection of Rayleigh line and adiabatic shock Hugoniot ($q = 0$). From VN state, reaction containing q leads to upper CJ point. Also, non-equilibrium weak detonation state is observed below CJ upper point, while strong detonation state is above this point.

By constant volume explosion, transition from VN state to upper CJ point can be estimated. In experiment, Shepherd [82] shows induction times obtained from ZND model and constant volume explosion are similar for H_2 concentration in range of 13-70 vol%.

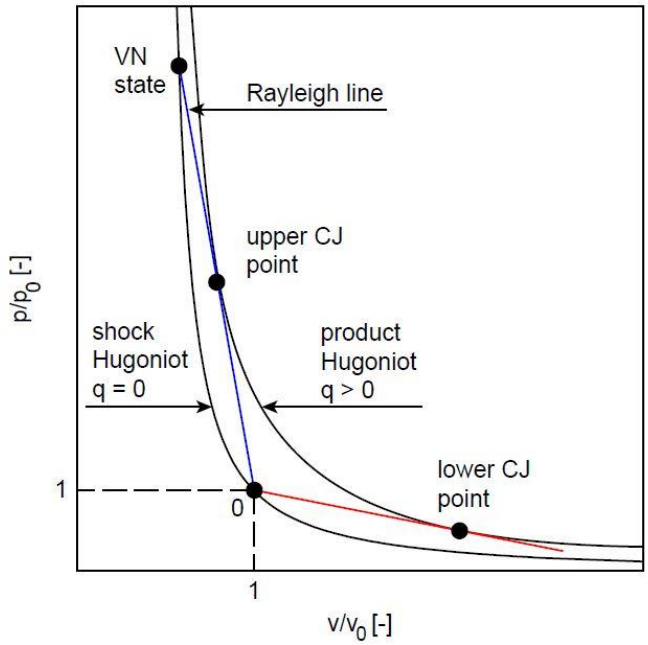

Figure 2.8. Hugoniot diagram with Rayleigh lines (Blue;Red) and CJ tangency solution [4].

Detonation in reality has three dimensional structures and includes transverse waves oscillating perpendicular to incident shock section. Depending on the number of these transvers waves, two main categories are defined as single-headed (one transverse wave) and multi-headed (more than one transverse wave) for detonation.

Figure 2.9 shows a two-dimensional structure of detonation front [78, 83] and there, Mach stem and triple points are formed as collision of incident shock and transverse waves. Cellular patterns are made by triple point trajectories and width of cell shown in this figure is known as detonation cell width λ. Gas velocity differences behind Mach stem and incident shock leads to appear shear layer. Reaction zone through detonation cell starts behind the Mach stem at triple point and propagates at higher rates of CJ velocity D_{CJ} like about 1.2 D_{CJ} [82]. Mach stem strength and velocity reduced. At end of cell, velocity decreases to about 0.8 D_{CJ} [82]. So, at first reaction and Mach stem are close to each and separates afterwards that is obvious significantly in end of cell.

Detonation propagation can be defined as continuous process of initiation at hot spot formed by transverse wave collision at triple point and based on mixture, fails by separation of reaction zone and incident shock. Also, CJ and ZND models correspond to ideal three-dimensional detonation without losses and are not capable to represent transient conditions in detonation cells.

There are correlations for detonation cell width λ as function of mixture properties, effective mixture activation energy and reaction zone length [82, 84, 85]. Experimental values for detonation cell width λ in H_2-air cloud can be shown as a function of equivalence ratio [86].

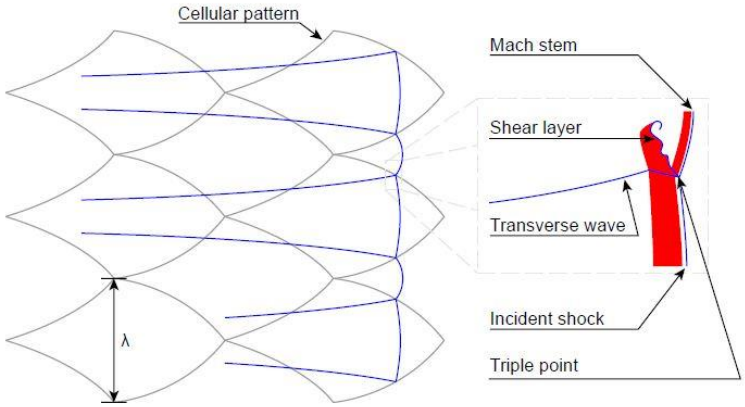

Figure 2.9. 2D Cellular structure (grey lines) of detonation front with shock wave and shear layer (blue lines) and reaction zone (red region) [78, 83]

Detonation cell width λ can be applied in order to determine possibility limits of detonation for mixture in specific geometry. Self-sustained detonation propagation for an unobstructed channel with height of H is possible if $H \geq \lambda$ [58] and for a flat mixture layers of height H (layer of reactive mixture confined by solid wall on one side and an inert on the other side) is possible if $H \geq 3\lambda$ investigated by Rudy et al. [87] and Gaathaug et al. [88]. For bigger Detonation cell widths detonation fails.

Effect of inhomogeneity in fuel-air cloud for detonation occurrence was studied in experimental works by consideration of inert layer in channel. Reinitiation of detonation across an inert region of air was experimentally studied by Bjerketvedt et al.[89] with consideration of gas mixture and width of inert region effects. They showed in similar conditions, reinitiation can occur for some mixtures while for other, they failed to reinitiate. Also, detonation reinitiation occurs with some delay and not instantly. Furthermore, they observed that CJ properties of detonation in upstream region of inert layer, width of inert region and reactivity of gas in downstream region of inert layer are governing parameters for detonation reinitiation and also this process is highly sensitive to sharpness of concentration gradients at boundaries of inert region. Besides, heat transfer and wall friction weaken the shock and delay reinitiation of detonation while presence of soot on tube walls enhance it.

Effect of inert layer on detonation reinitiation/failure and other detonation parameters was also studied with multiple inert layer perpendicular to detonation propagation direction for stoichiometric $H_2/O_2/N_2$ mixture[90]. Here in this inhomogeneous mixture, it was observed that detonation reinitiation occurs only at relatively small amounts of inert layer thickness and spacing between two consecutive inert layers. A critical thickness for each amount of spacing was observed that above it, detonation fails while passing inert layers. By having more spacing, critical thickness starts to reduce. Also, due to cellular structure with triple point in 2D propagation case, larger amount of this critical inert layer thickness was found than in 1D case. Average detonation propagation speed of inhomogeneous mixture was compared to CJ speed with good agreement that shows inert layer does not affect detonation propagation speed since a successful detonation reinitiation occurs. In contrast, detonation cell structure and cell size are significantly affected by inert layer and results in large cellular structure which its size is linearly proportional to inert layer spacing. Furthermore, in large amount of spacing between inert layers, double cellular structure or substructure in large cellular structure can be seen.

2.4.1 Detonation in inhomogeneous condition of H_2-air mixture

In order to investigate detonation in inhomogeneous H_2-air mixture, effect of vertical concentration gradients was considered for inhomogeneity in experiments [4] and detonation velocity and shape was compared with homogeneous mixture.

2.4.1.1 Detonation velocity

For homogeneous H_2-air mixtures, detonation velocity is close to Chapman-Jouguet velocity D_{CJ}. By increasing H_2 concentration and having richer mixture, triple point is less obvious and reaction zone behind the leading shock becomes thinner.

For inhomogeneous H_2-air mixture, detonation velocity is less than for homogeneous mixture at same average H_2 concentration and have slower propagation. It is different from deflagration regime observation in experiments. By having more inhomogeneity, this velocity becomes less. In richer H_2-air mixtures, difference of velocity with Chapman-Jouguet velocity D_{CJ} is smaller than for leaner ones. In spite of this deficit, it can be observed that maximum inhomogeneity also support detonation propagation and velocity difference is less than 10% compared to Chapman-Jouguet velocity D_{CJ} [4, 91, 92].

2.4.1.2 Detonation shape

Detonation shape is classified in two main categories. First one is Single-headed detonation regime that occurs in high inhomogeneity of H_2-air mixtures. It exhibits a strong transverse wave through the channel reflecting off the walls periodically and keep the pressure differences behind the detonation front balanced. By reflection of the wave at top of channel, strong local explosions occur and cause reinitiation of detonation. This local explosion result to single-headed regime. Reaction and shock are coupled behind the Mach stem after local explosion and also when wave reflecting off the wall. But afterwards, they decoupled in upper region of channel. By reaching the top of channel, reflected wave results to local explosion and it completes one cell cycle. This regime as a near limit phenomenon can be considered like spinning detonation [93] and compared with detonation of high activation energy mixtures [88]. To reach the single-headed regime, at a constant H_2 concentration, inhomogeneity of mixture should be increased or at a constant inhomogeneous mixture, H_2 concentration should be decreased [4]. Second category is multi-headed detonation regime that in inhomogeneous H_2-air mixture occurs in rich conditions with high amount of H_2 concentration. It also happens at leaner mixtures but with more homogeneity. Transverse waves are produced consistently by reflecting off the channel wall and collision with other waves. There is no Mach stem formation on walls in contrast to lower H_2 concentration. In this regime, reaction zone is significantly thinner which means more part of mixture is consumed by auto-ignition and interprets lower velocity differences than single-headed detonation. In contrast to homogeneous mixtures, inhomogeneous ones have not symmetric detonation cells, and they are larger adjacent the walls.

Detonation cell width for homogeneous mixture is identical within the channel height while for inhomogeneous mixtures, can be related to H_2 concentration and has a non-linear relationship with local H_2 concentration. It can be observed that at top of channel where high H_2 concentration is present, cell width is smaller and by reduction of H_2 concentration through the bottom of channel, significant increase in cell width even larger than channel height can be

happened. Single-headed regime shows significant rise in cell width in contrast to multi-headed regime and happens when bottom of channel reaches low H_2 concentration. Cells with smaller width than channel height are considered to show lower limit of detonation. It can be observed that detonable layer height for single-headed cases is lower than multi-headed ones. Experiments shows that about two detonation cells required to be present in detonable layer to have stable multi-headed propagation while for single-headed it is less than two cells in region. So, by lower detonable height, unstable single-headed detonation occurs and by even reducing this height for more inhomogeneity, detonation fails to occur.

2.5 Conclusion

As observed in experiments, H_2-air explosion starts from slow deflagration with maximum pressure of almost 1 bar and maximum flame speed of 100 m/s and continues to detonation propagation with maximum overpressure of 10 bar and supersonic propagation speed of up to 2000 m/s. Because of high ignition energy needed for direct detonation of H_2-air cloud, strong ignition is not probable.

It can be observed that in vertical concentration gradients for inhomogeneous H_2-air mixture, they show much higher explosion, stronger FA, and earlier DDT in closed channel than homogeneous mixture at equal average H_2 concentration. Two main effects of flame surface area enlargement and effective flame speed influence FA for inhomogeneous mixtures in these experiments. In unobstructed configuration flame elongation leads to enlargement of flame surface area and consequently flame accelerates much stronger further with earlier DDT for inhomogeneous mixtures than homogeneous ones. For low H_2 concentration, DDT occurs for inhomogeneous mixture, while it happens for homogeneous mixture when there are obstacles in channel. At higher H_2 concentration in obstructed configuration, inhomogeneous mixtures postpone DDT and lead to have upper limit of DDT. It can be interpreted as flame of inhomogeneous mixture need to accelerate to a local flame Mach number same as homogeneous mixture to reach the peak overpressure. Effective flame speed of inhomogeneous mixtures with H_2 concentration more than 24 vol% remains constant, while flame speed needed for onset of detonation increases by rising H_2 concentration. So, critical flame speed and consequently flame Mach number cannot lead to have onset of detonation for inhomogeneous condition. By having more homogeneity, effective flame speed increases significantly and there will be high probability of DDT. Therefore, flame in both mixtures need to accelerate to same critical flame Mach number to reach DDT.

Detonation propagation of H_2-air mixture is different from deflagration regime observation in experiments. In same H_2 concentration, inhomogeneous H_2-air mixtures have slower detonation propagation velocity than homogeneous ones, but it can be observed even in high inhomogeneity. Single-headed detonation regime has one strong transverse wave, and it is observable in leaner condition of inhomogeneous mixture, while multi-headed regime has a constant macroscopic front curvature over time and some weak transverse waves which is observable in rich condition of inhomogeneous mixtures or lean homogeneous mixtures.

Finally, it can be concluded that flame elongation and enlargement of flame surface area is the most dominant mechanism for FA of inhomogeneous mixtures. So, understanding this mechanism for unobstructed configuration and preventing of it due to obstacle in obstructed configuration is fundamental in explosion study of inhomogeneous H_2-air mixture.

3 Finite Volume method and Case Study Simulation

Computational fluid dynamics (CFD) is a computer-based simulation for analyzing systems involve with fluid flow, heat transfer, chemical reactions, etc. This technique uses numerical algorithm for codes with reasonable error in order to approach and compute behavior of system. It helps users to compare results with other methods and experiments. CFD codes are in three main elements as pre-processor, solver, and post-processor. Definition of these codes are different and important for getting accurate results. One significant advantage of using CFD technique is lower cost of implementation in comparison with real scale experiments [2]. Here, openFOAM (open-source Field Operation And Manipulation) software has been employed as an open-source CFD toolbox to simulate case study.

Since present work is based on combustion modelling, in following sections equations govern on combustion process in CFD simulation are expressed.

In this chapter, first governing equations for combustion flows as fundamental of finite volume discretization technique are discussed. Then turbulence model and combustion flame wrinkling model are described separately which have been implemented for present work. Finally, numerical method for objective case and corresponding setup are described for simulation of desired gas explosion.

3.1 Governing equations in combustion modelling[2]

3.1.1 Transport equation

For any scalar property of fluid named as φ, conservative equation can be shown in general transport equation.

$$\frac{\partial(\rho\varphi)}{\partial t} + div(\rho\varphi\boldsymbol{u}) = div\,(\Gamma\, grad\varphi) + S_\varphi \tag{3.1}$$

Where Γ is diffusion coefficient and S_φ is source term.

By adopting proper value of φ (e.g.,1, u_i, Y_k, h, etc.) and corresponding diffusion coefficient Γ and source term S_φ, transport equation can result to conservation equations that introduce as follows. Transport equation is start point for computational procedure in finite volume method.

In finite volume method, domain is discretized into control volume. CFD uses numeric algorithm to integrate the general transport equation over time and over control volume and solve any property of fluid in nodal of this discretized grid.

3.1.1.1 Continuity equation

First equation in transport is mass conservation or mass continuity ($\varphi = 1$). It shows that rate of increase of mass in fluid element is equal to net rate of flow of mass into fluid element. For reacting and non-reacting flows since there is no generation or consumption of mass, so it

conserved. In combustion flows, density is changing and depends on pressure, temperature, and species concentration. So, continuity equation can be expresses as equation below.

$$\frac{\partial \rho}{\partial t} + \frac{\partial}{\partial x_i}(\rho u_i) = 0 \tag{3.2}$$

Where: ρ is mass density and u_i is velocity component in i direction.

3.1.1.2 Momentum equation

Momentum equation is next conservation equation that derived from Newton`s second law ($\varphi = u_i$). By definition, momentum is product of mass and velocity of particle. These equations show that momentum increasing rate of fluid particle equals to summation of forces on that fluid particle. Two main types of forces have effects on fluid particles. First one is surface forces that contains pressure and viscous forces (based on viscous stresses) and second one is body forces that mostly contains gravity forces. In momentum equation, effect of body forces shows in a separate term as source. In many fluids flows, viscous stresses are proportional to local deformation rates or strains rate. They are known as Newtonian fluids and Strain rates is composed of linear deformation rate and volumetric deformation rate. So, substitution of viscous stresses with relevant deformation components are known as Navier-stokes equations. Momentum equation can be shown as below for combustion flows.

$$\frac{\partial}{\partial t}(\rho u_i) + \frac{\partial}{\partial x_i}\left(\rho u_i u_j\right) = -\frac{\partial P}{\partial x_i} + \frac{\partial \tau_{ij}}{\partial x_i} + F_i \tag{3.3}$$

Where p is pressure, τ_{ij} is viscous stress component acts in j direction on surface normal to the i direction and calculated from equation below proposed by Boussinesq in 1877 based on proportionality to rates of deformation (velocity gradients) in Newtonian fluids and F_i is body force which includes gravity.

$$\tau_{ij} = \mu\left(\frac{\partial u_i}{\partial x_j} + \frac{\partial u_j}{\partial x_i} - \frac{2}{3}\delta_{ij}\frac{\partial u_k}{\partial x_k}\right) \tag{3.4}$$

Where μ is dynamic viscosity and δ_{ij} is Kronecker delta that gets value $\delta_{ij} = 1$ if $i = j$ and $\delta_{ij} = 0$ if $i \neq j$.

3.1.1.3 conservation of species

In combustion flow, transport equation can be shown for reacting flows as conservation of mass of a species k. By adopting $\varphi = Y_k$ as mass fraction of species k, general transport equation (3.1) presents as equation below. It shows that:

(Rate of change of mass of species k) + (Net rate decrease of mass of species k due to Convective) = (Net rate increase of mass of species k due to diffusion) + (Net rate increase of mass of species k due to sources)

$$\frac{\partial}{\partial t}(\rho Y_k) + \frac{\partial}{\partial x_i}(\rho u_i Y_k) = \frac{\partial}{\partial x_i}\left(\rho D_k \frac{\partial Y_k}{\partial x_i}\right) + \dot{\omega}_k \tag{3.5}$$

Where D_k is species diffusion coefficient in unit (m^2/s) and $\dot{\omega}_k$ is reaction rate source (or sink) term also in unit ($kg/m^3.s$), in which volumetric rate of generation (or destruction) of a species occurs due to chemical reaction.

There are various models for physically controlled combustion where reaction rate source term takes the form of that model. For example, kinetically controlled combustion leads to source term takes the form of:

$$\dot{\omega}_k = MW_k \dot{q}_k \tag{3.6}$$

where MW_k is molecular weight of species k , $\dot{q}_k$ is total reaction rate of species k which is summation of reaction rate of species k produced by each specific reaction.

For a simple forward reaction as: $aA + bB \rightarrow cC + dD$, progress rate for consumption of species A can be shown as follows:

$$\dot{q}_A = \frac{dC_A}{dt} = -ak_f (C_A)^a (C_B)^b \tag{3.7}$$

Where C_A and C_B are molar concentration of A and B and k_f is forward reaction rate that is expressed based on Arrhenius law as follows.

$$k_f = AT^\alpha \exp\left(-\frac{E_a}{RT}\right) \tag{3.8}$$

Where A is pre-exponential factor, E_a is activation energy and $R = 8.314\ kJ/kmol.K$ is universal molar gas constant.

So, expression for reaction rate source term of chemical kinetics is consumption of species A that will be:

$$\dot{\omega}_k = AT^\alpha (C_A)^a (C_B)^b \exp\left(-\frac{E_a}{RT}\right) \tag{3.9}$$

Another expression is:

$$\dot{\omega}_k = A'[Y_A]^a [Y_B]^b \exp\left(-\frac{E_a}{RT}\right) \tag{3.10}$$

Where:

$$A' = (MW)_A a A T^\alpha \left(\frac{\rho}{(MW)_A}\right)^a \left(\frac{\rho}{(MW)_B}\right)^b \tag{3.11}$$

that contains density, molecular weight and comes from conversion of molar concentration C_A and C_B to mass fraction Y_A and Y_B in purpose of using in CFD calculation.

3.1.1.4 Energy equation

Energy equation is another conservation equation that derived from first law of thermodynamics ($\varphi = h$). It shows that energy change rate of fluid particle is equal to net rate of heat added to and net rate of work done on that fluid particle. The rate of work done by surface force is equal to product of force and velocity component in direction of force. Also, net rate of heat transfer to fluid particle is difference of heat input rate and heat loss rate from fluid particle.

Energy of fluid particle can be defined as internal energy and kinetic energy produced by each velocity vector. Gravitational potential energy can be considered as a source term since it originates from body forces.

For compressible flows it can be shown that enthalpy related to internal and kinetic energy and in combustion flows, as combustion goes ahead, chemical energy released in form of heat. Thus, transport equation (3.1) can be written for obtained enthalpy as follow.

$$\frac{\partial}{\partial t}(\rho h) + \frac{\partial}{\partial x_i}(\rho u_i h) = \frac{\partial}{\partial x_i}\left[\frac{\mu}{\sigma_h}\frac{\partial h}{\partial x_i} + \mu\left(\frac{1}{S_{c_k}} - \frac{1}{\sigma_h}\right)\sum_{k=1}^{N} h_k \frac{\partial Y_k}{\partial x_i}\right] + \frac{\partial p}{\partial t} + S_{rad} \qquad (3.12)$$

It shows that rate of change of enthalpy + Net rate of decrease of enthalpy due to convection= Net rate of increase of enthalpy due to diffusion along gradients of enthalpy+ Net rate of increase of enthalpy due to mass diffusion along gradients of species concentration+ Net rate of increase of enthalpy due to pressure work + Net rate of increase of enthalpy due to radiative heat transfer.

In transport equation of enthalpy (3.12), h is mixture enthalpy per unit mass, h_k is specific enthalpy of species k, $\sigma_h$is Prandtl number, S_{c_k} is Schmidt number and S_{rad} is Source term of radiation loss or gain.

Prandtl number σ_h is defined as rate of momentum transport to rate of energy transport as below.

$$\sigma_h = \frac{c_p \mu}{K} \qquad (3.13)$$

And Schmidt number as rate of momentum transport to rate of mass transport,

$$S_{c_k} = \frac{\mu}{\rho D_k} = Le\,\sigma_h \qquad (3.14)$$

Here, Lewis number Le is defined as rate of energy transport to rate of mass transport,

$$Le \equiv \frac{K}{\rho c_p D_k} \qquad (3.15)$$

Where K is thermal conductivity.

So, transport equation for enthalpy (3.11) can be written as follows,

$$\frac{\partial}{\partial t}(\rho h) + \frac{\partial}{\partial x_i}(\rho u_i h) = \frac{\partial}{\partial x_i}\left[\frac{\mu}{\sigma_h}\frac{\partial h}{\partial x_i} + \frac{\mu}{\sigma_h}\left(\frac{1}{Le} - 1\right)\sum_{k=1}^{N} h_k \frac{\partial Y_k}{\partial x_i}\right] + \frac{\partial p}{\partial t} + S_{rad} \qquad (3.16)$$

If S_{rad} is small, enthalpy is conserved or passive scalar.

Lewis number for different species in H_2-air mixture can be read for example from [94], and it can be seen that except H and H_2 which are less than unity, other species has a Lewis number near unity. In combustion modelling, CHEMKIN package [95] for instance, can calculate required diffusion coefficients and other transport properties.

3.1.2 Equations of state

Four thermodynamics variables i, p, ρ and T for fluid relate to each other based on thermodynamic equilibrium. Equations of state relate variables to two state variables. For perfect gas by considering ρ and T as state variables, there are equations for pressure and internal energy based on these two state variables as follows.

$$p = \rho R T \qquad ; \qquad i = C_v T \qquad (3.17)$$

For compressible fluids, equations of state link energy equation to mass conservation and momentum equations that rise possibility of change in density as result of pressure and temperature change in field of flow.

3.2 Turbulence model[2]

In combustion flows like many other flows, chaotic and random behavior of flow which known as turbulence appears above a certain number of Reynolds number.

In order to consider this phenomenon and effects of instabilities in flows there is a need to define a suitable turbulence model. This condition takes place when viscous forces are not sufficient to resist instabilities in flow, hence Reynolds number appears to evaluate this situation. By defining a critical Reynold number $R_{e_{Crit}}$, laminar and turbulent regimes are separated from each other. So, calculation of turbulence is important in combustion flows. There are three main groups to calculate turbulence as mentioned below:

- Reynolds-average Navier-stokes (RANS) equations: Reynolds decomposes any flow properties to two parts as mean flow and fluctuation flow. This model focuses mainly on mean flow and effects of mean flow properties and implements time averaging of Navier-stokes equations. Extra terms appear in time-averaged (or Reynolds averaged) flow equations due to interactions among turbulent fluctuations. Extra terms are modelled with turbulence model such as $\kappa - \varepsilon$ and Reynolds stress models.
- Large eddy simulation (LES): intermediate form of turbulence calculation that follows large eddies behavior and filter unsteady Navier-stokes equations. This model passes large eddies and rejects small eddies.
- Direct numerical simulation (DNS): calculate all mean flow and turbulent velocity fluctuations. Unsteady Navier-stokes equation are computed on spatial grid. So, it is fine enough to consider small time step and resolve period of fastest fluctuations.

In following subchapters, two kinds of averaging method, Reynolds averaging, and Favre averaging for RANS turbulence calculation are introduced. Furthermore, $\kappa - \varepsilon$ turbulence model is discussed in order to estimate Reynolds stresses and scalar transport terms for turbulent flows computation in RANS. Finally, characteristic scales in turbulent flows are described.

3.2.1 Reynolds averaging

For every single fluid property of φ, Reynolds divided it to two composition as mean value and fluctuation value. It is known as Reynold decomposition of Reynolds averaging of that flow variable and is shown as follows:

$$\varphi(t) = \bar{\varphi} + \varphi'(t) \tag{3.18}$$

Where time average value is:

$$\bar{\varphi} = \frac{1}{\Delta t}\int_{t_0}^{t_0+\Delta t} \varphi(t)dt \tag{3.19}$$

Selecting Δt is wisely to be large enough compared to period of random turbulence fluctuation and small enough compared to slow variations time constant in ordinary unsteady flows.

Also, average value of fluctuation φ' is zero.

$$\overline{\varphi'}(t) = \frac{1}{\Delta t}\int_{t_0}^{t_0+\Delta t} \varphi'^{(t)} dt = 0 \tag{3.20}$$

In combustion flows, due to high and strong heat generation, density varies as a function of position. Furthermore, by turbulent flow, fluctuation of density is observable. So, it is practical to show density in form of Reynolds decomposition $\rho = \bar{\rho} + \rho'$.

This Reynolds decomposition can be generalized to other variables like u_i,p,T,Y_k,h in reacting flows ($u_i = \overline{u_\iota} + u_i'$, etc.).

By implementing Reynolds averaging of u_i and ρ in continuity equation (3.2) it would result to following equation.

$$\frac{\partial \bar{\rho}}{\partial t} + \frac{\partial(\overline{\rho u_\iota})}{\partial x_i} + \frac{\partial\overline{(\rho' u'_\iota)}}{\partial x_i} = 0 \tag{3.21}$$

Thus, density fluctuations show additional term by using Reynolds averaging system. This additional term $\frac{\partial\overline{(\rho' u'_\iota)}}{\partial x_i}$ has to be modelled since it comes from correlation between velocity and density fluctuations in reacting flow. Other additional terms also can be derived from momentum, species and other transport equations which need to be modelled. Momentum transport equations (3.3) by implementing Reynolds decomposition is expressed as below.

$$\frac{\partial}{\partial t}\left(\bar{\rho}\overline{u_\iota} + \overline{\rho' u'_\iota}\right) + \frac{\partial}{\partial x_j}\left(\bar{\rho}\overline{u_\iota}\overline{u_j} + \overline{u_\iota}\overline{\rho' u'_j}\right) = -\frac{\partial \bar{p}}{\partial x_i} + \frac{\partial}{\partial x_j}\left(\bar{\tau}_{ij} - \overline{u_j}\overline{\rho' u'_\iota} - \bar{\rho}\overline{u'_\iota u'_j} - \overline{\rho' u'_\iota u'_j}\right) \tag{3.22}$$

Where:

$$\bar{\tau}_{ij} = \mu\left[\left(\frac{\partial \overline{u_i}}{\partial x_j} + \frac{\partial \overline{u_j}}{\partial x_i}\right) - \frac{2}{3}\delta_{ij}\frac{\partial \overline{u_k}}{\partial x_k}\right] \tag{3.23}$$

In purpose of reducing these number of additional terms, it has been proposed to use a density-weighted averaging procedure named as Favre averaging by Favre[96] and Jones and Whitelaw[97].

3.2.2 Favre averaging

As mentioned above, Favre averaging is used in order to simplify averaging procedure by means of reducing additional terms. It is known as mass- weighted or density- weighted averaging. Same as Reynolds averaging procedure, Favre averaging, or Favre decomposition defined for any single fluid property of φ as two parts of mean value $\tilde{\phi}$ and fluctuation value φ''.

$$\varphi = \tilde{\varphi} + \varphi'' \tag{3.24}$$

Where:

$$\tilde{\varphi} = \frac{\overline{\rho\varphi}}{\bar{\rho}} \tag{3.25}$$

So, by substituting eq. (3.25) in eq. (3.24) it results,

$$\varphi = \frac{\overline{\rho\varphi}}{\bar{\rho}} + \varphi'' \tag{3.26}$$

It should be considered that mass averaged is only for velocity components and thermal variables. Fluid properties like density and pressure are treated as before.

In contrast to Reynolds decomposition shown in equation (3.20), mean value of fluctuations φ'' is not zero ($\overline{\varphi''} \neq 0$).

In Favre decomposition, it can be shown that $\overline{\rho\varphi''} = 0$ same as $\overline{\rho\varphi'} = 0$ for Reynolds decomposition. Also, it can be result that φ' shows a turbulent fluctuation of property φ, while φ'' include effect of density fluctuation rather than fluctuation of property φ.

By implementing ρ and u in convective term of continuity equation with Favre averaging it can be shown that:

$$\rho u = \rho(\tilde{u} + u'') = \rho\tilde{u} + \rho u'' \tag{3.27}$$

By time averaging it will be:

$$\overline{\rho u} = \bar{\rho}\tilde{u} + \overline{\rho u''} = \bar{\rho}\tilde{u} \tag{3.28}$$

So, continuity equation (3.2) will be as follows:

$$\frac{\partial \bar{\rho}}{\partial t} + \frac{\partial(\bar{\rho}\widetilde{u_i})}{\partial x_i} = 0 \tag{3.29}$$

In contrast to Reynolds averaging form of continuity equation, above equation is in same form of original continuity equation, but with this difference that mean velocity here is density-weighted Favre-average velocity.

So, it can be observed that Favre averaging procedure, reduces similarly the number of additional terms which are product of fluctuation in other transport equations. But it should be considered that results from Favre averaging need to be converted to time averaging to compare with experimental result.

Other Favre averaging equations to be used in combustion modelling for transport equations are as follows.

Momentum equation (3.3) by implementing Favre averaging is expressed as:

$$\frac{\partial}{\partial t}(\bar{\rho}\widetilde{u_\iota}) + \frac{\partial}{\partial x_j}\left(\bar{\rho}\widetilde{u_\iota}\widetilde{u_\jmath}\right) = -\frac{\partial \bar{p}}{\partial x_i} + \frac{\partial}{\partial x_j}\left(\bar{\tau}_{ij} - \overline{\rho u''_\iota u''_\jmath}\right) \tag{3.30}$$

Where:

$$\bar{\tau}_{ij} = \mu\left[\left(\frac{\partial \widetilde{u_i}}{\partial x_j} + \frac{\partial \widetilde{u_j}}{\partial x_i}\right) - \frac{2}{3}\delta_{ij}\frac{\partial \widetilde{u_k}}{\partial x_k}\right] + \mu\left[\left(\frac{\partial \overline{u''_i}}{\partial x_j} + \frac{\partial \overline{u''_j}}{\partial x_i}\right) - \frac{2}{3}\delta_{ij}\frac{\partial \overline{u''_k}}{\partial x_k}\right] \tag{3.31}$$

Here viscosity fluctuations are neglected. Also, practically, second viscous term in equation (3.31) is too small compared to other term that can be neglected.

Furthermore, Boussinesq expressed turbulent Reynolds stresses $\overline{\rho u''_\iota u''_\jmath}$ term in equation (3.30) as follows:

$$\overline{\rho u''_\iota u''_\jmath} = \bar{\rho}\widetilde{u''_\iota u''_\jmath} = -\mu_t\left(\frac{\partial \widetilde{u_i}}{\partial x_j} + \frac{\partial \widetilde{u_j}}{\partial x_i} - \frac{2}{3}\delta_{ij}\frac{\partial \widetilde{u_k}}{\partial x_k}\right) + \frac{2}{3}\bar{\rho}\kappa \tag{3.32}$$

Where κ is turbulent kinetic energy and expressed in three directions as follows:

$$\kappa = \frac{1}{2}\sum_{j=1}^{3}\widetilde{u''_\iota u''_\jmath} = \frac{1}{2}\left(\widetilde{u''^2_1} + \widetilde{u''^2_2} + \widetilde{u''^2_3}\right) \tag{3.33}$$

Species conservation equation (3.5) by implementing Favre averaging is:

$$\frac{\partial}{\partial t}\left(\bar{\rho}\widetilde{Y_k}\right)+\frac{\partial}{\partial x_j}\left(\bar{\rho}\,\widetilde{u_j}\widetilde{Y_k}\right)=\frac{\partial}{\partial x_j}\left(\bar{\rho}D_k\frac{\partial\widetilde{Y_k}}{\partial x_j}-\overline{\rho Y''_k u''_j}\right)+\frac{\partial}{\partial x_j}\left(\bar{\rho}D_k\frac{\overline{\partial Y''_k}}{\partial x_j}\right)+\widetilde{\dot{\omega}_k} \tag{3.34}$$

Where $\widetilde{\dot{\omega}_k}$ is Favre-averaged reaction rate of production or consumption of species k. By using gradient diffusion assumption, turbulent species will be:

$$\overline{\rho Y''_k u''_j}=\frac{\mu_t}{S_{c_k}}\frac{\partial\widetilde{Y_k}}{\partial x_j} \tag{3.35}$$

Where: S_{c_k} is turbulent Schmidt number for species k.

Finally, by substitution of equation (3.35) in (3.34) species equations will be:

$$\frac{\partial}{\partial t}\left(\bar{\rho}\widetilde{Y_k}\right)+\frac{\partial}{\partial x_j}\left(\bar{\rho}\,\widetilde{u_j}\widetilde{Y_k}\right)=\frac{\partial}{\partial x_j}\left(\Gamma_k\frac{\partial\widetilde{Y_k}}{\partial x_j}\right)+\frac{\partial}{\partial x_j}\left(\bar{\rho}D_k\frac{\overline{\partial Y''_k}}{\partial x_j}\right)+\widetilde{\dot{\omega}_k} \tag{3.36}$$

Where:

$$\Gamma_k=\left(\frac{\mu}{\sigma}+\frac{\mu_t}{S_{c_k}}\right) \tag{3.37}$$

Energy in form of enthalpy transport equation (3.16) can be shown as follows after implementing Favre averaging:

$$\frac{\partial}{\partial t}\left(\bar{\rho}\tilde{h}\right)+\frac{\partial\left(\bar{\rho}\widetilde{u_j}\tilde{h}\right)}{\partial x_j}=\frac{\partial}{\partial x_j}\left(\Gamma_h\frac{\partial\tilde{h}}{\partial x_j}\right)+\bar{S}_h \tag{3.38}$$

Where:

$$\Gamma_h=\left(\frac{\mu}{\sigma}+\frac{\mu_t}{\sigma_h}\right) \tag{3.39}$$

and σ_h is turbulent Prandtl number.

In order to calculate μ_t in momentum, species and enthalpy equations, proper turbulent model should be selected. These models are classified based on number of additional transport equations need to be computed along with RANS flow equations. Some turbulent model examples are: Mixing length model with zero extra transport equation, Spalart-Allmaras model with one extra transport equation, $\kappa-\varepsilon$, $\kappa-\omega$ and Algebraic stress models which use two extra transport equations and Reynold stress model that uses seven extra transport equations.

In following subchapter, $\kappa-\varepsilon$ model is discussed as one of the frequent models in RANS turbulence calculations.

3.2.3 $\kappa-\varepsilon$ turbulence model

In this model, two additional transport equations are used in order to describe turbulence due to consideration effects of transport of turbulence properties by convection and diffusion and production and destruction of turbulence. First equation is for turbulent kinetic energy κ as follows.

$$\frac{\partial}{\partial t}\left(\bar{\rho}\kappa\right)+\frac{\partial}{\partial x_j}\left(\bar{\rho}\,\widetilde{u_j}\kappa\right)=\frac{\partial}{\partial x_j}\left[\left(\mu+\frac{\mu_t}{\sigma_\kappa}\right)\frac{\partial\kappa}{\partial x_j}\right]+\mathrm{P}_k-\bar{\rho}\varepsilon \tag{3.40}$$

Where σ_κ is turbulent Prandtl number for κ and source term P_κ is:

$$P_\kappa = -\bar{\rho}\widetilde{u''_\iota u''_J}\frac{\partial \widetilde{u_J}}{\partial x_j} \tag{3.41}$$

Also $\bar{\rho}\widetilde{u''_\iota u''_J}$ was defined as Boussinesq equation (3.31).

Another extra equation is for rate of dissipation of turbulent kinetic energy ε as follows.

$$\frac{\partial}{\partial t}(\bar{\rho}\varepsilon) + \frac{\partial}{\partial x_j}\left(\bar{\rho}\,\tilde{u}_j\varepsilon\right) = \frac{\partial}{\partial x_j}\left[\left(\mu + \frac{\mu_t}{\sigma_\varepsilon}\right)\frac{\partial \varepsilon}{\partial x_j}\right] + C_{1\varepsilon}\frac{\varepsilon}{\kappa}P_\kappa - C_{2\varepsilon}\bar{\rho}\frac{\varepsilon^2}{\kappa} \tag{3.42}$$

Where σ_ε is turbulent Prandtl number for ε.

The κ and ε are used to define integral length scale ℓ_T , integral time scale τ_T and velocity scale ϑ.

$$\ell_T = \frac{\kappa^{\frac{3}{2}}}{\varepsilon} \quad ; \quad \tau_T = \frac{\kappa}{\varepsilon} \quad ; \quad \vartheta = \kappa^{\frac{1}{2}} \tag{3.43}$$

So, Turbulence viscosity μ_t will be:

$$\mu_t = \bar{\rho}\, C_u \frac{\kappa^2}{\varepsilon} \tag{3.44}$$

Standard values for constants in equations (3.40), (3.42) and (3.44) are obtained from data fitting over a wide range of turbulent flows are mentioned below.

$$C_u = 0.09 \;;\; \sigma_\kappa = 1.00 \;;\; \sigma_\varepsilon = 1.30 \;;\; C_{1\varepsilon} = 1.44 \;;\; C_{2\varepsilon} = 1.92 \tag{3.45}$$

3.3 Combustion model

In a premixed flame during combustion, flame front propagates at certain speed and leaves burnt products. As mentioned in section 2.2, laminar and turbulent flame speed and a parameter named as reaction progress variable c are used to model the combustion. This variable shows that flame propagates from burned to unburned mixtures and describes progress of reaction toward unburned gas. If temperature of unburnt gas is considered as T_u , temperature of burnt gas as T_b , and flame temperature as T , reaction progress variable c can be defined as follows.

$$c = \frac{T - T_u}{T_b - T_u} \tag{3.46}$$

Based on reaction progress variable definition, $c = 0$ where mixture is unburnt and $c = 1$ where mixture is fully burnt [2].

For modelling premixed turbulent combustion, Weller [98] proposed a model named Flame wrinkling combustion model, based on wrinkle density Ξ transport equation and corresponding equation for regress variable b that is implemented in present work.

3.3.1 Flame wrinkling combustion model

This model was proposed by Weller [98] to satisfy needs of turbulent combustion modelling. He suggested a simple model compared to multi equation ones that were used for this reason before. A comprehensive mathematical model of turbulent combustion including mass, momentum, energy, and mass fraction conservation of all components by density weighted applied and sub-grid scales (SGS) is introduced.

It was assumed that turbulent flame may expressed as distribution of reaction zones named flamelets, that considered as laminar flame evaluated at local conditions. Previously, extended laminar flamelet approaches, considered flame as a sheet that propagate locally as laminar flame and increase in area due to formation of distortion by its interaction with turbulent flow. These approaches included progress variable and flame area per unit volume transport equations that make them develop in many directions. But Weller proposed alternative approach of flame area to these traditional models. He introduced flame wrinkle density Ξ which is flame area per unit area solve in mean direction of propagation. Also, he introduced correspond equation for regress variable b which is in contrast to progress variable that was defined previously.

$$b = 1 - c \tag{3.47}$$

Therefore, $b = 1$ is unburnt region and $b = 0$ is burnt region in contrast to progress variable.

As proposed Weller et al. [99] to produce transport equations, laminar flamelet approach is used with conditional filtering. Such procedure was used in RANS successfully for combustion cases.

By introducing $\tilde{b}$ as density- weighted regress variable, transport equation for resolved part of unburned gas mass fraction or regress variable $\tilde{b}$ can be expressed as below.

$$\frac{\partial}{\partial t}\left(\bar{\rho}\tilde{b}\right) + \nabla.\left(\bar{\rho}\tilde{u}\tilde{b}\right) - \nabla.\left(\bar{\rho}D\nabla\tilde{b}\right) = -\bar{\rho}_u S_L \Xi\left|\nabla\tilde{b}\right| \tag{3.48}$$

Where: $\bar{\rho}_u$ is unburned mixture density, D is sub-grid diffusion coefficient, Ξ is sub-grid flame wrinkling and can be considered as ratio of turbulent flame speed S_T to laminar flame speed S_L.

$$\Xi = \frac{S_T}{S_L} \tag{3.49}$$

Transport equation for sub-grid flame wrinkling Ξ would be,

$$\frac{\partial \Xi}{\partial t} + U_s\,.\nabla\Xi = G\Xi - R(\Xi - 1) + (\sigma_s - \sigma_t)\Xi \tag{3.50}$$

Where U_s is surface-filtered velocity of flame, σ_s is surface-filtered resolved strain rate and σ_t is resolved strain rates that are related to surface-filtered velocity of flame, respectively. $G\Xi$ and $R(\Xi - 1)$ are sub-grid turbulent generation and removal rates, respectively where rate coefficients G and R are modelled as below. Current approach is based on flame-speed correlation of Gülder [52].

$$G = R\frac{\Xi_{eq} - 1}{\Xi_{eq}} \tag{3.51}$$

$$R = \frac{0.28}{\tau_\eta}\frac{\Xi^*_{eq}}{\Xi^*_{eq} - 1} \tag{3.52}$$

Where: $\Xi^*_{eq}$is equilibrium wrinkling at Kolmogrov turbulence length scale proposed by Gülder correlation as algebraic equation (2.23) mentioned in section 2.2.3. So, algebraic equations for flame wrinkling factor are as follows.

$$\Xi^*_{eq} = 1 + 0.62\sqrt{\frac{u'}{S_L}}\mathcal{R}_{e\eta} \tag{3.53}$$

Equilibrium wrinkling Ξ_{eq} obtained from algebraic equation:

$$\Xi_{eq} = 1 + 2(1 - b)(\Xi^*_{eq} - 1) \tag{3.54}$$

3.4 Numerical method and pre-processing case setup

In present work openFOAM CFD toolbox has been employed. This open-source package employs finite volume discretization technique in order to compute fluid dynamics. For simulation of premixed turbulent combustion in openFOAM, Weller $b - \Xi$ flame surface wrinkling combustion model is implemented by XiFoam solver. This solver covers compressible premixed and partially premixed turbulent combustion models and employs density weighted conservation equations and equation of state in addition to transport equation of density weighted regress variable, which is used for flame front propagation as described before. Here, burning velocity or turbulent flame speed has been modeled as product of sub-grid flame wrinkling factor and laminar flame speed. In XiFoam solver, Xi expressed as ratio of turbulence to laminar flame speed,

$$Xi = \frac{S_T}{S_L} \tag{3.55}$$

In following subchapters, case setup and corresponding adjustment for running XiFoam solver in openFOAM has been described.

3.4.1 Case geometry

In this project, simulation geometry consists of a simple 2D horizontal channel with rectangular section and dimensions of 1700 mm length, 100 mm height and 1 mm width with unobstructed configuration. Channel is closed in left end as wall and open in the right end as patch. Upper and lower sides are defined as wall. Since this geometry is a 2D case, front and back sides are empty. Creating the geometry dimension, cell size and defining type of inlet, outlet and walls has been implemented in BlockMeshDict file in system folder. Mesh size has been selected small enough to have precise computation with minor error and large enough to reduce the computational time. Computational domain consists of 42500 cells that uniformly distributed with mesh size of 2 mm.

3.4.2 Case setup and initial field in channel

Here, homogeneous cases are defined by having H_2-air mixture within the whole domain of geometry and this flammable cloud is distributed in total of channel. In contrast, in order to define inhomogeneous cases of H_2-air mixture, channel has been divided into two homogeneous layers. In half top of channel, there is homogeneous mixture of H_2-air and in half bottom of channel, there is air as inert gas. This condition makes inhomogeneous H_2-air mixture. So, reacting mixture is just in top half of channel. To reach this inhomogeneous conditions, setFields utility file in system folder has been applied. It requires a dictionary whose entry for this case is fuel mass fraction variable as ft.

By definition:

$$ft = \text{mass of fuel}/(\text{mass of fuel} + \text{mass of oxidizer}) \tag{3.56}$$

For defaultFieldValues, ft gets the calculated amount of fuel mass fraction corresponds to equivalence ratio of mixture. it means that the region takes this value unless specified region. So, in regions section, half bottom of channel is specified and here ft get zero value since there is only air.

setFields utility reads ft field from file and after re-calculation, will write back to another file. So, it is essential to define a file name as ft.orig in 0 folder that initially stored ft as backup. After calculation, there would be another generated ft file in 0 folder which write calculated field.

3.4.3 Time step and duration of simulation

In order to have precise calculation over the computational domain, it is required to define a suitable time step to evaluate the variable. In combustion simulation, Courant number Co is defined to consider flow velocity and cell size to calculate proper time step. This number is defined as

$$Co = u.\delta t/\delta x \tag{3.57}$$

Maximum Courant number for present work is considered as 0.2 and time step will be adjusted based on this amount. Also, duration of simulation is considered long enough have flame reach the end of channel. These setting are implemented in contolDict file in system folder.

3.4.4 Pressure probes

In order to trace value of pressure in certain points in channel, eight pressure probes have been defined around the geometry. Table 3.1 shows location of these probes. Probe function has been implemented at the end of controlDict file in system folder to write corresponding pressure of probes at each time step.

Table 3.1- location of pressure probes in channel

Probe No.	Location (x, y, z) mm
# 1	(0, 50, 0.5)
# 2	(500, 100, 0.5)
# 3	(1000, 100, 0.5)
# 4	(1500, 100, 0.5)
# 5	(1700, 50, 0.5)

3.4.5 Turbulence model

Proper turbulence model has been defined in turbulenceProperties file in constant folder. As discussed before, RANS turbulent model is selected for simulationType and corresponding sub model has been selected as LaunderSharmaKE which is based on Launder-Sharma [100] low Reynolds $\kappa - \varepsilon$ model.

3.4.6 Thermophysical model [101]

Thermophysical model is related to energy, heat, and physical properties. For this reason, thermophysicalProperties dictionary is used and is read by solver. This model is formed as a

pressure-temperature system from which other properties are computed. There is one compulsory dictionary that specify thermophysical modelling which called thermoType entry. It reflects multiple layers of modelling and underlaying framework where they combined.

In present work, thermophysicalProperties file in constant folder contains thermoType and is adjusted with following keywords.

- type: In this entry type gets the heheuPsiThermo keyword for present work. It is for XiFoam solver that construct psiuReactionThermo thermophysical model for combustion based on compressibility of unburnt gas.
- mixture: Since the desired mixture for this work is inhomogeneous, so mixture gets inhomogeneous keyword. Combustion is based on regress variable b and fuel mass fraction ft.
- transport: the transport modelling considers evaluating of dynamic viscosity μ, thermal conductivity K and thermal diffusivity α (for internal energy and enthalpy equations). In present work, transport gets sutherland keyword and calculates μ as a function of temperature T from Sutherland coefficients A_s and Sutherland temperature T_s according to following equation [102].

$$\mu = \frac{A_s\sqrt{T}}{1+T_s/T} \tag{3.58}$$

- thermo: thermodynamics model concerns evaluating c_p from which other properties are derived. In this work, thermo gets janaf keywords. It calculates c_p as a function of temperature T from a set of coefficients from JANAF table of thermochemical [103]. It is valid between lower temperature T_l and upper T_h temperature limit. There are two sets of coefficients for each specie. First set is for temperature above common temperature T_c (and below T_h) and second set is for temperature below common temperature T_c (and above T_l). Calculated thermodynamic properties were polynomialized and represented in polynomial form and known as NASA polynomial format [104]. This format is suitable for use in computer programs. Molar standard thermochemical functions for specific heat capacity, enthalpy and entropy can be obtained from polynomial coefficients $(a_1, a_2, a_3, \dots)$ as follows.

$$\frac{C_p^0}{R} = a_1 + a_2T + a_3T^2 + a_4T^3 + a_5T^4 \tag{3.59}$$

$$\frac{H_T^0}{RT} = a_1 + \frac{a_2}{2}T + \frac{a_3}{3}T^2 + \frac{a_4}{4}T^3 + \frac{a_5}{5}T^4 + \frac{a_6}{T} \tag{3.60}$$

$$\frac{S_T^0}{R} = a_1 \ln T + a_2T + \frac{a_3}{2}T^2 + \frac{a_4}{3}T^3 + \frac{a_5}{4}T^4 + a_7 \tag{3.61}$$

- equationOfState: for present work is chosen perfectGas keyword.

$$\rho = \frac{p}{RT} \tag{3.62}$$

- specie: This model specifies composition of each constituent and since there is only one option for this, it gets specie keyword named as itself.
- energy: form of energy in solution and inclusion of heat of formation is specified. In this work, energy gets absoluteEnthalpy keyword to consider heat of formation.

$$h = h_s + \sum_i c_i \Delta h_f^i \tag{3.63}$$

Here: h_s is sensible enthalpy, c_i is molar fraction and h_f^i is heat of formation of species i.

- stoichiometricAirFuelMassRatio: since for present work, hydrogen is considered for reacting in air, it gets value of 34.0751.

Since in this simulation, inhomogeneous has been defined in mixture keyword, thermophysical properties data, should be specified for three species as fuel, oxidant and burntProducts at the end of thermophysicalProperties file. For all of these three species molWeight as species sub-dictionary, NASA polynomial coefficients as thermodynamics sub-dictionary and Sutherland coefficients as transport sub-dictionary should be specified and implemented in this file.

3.4.7 Combustion properties [105]

In combustionProperties file in constant folder following keywords are determined for each entry,

- laminarFlameSpeedCorrelation: it specified by Gulders keyword. So laminar flame speed is calculated based on Gülder correlation expressed in equation (2.23).
- fuel: HydrogenInAir keyword has been defined.
- Su: represents laminar flame speed, if correlation of laminar flame speed was selected by constant keyword, then value of Su should be mentioned here.
- SuModel: there are three keywords as unstrained, equilibrium and transport and in this work, it gets unstrained keyword.
- equivalenceRatio: it gets the corresponded amounts for simulation as 0.8,1 and 1.2 values.
- sigmaExt: is strain rate at extinction that calculated from Markstein length by extrapolating to Su→0. Markstein length measures effect of curvature on flame and for larger Markstein length, there is greater effect of curvature on burning velocity. Makstein number is Markstein length divided by flame thickness.
- XiModel: there are three different keywords as fixed, algebraic and transport to calculate Xi. Fixed model considers Xi constant. Algebraic model calculates Xi based on algebraic equations (3.53) and (3.54) expressed in section 3.3.1. Transport model solves transport equation for Xi. For present work transport keyword is selected for Xi model.
- XiCoef and XiShapeCoef: If algebraic model for Xi calculation is selected, values for these keywords should be imported.
- uPrimeCoef: is used for calculation of velocity fluctuation according to below.

$$u' = \text{uprimeCoef} * (\frac{2\kappa}{3})^2 \tag{3.64}$$

- GuldersCoeffs: By selecting Gülder correlation for laminar flame speed calculation, corresponding coefficients of hydrogen as fuel for this correlation as defined in equation (2.6) should be determined.

After implementing Gulders coefficients, specification of ignition source such as location, dimeter, start and duration and strength can be defined at the end of combustionProperties file. In this work, location of ignition is defined at near top of end left wall.

3.4.8 Initial and boundary conditions

Initial and boundary conditions for variables are defined in 0 folder. Table 3.2 shows corresponding initial and boundary conditions for different variables. In this table (*) get proper amount of ft variable according to selected equivalence ratio.

Table 3.2 – Initial and boundary conditions of variables for all surfaces of geometry

Variable	wall (Left, Top and Bottom)	patch (Right)	frontAndBack
alphat	type compressible::alphatWallFunction; prt 0.85; value uniform 0;	type calculated; value uniform 0;	empty
b	type zeroGradient;	type inletOutlet; inletValue uniform 1; value uniform 1;	empty
epsilon	type epsilonWallFunction; value uniform 0.001;	type zeroGradient;	empty
ft	type zeroGradient;	type inletOutlet; inletValue 0; value uniform (*);	empty
fu	type zeroGradient;	type inletOutlet; inletValue 0; value uniform 0;	empty
k	type kLowReWallFunction; value uniform 0.001;	type zerpGradient;	empty
nut	type nutkWallFunction; value uniform 0;	type calculated; value uniform 0;	empty
p	type zeroGradient;	type totalPressure; p0 uniform 101325; value uniform 101325;	empty
Su	type zeroGradient;	type zeroGradient;	empty
T	type zeroGradient;	type totalTemperature; gamma 1.41; T0 uniform 298;	empty
Tu	type zeroGradient;	type totalTemperature; gamma 1.41; T0 uniform 298;	empty
U	type noSlip;	type pressureInletOutletVelocity; value uniform (0 0 0);	empty
Xi	type zeroGradient;	type inletOutlet; inletValue uniform 1; value uniform 1;	empty

4 Post processing results

In present work, simulation has been performed for two cases of homogeneous and inhomogeneous H_2-air mixture as described in section 3.4.2 with further consideration of various H_2 concentration by having different equivalence ratio ϕ equals to 0.8, 1 and 1.2. By running XiFoam solver in openFOAM, numerical simulation is executed, and results can be obtained. The simulation results mainly focus on effect of homogeneity and inhomogeneity of H_2-air explosion, with further effects of mixture properties on flame propagation and acceleration, front position, velocity, and pressure. Initial conditions of simulations considered by atmospheric pressure and temperature as mentioned in section 3.4.8 and ignition starts from beginning of simulations and has duration of 3 milliseconds. In following sections in this chapter, six simulation cases as mentioned above are presented with illustration of flame propagation sequences and other related results in corresponded figures.

4.1 Case 1: Homogeneous H_2-air mixture with fuel-lean condition ($\phi = 0.8$)

In simulation case 1, homogeneous flammable H_2-air cloud with lean condition of hydrogen is distributed within the whole domain of channel. This case considers low concentration of H_2 in homogeneous mixture. After ignition, flame starts to propagate from ignition point through the whole of channel. Figure 4.1 shows some flame propagation sequences during this simulation.

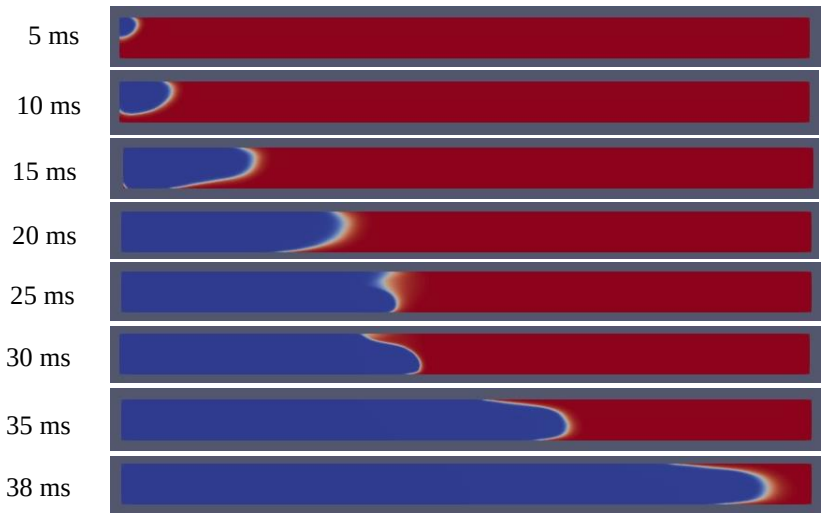

Figure 4.1. Flame propagation sequences in homogeneous H_2-air mixture-equivalence ratio 0.8

Flame front position in this case can be seen in figure 4.2 It shows flame propagation toward the end of channel. From this figure it can be observed that flame propagates almost constantly in the channel until 0.014 seconds after simulation, and after that it propagates slowly until it reaches 700 mm of channel from ignition point origin. For 0.02-0.027 seconds flame does not go further in channel. But afterward, flame front starts to propagate faster and significantly accelerates toward the end of channel with much higher speed.

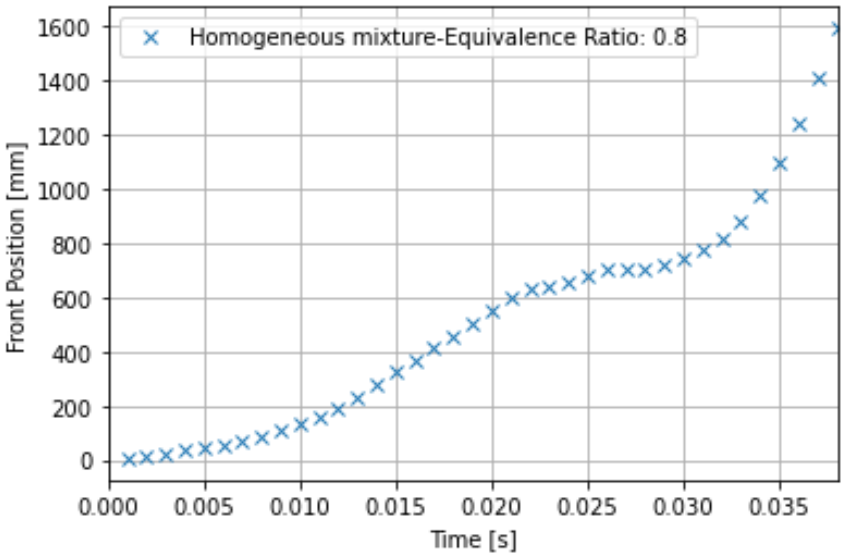

Figure 4.2. Flame front position in homogeneous H_2-air mixture-equivalence ratio 0.8

Also from front position, velocity of flame front can be obtained and presents in figure 4.3. In this figure, it can be observed that flame front velocity grows up constantly to 50 m/s in 0.014 seconds of simulation and after reaching this velocity, since flame does not go further in channel, velocity reduces to nearly zero after 0.027 seconds. It shows that flame front has low propagation progress as presented in figure 4.2. After this time, flame front speed rises drastically to almost 175 m/s toward the end of channel that shows flame acceleration in this condition.

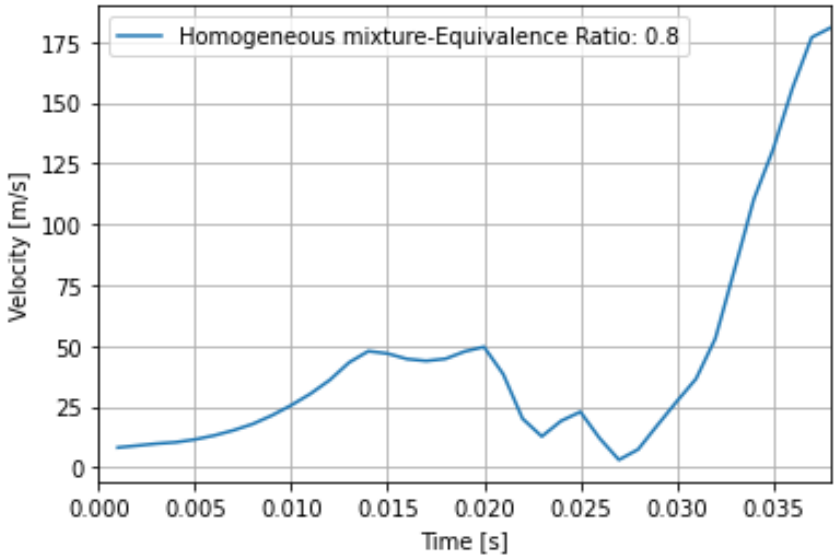

Figure 4.3. Flame front velocity in homogeneous H_2-air mixture-equivalence ratio 0.8

Figure 4.4 shows pressure behavior at different probes which are located according to table 3.1. Pressure near the ignition point (probe1) has highest values and by going far from ignition location, it goes down as seen in subsequent probes in this figure. It also shows that wave of explosion due to ignition, raises pressure up to 110 kpa after 0.014 seconds from beginning and then by reduction of pressure wave it hinders flame propagation as observed in figure 4.2 and

4.3. finally, pressure increases significantly to 130 kpa near ignition point that results the flame acceleration. By reaching flame to end of channel pressure reduces afterwards.

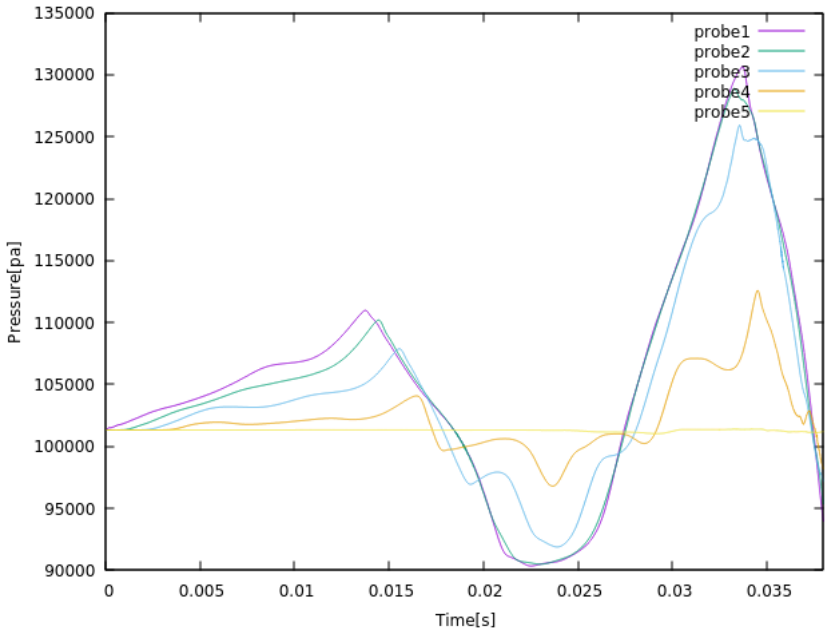

Figure 4.4. Pressure changes in probes of homogeneous H_2-air mixture-equivalence ratio 0.8

4.2 Case 2: Homogeneous H_2-air mixture with stoichiometric condition ($\phi = 1$)

In this simulation case, homogeneous H_2-air cloud is considered by having stoichiometric condition. Flame propagation sequences during this simulation case is shown in figure 4.5.

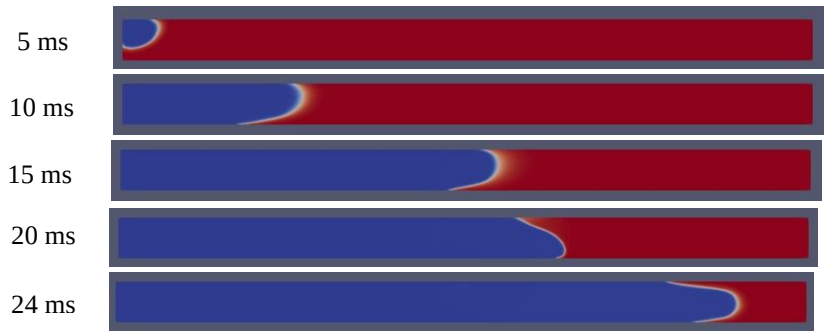

Figure 4.5. Flame propagation sequences in homogeneous H_2-air mixture-equivalence ratio 1

Figure 4.6 shows flame front position and exhibits propagation of flame until 0.014 seconds. After that, it reduces and remains constant until 0.02 seconds. In this time flame reaches 1100 mm of channel from ignition point. Afterward, flame starts to accelerate and exits the channel with higher rate of propagation.

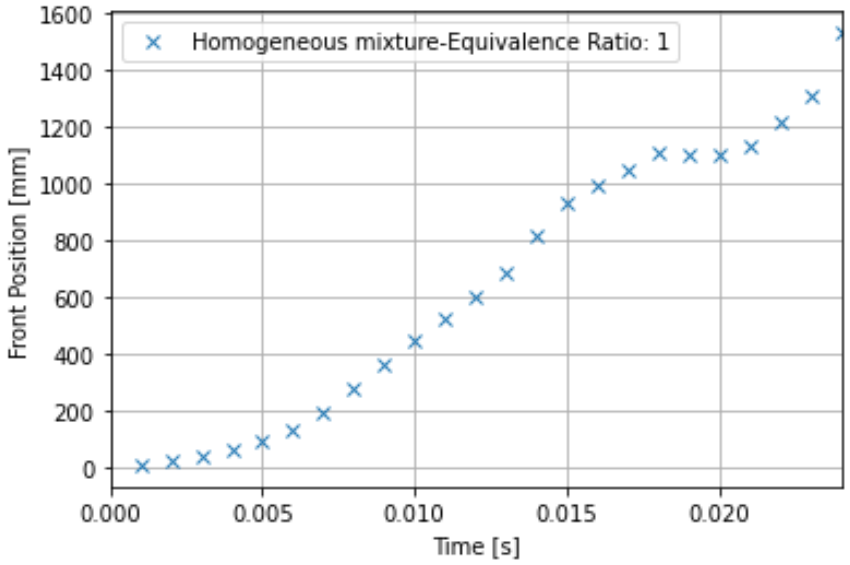

Figure 4.6. Flame front position in homogeneous H_2-air mixture-equivalence ratio 1

From figure 4.7, velocity of flame front can be observed. It shows that flame reaches to speed of 120 m/s after 0.014 seconds and due to low rate of propagation, it goes down until about 0.02 seconds. Afterward, velocity rises to 225 m/s and flame accelerates when it reaches almost end of the channel.

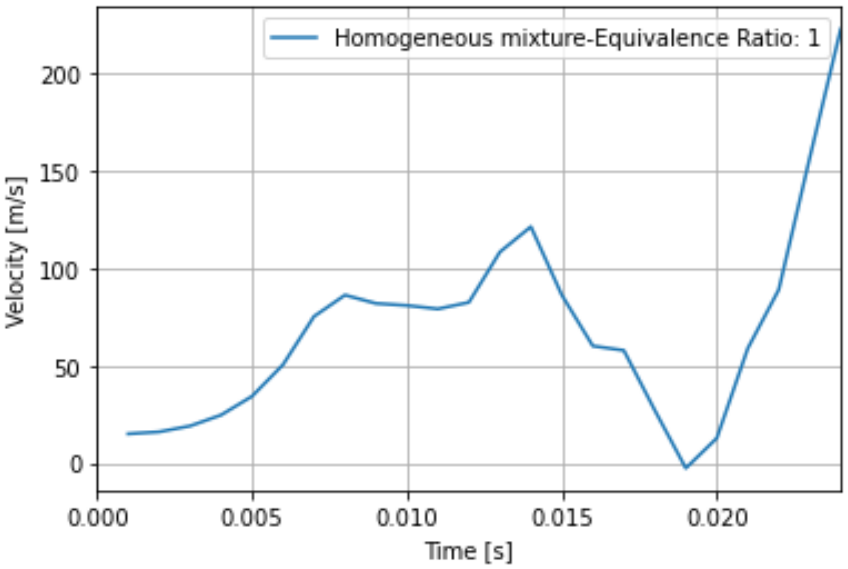

Figure 4.7. Flame front velocity in homogeneous H_2-air mixture-equivalence ratio 1

In figure 4.8, pressure in probes can be seen. Same as previous case, probe 1 near ignition point records highest pressure during simulation. It shows due to explosion wave, pressure increases to almost 130 kpa and then, it reduces until 0.02 seconds. This pressure wave prevents propagation of flame and afterward by having forward explosion wave, pressure grows to 175 kpa and helps flame to accelerates.

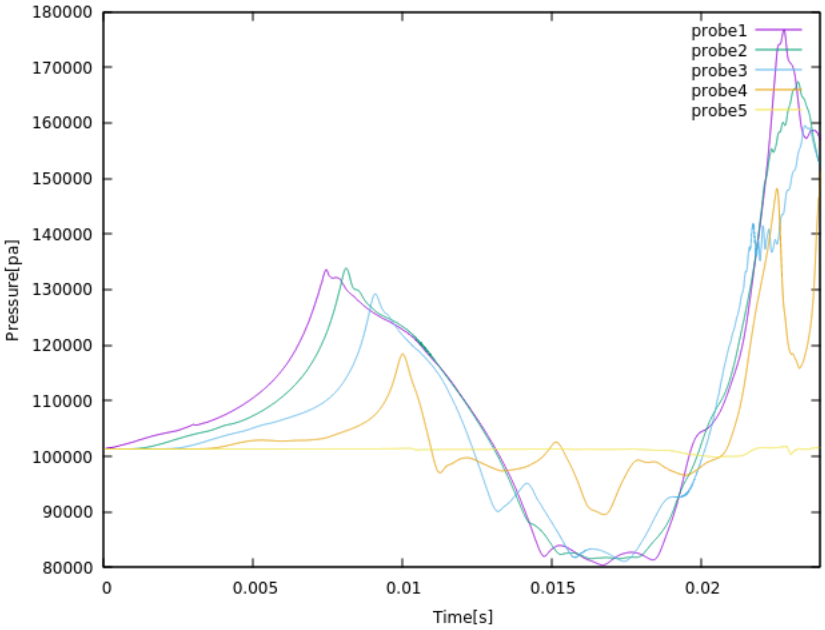

Figure 4.8. Pressure changes in probes of homogeneous H_2-air mixture-equivalence ratio 1

4.3 Case 3: Homogeneous H_2-air mixture with fuel-rich condition ($\phi = 1.2$)

In this case homogeneous H_2-air mixture with rich condition of hydrogen is considered by implementing equivalence ratio $\phi = 1.2$. This case considers high H_2 concentration in mixture and figure 4.9 shows flame propagation sequences during simulation.

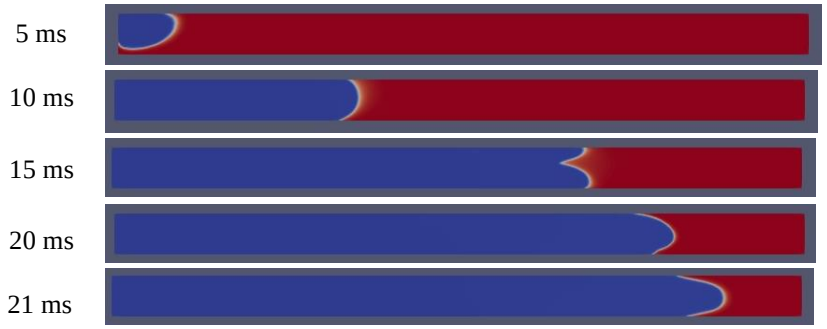

Figure 4.9. Flame propagation sequences in homogeneous H_2-air mixture-equivalence ratio 1.2

Figure 4.10 presents flame front position in this simulation case. It shows flame propagates by 0.016 seconds after start of ignition. In this time, flame reaches 1300 mm of channel from ignition point and it remains constant until 0.018 seconds. Afterward, flame propagates and exits the channel.

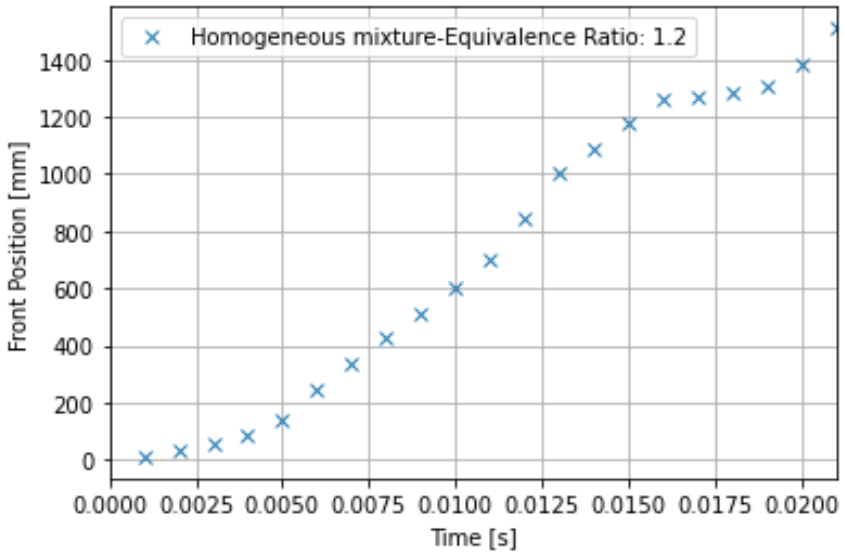

Figure 4.10. Flame front position in homogeneous H_2-air mixture-equivalence ratio 1.2

In figure 4.11 flame front velocity can be seen. It shows that flame reaches the maximum speed of 150 m/s after 0.012 seconds from start of ignition, then it reduces continuously. Again, after 0.0175 seconds flame starts to propagate constantly and exits the channel, but it cannot reach the maximum velocity at the end since channel is short for this case.

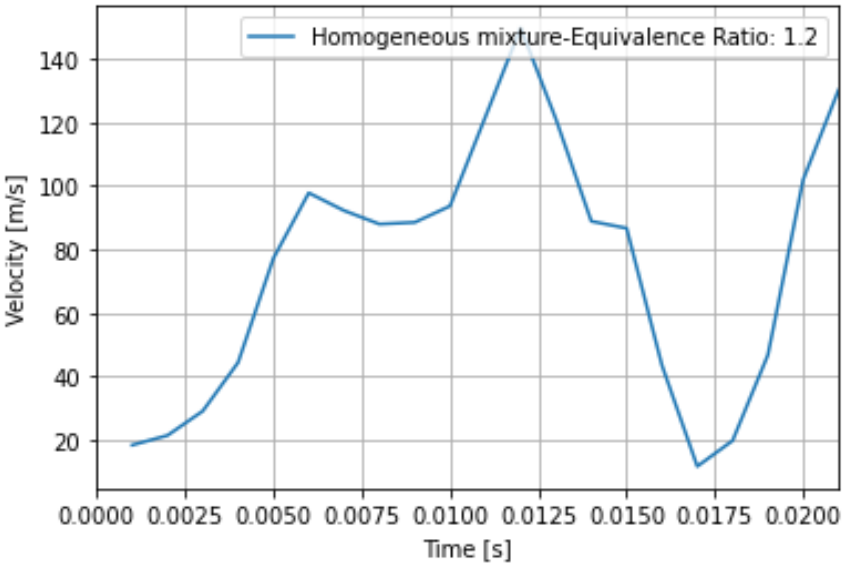

Figure 4.11. Flame front velocity in homogeneous H_2-air mixture-equivalence ratio 1.2

Figure 4.12 presents pressure changes during simulation. It shows that explosion wave raises pressure in probes up to 140 kpa and by going further of wave through the channel, pressure reduces by 0.0175 seconds. Due to explosion wave in channel after this time, pressure increases again and reaches 145 kpa.

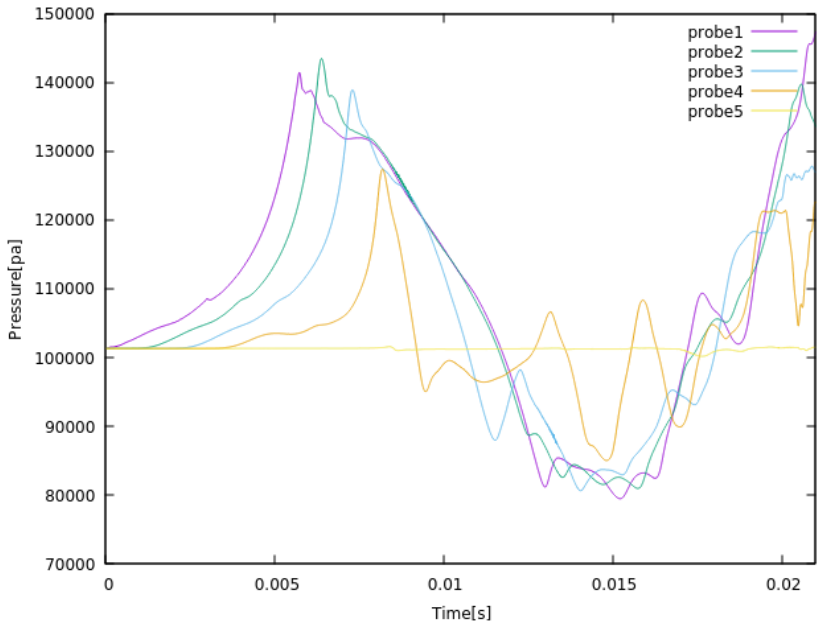

Figure 4.12. Pressure changes in probes of homogeneous H_2-air mixture-equivalence ratio 1.2

4.4 Case 4: Inhomogeneous H_2-air mixture with fuel-lean condition ($\phi = 0.8$)

In case 4, inhomogeneous flammable H_2-air cloud with lean condition of hydrogen is considered. Here as described in section 3.4.2 in purpose of having inhomogeneous condition, two homogeneous layers in channel are defined as homogeneous mixture of H_2-air distributed in half top of channel and air distributed in half bottom of it. This case considers low H_2 concentration in inhomogeneous mixture. After ignition, flame starts from ignition point and propagates through the channel. Figure 4.13 shows flame propagation sequences during simulation of this case.

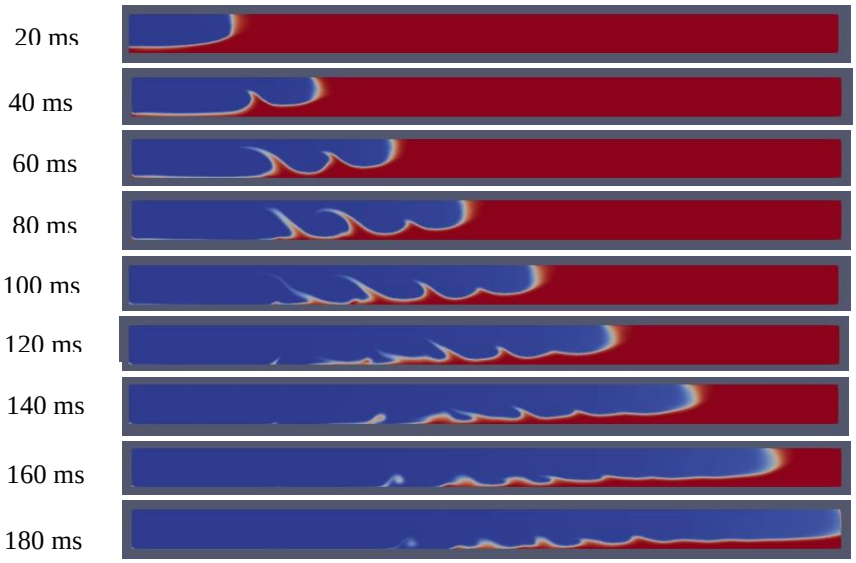

Figure 4.13. Flame propagation sequences in inhomogeneous H_2-air mixture-equivalence ratio 0.8

Figure 4.14 shows flame front position in this simulation and reveals flame propagation with a nearly constant rate through the channel.

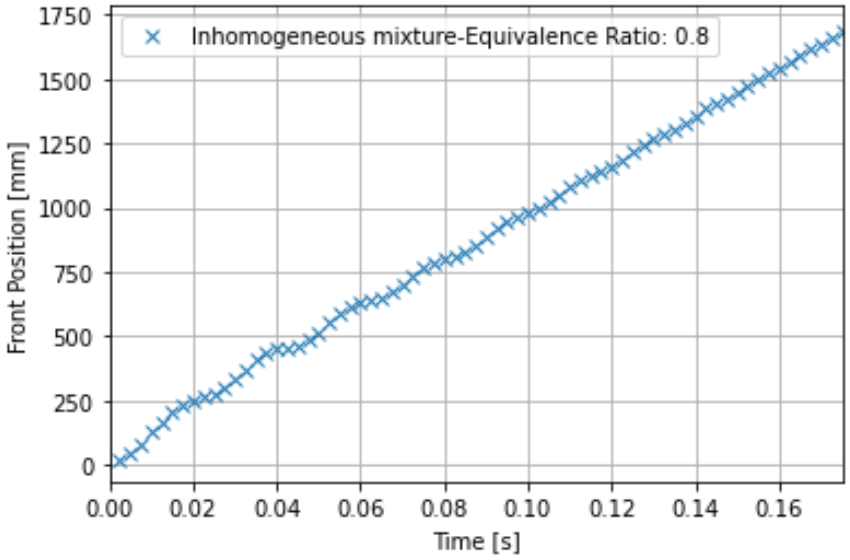

Figure 4.14. Flame front position in inhomogeneous H_2-air mixture-equivalence ratio 0.8

In figure 4.15 it can be seen that velocity of flame front has fluctuation during simulation and by increasing simulation time, rate of fluctuation reduced. However, flame front never reaches zero velocity within the channel. Maximum velocity in this condition is around 17 m/s after 0.01 seconds from start of ignition.

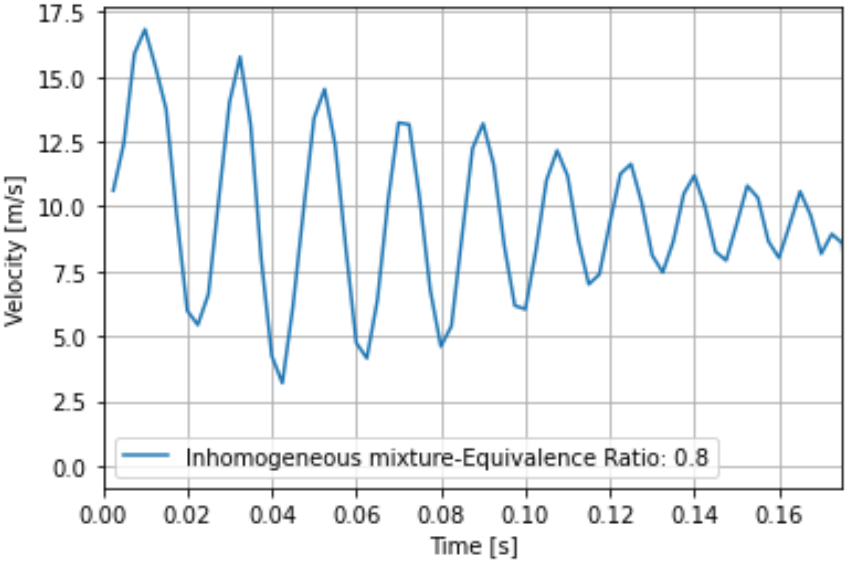

Figure 4.15. Flame front velocity in inhomogeneous H_2-air mixture-equivalence ratio 0.8

Figure 4.16 shows pressure oscillation during simulation period and it shows that along the simulation, explosion wave helps the flame to propagates and accelerate faster. By passing the time, pressure changes reduced oscillatory according to velocity fluctuation as observed in figure 4.15. Maximum pressure can be seen about 106 kpa at probe 1 near the ignition point.

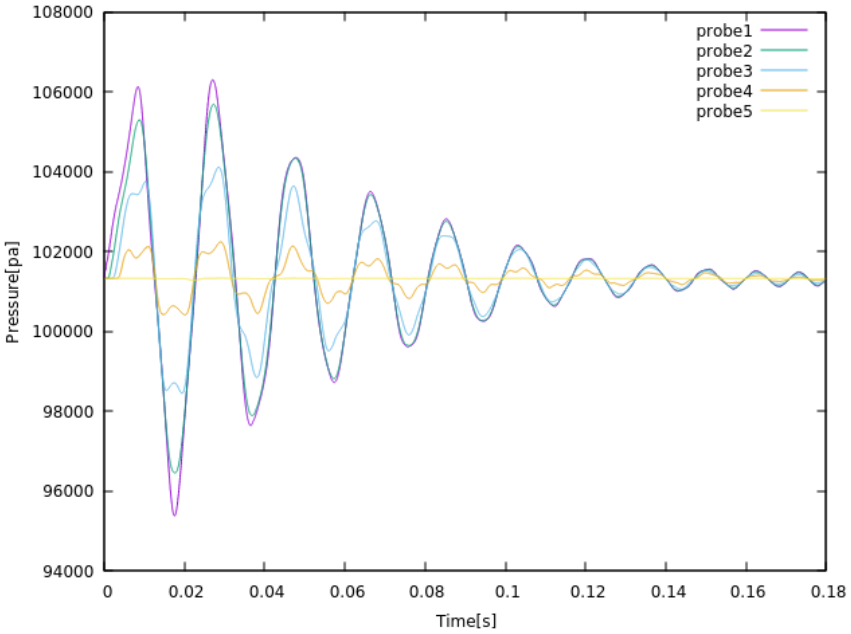

Figure 4.16. Pressure changes in probes of inhomogeneous H_2-air mixture-equivalence ratio 0.8

4.5 Case 5: inhomogeneous H_2-air mixture with stoichiometric condition ($\phi = 1$)

In case 5, inhomogeneous H_2-air cloud is considered as previous case but with this difference that stoichiometric condition governs here by having equivalence ratio $\phi = 1$. Flame propagation sequences during this simulation case is shown in figure 4.17.

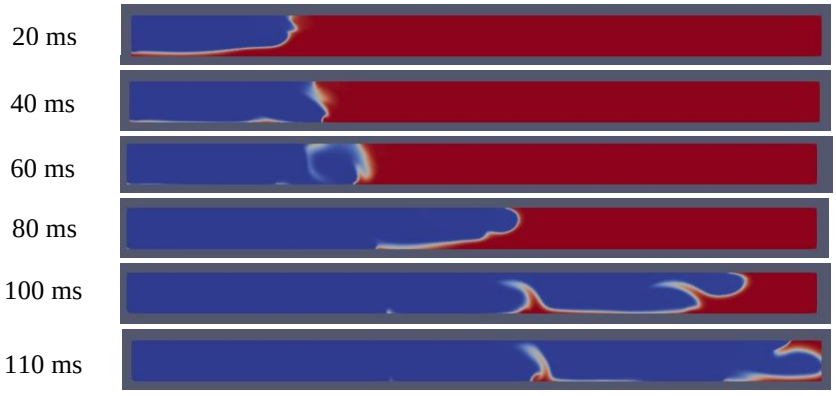

Figure 4.17. Flame propagation sequences in inhomogeneous H_2-air mixture-equivalence ratio 1

Figure 4.18 shows flame front position in stoichiometric condition of inhomogeneous mixture. Obviously, flame propagates periodically through the channel and in some steps, it has low progress in propagation. By reaching end of the channel, flame front propagates faster.

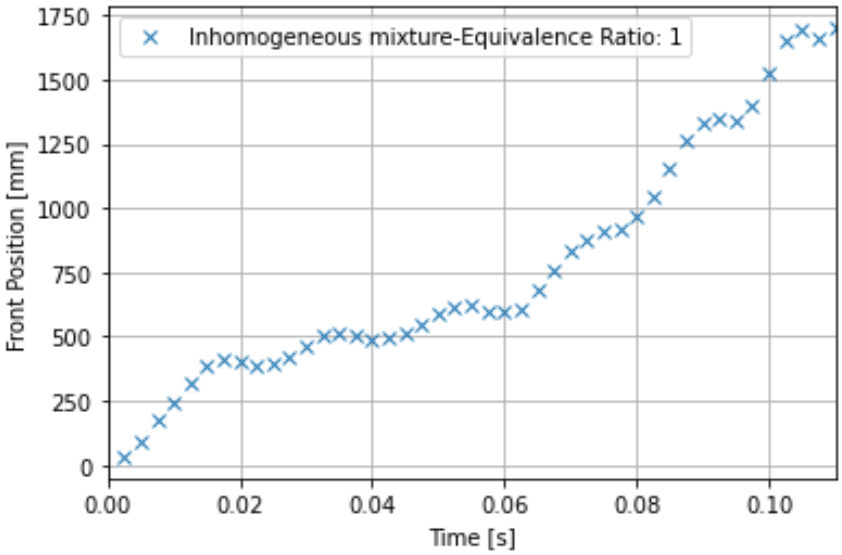

Figure 4.18. Flame front position in inhomogeneous H_2-air mixture-equivalence ratio 1

Figure 4.19 presents velocity of flame front according to flame front position within the channel. It shows that after some reduction in velocity fluctuation and low propagation, it increases and reaches the maximum value of 50 m/s after 0.1 seconds.

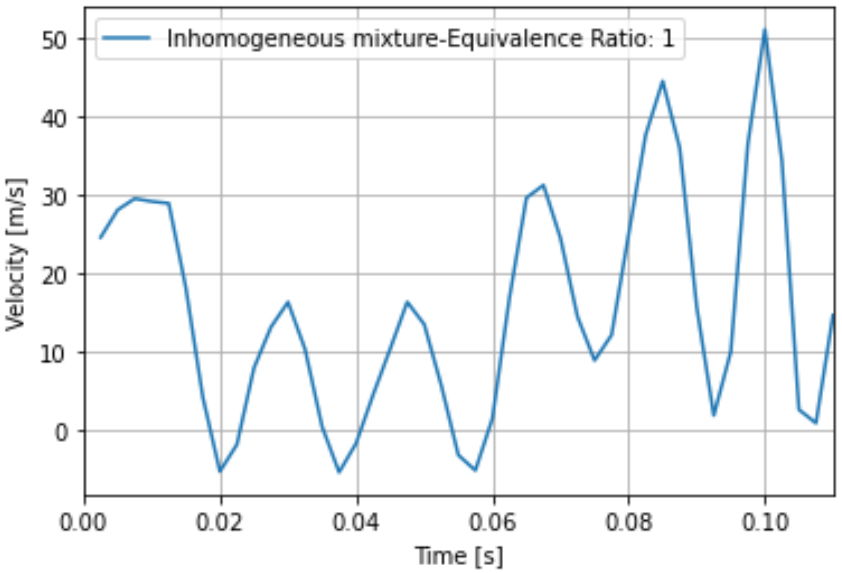

Figure 4.19. Flame front velocity in inhomogeneous H_2-air mixture-equivalence ratio 1

Figure 4.20 presents pressure oscillation due to explosion wave during the simulation. It shows reduction of pressure by reaching the flame to end of channel. Maximum amount of pressure is around 110 kpa at probe 1.

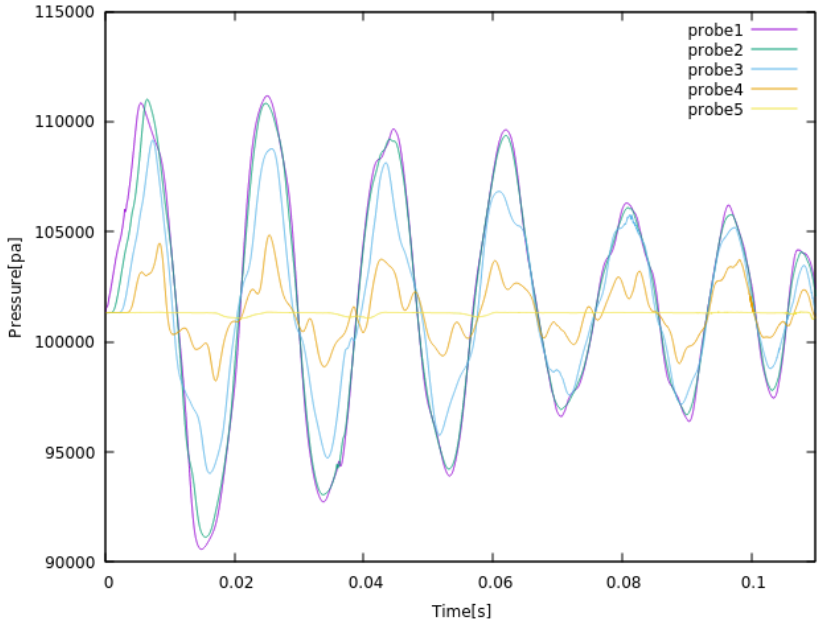

Figure 4.20. Pressure changes in probes of inhomogeneous H_2-air mixture-equivalence ratio 1

4.6 Case 6: inhomogeneous H_2-air mixture with fuel-rich condition ($\phi = 1.2$)

Here in last case, there is inhomogeneous H_2-air mixture with rich condition of hydrogen by considering equivalence ratio $\phi = 1.2$. figure 4.21 shows flame propagation sequences during simulation.

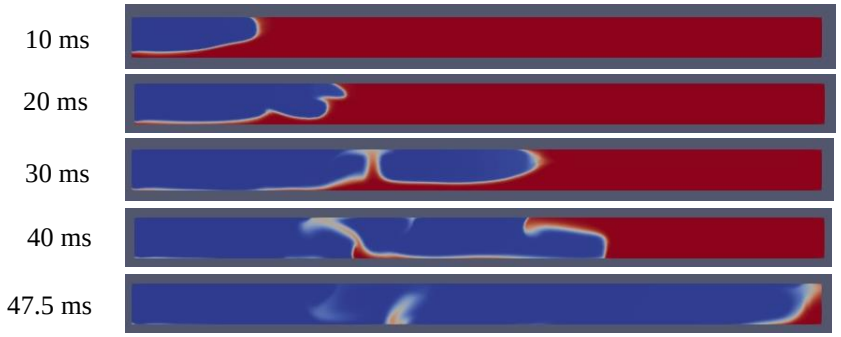

Figure 4.21. Flame propagation sequences in inhomogeneous H_2-air mixture-equivalence ratio 1.2

Figure 4.22 exhibits flame front position. It shows flame propagation through the channel and by reaching end of it, flame propagates faster.

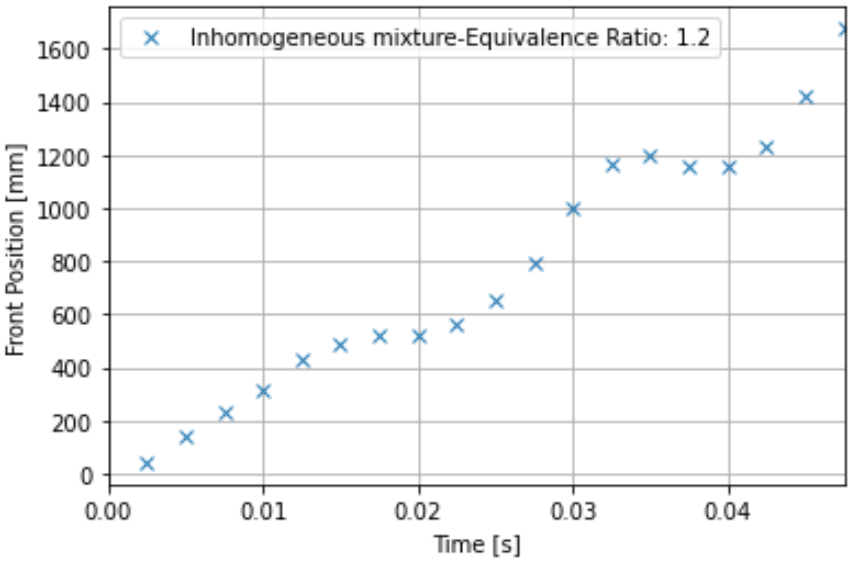

Figure 4.22. Flame front position in inhomogeneous H_2-air mixture-equivalence ratio 1.2

In figure 4.23 velocity of flame front can be observed. It shows that velocity fluctuates during simulation and by reaching end of the channel, it increases to maximum amount of 100 m/s after 0.0475 seconds.

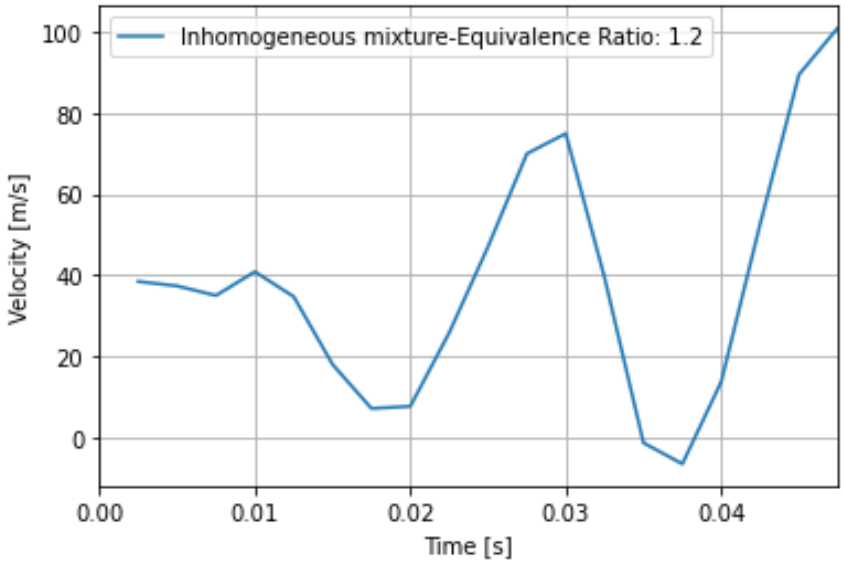

Figure 4.23. Flame front velocity in inhomogeneous H_2-air mixture-equivalence ratio 1.2

Figure 4.24 shows pressure oscillation due to explosion wave in simulation and by reaching end of the channel, pressure changes increase, and it has maximum value of 117 kpa at probe1.

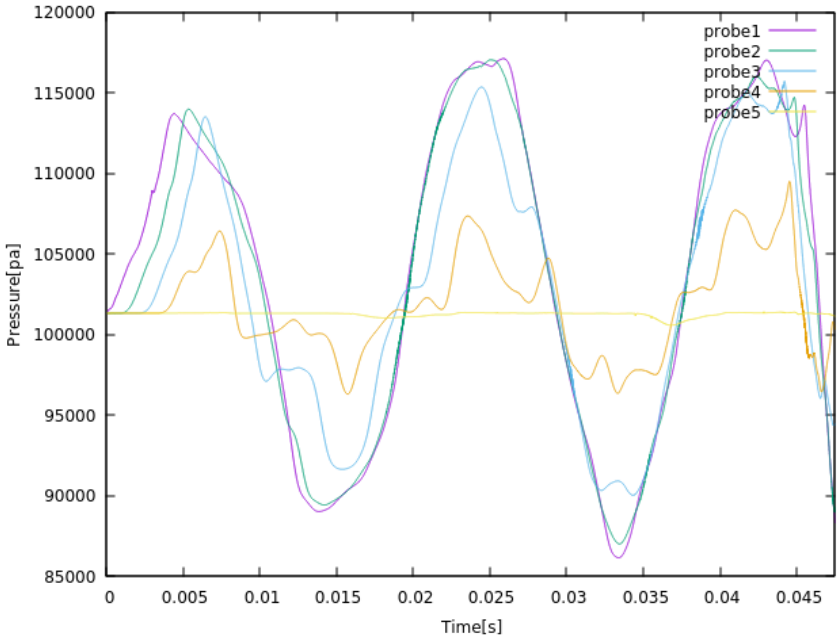

Figure 4.24. Pressure changes in probes of inhomogeneous H_2-air mixture-equivalence ratio 1.2

5 Discussion

In this chapter, results of six simulation cases as introduced in chapter 4 are discussed. First homogeneous mixtures presented in section 4.1 to 4.3 are compared with each other by investigation H_2 concentration effect. Then inhomogeneous mixtures as described in sections 4.4 to 4.6 are compared with each other by evaluation effects of H_2 concentration. Finally, homogeneity and inhomogeneity of H_2-air mixtures are compared in same H_2 concentration of lean, stoichiometry and rich conditions.

5.1 Homogeneous H_2-air mixture

For homogeneous cases as introduced in sections 4.1-4.3, flame elongates continuously through the whole domain of geometry. Here, flame elongation and enlargement of flame surface area causes increase in reaction rate and consequently results to higher flame acceleration. In beginning of explosion in these cases, flame propagates faster at top of channel rather than in bottom and it is inclined near the lower wall. But after a while as flame goes further in the channel, it quenches and its propagation and velocity decrease. Here a notch appears in the flame tip and results faster propagation in bottom of channel than in top. This behavior is similar for all homogeneous cases. Afterwards, flame propagates uniformly which is obvious specifically in rich condition. Finally, by reaching end of the channel, flame accelerates again, and pressure increases rapidly. Shape of flame front is almost symmetric at end. This observation of flame front shape is in good agreement with that in experiments as discussed in section 2.2.5.

By comparison among homogeneous cases as shown in figure 5.1, it is obvious that flame front propagates faster and reach the end of channel sooner by increasing H_2 concentration. Also, velocity as observed in figure 5.2 is higher in the channel by having fuel-rich condition. Furthermore, pressure probes record higher pressure by this increase as presented in figure 5.3.

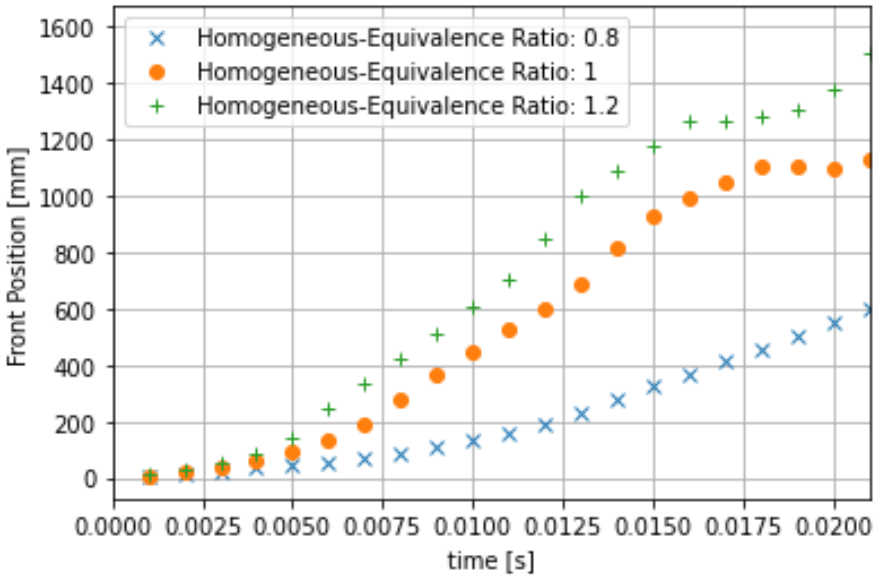

Figure 5.1. Flame front position in homogeneous H_2-air mixture with different equivalence ratio

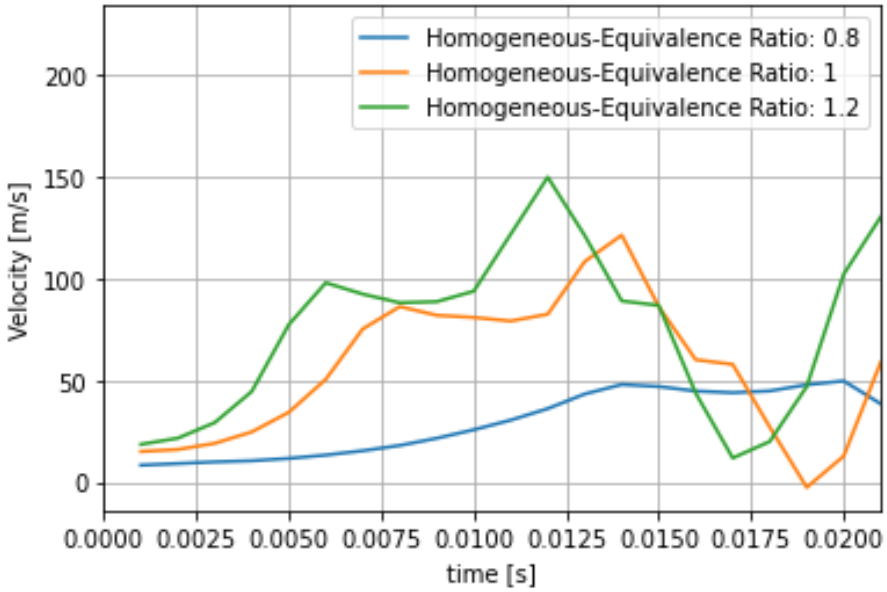

Figure 5.2. Flame front velocity in homogeneous H_2-air mixture with different equivalence ratio

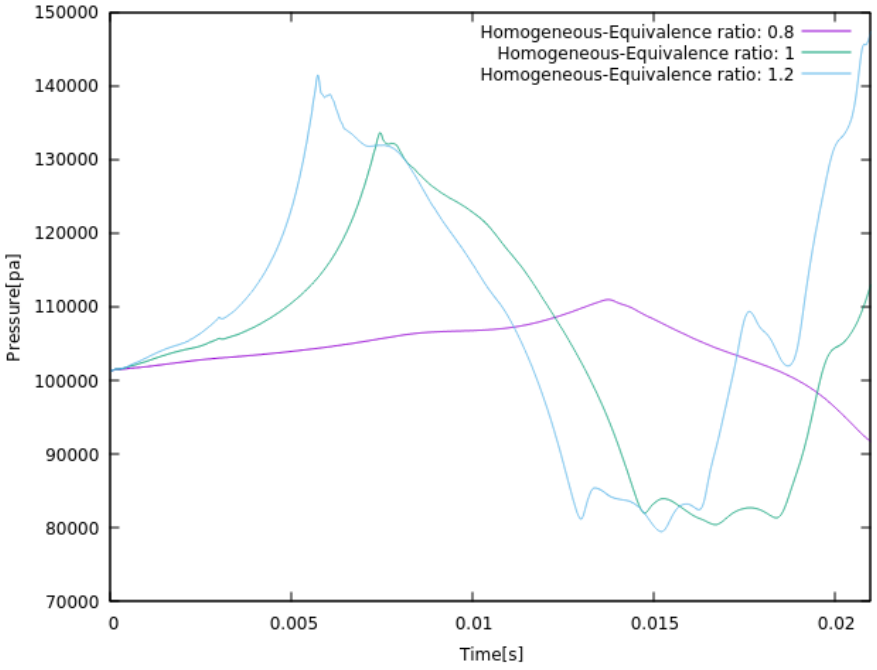

Figure 5.3. Pressure of probe1 in homogeneous H_2-air mixture with different equivalence ratio

5.2 Inhomogeneous H_2-air mixture

For inhomogeneous cases as introduced in sections 4.4-4.6, flame start to propagate from upper layer of flammable H_2-air mixture and goes further into lower inert layer of air. In these cases, flame propagates faster at top of channel rather than bottom and it is inclined near the lower wall. This observation could be as results of higher H_2 concentration around upper wall and

due to stratification of hydrogen in channel. Flame tip has a finger shape in this condition. This flame front observation is also in good agreement with that observed in experiments as discussed in section 2.2.5. As flame goes further in the channel, flame front propagates irregularly and oscillates that prevents flame elongation. It is highly obvious in lean mixture. This oscillation presented in pressure and fluctuation in flame velocity. This behavior of velocity is as results of explosion wave during simulation that goes back and forth. Finally, by reaching end of the channel, flame accelerates and exit the geometry. In lean mixture, as observed in experiments described in section 2.2.5 flame cannot propagates downward in the channel since concentration of H_2 is low. While by increasing H_2 concentration and having rich condition, flame propagates downward and governs in whole domain.

By comparison among inhomogeneous cases as shown in figure 5.4, it is obvious that flame front propagates faster and reach end of the channel sooner by increasing H_2 concentration. Maximum local flame speed occurs at top of channel and flame propagates there faster in these cases. So, by increasing H_2 concentration, flame elongation enhanced and mixture ahead of flame accelerates more. Velocity fluctuation and its value goes higher by this increase within the channel as observed in figure 5.5. Furthermore, in similar behavior of velocity, pressure probes record bigger oscillation and higher values as seen in figure 5.6.

Pressure oscillations and behavior for inhomogeneous cases are in good accordance with structural response analysis performed for inhomogeneous H_2-air mixture experiments[106].

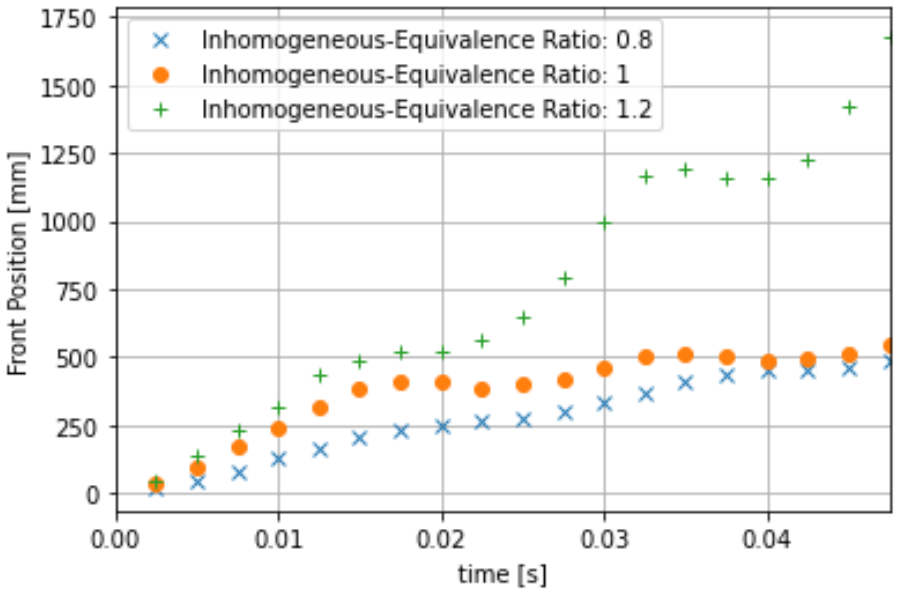

Figure 5.4. Flame front position in inhomogeneous H_2-air mixture with different equivalence ratio

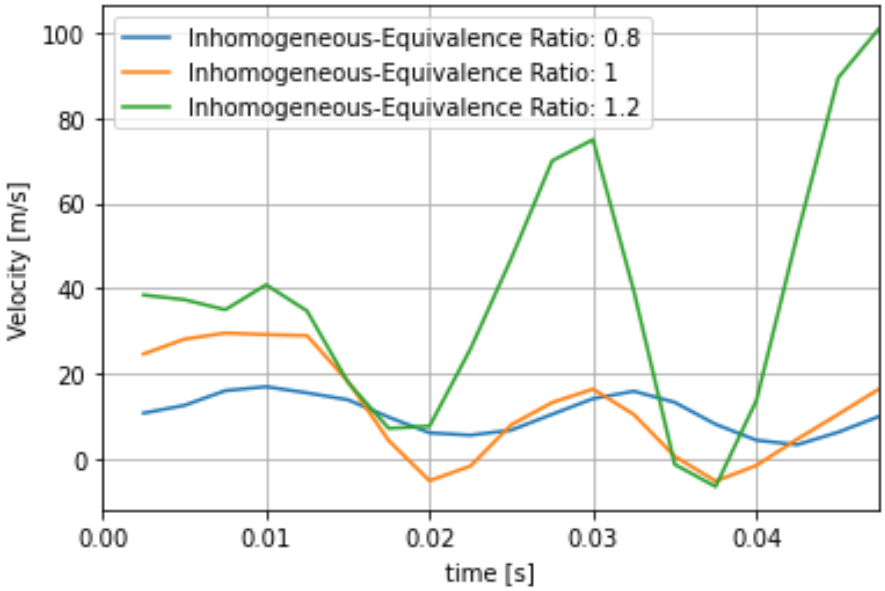

Figure 5.5. Flame front velocity in inhomogeneous H_2-air mixture with different equivalence ratio

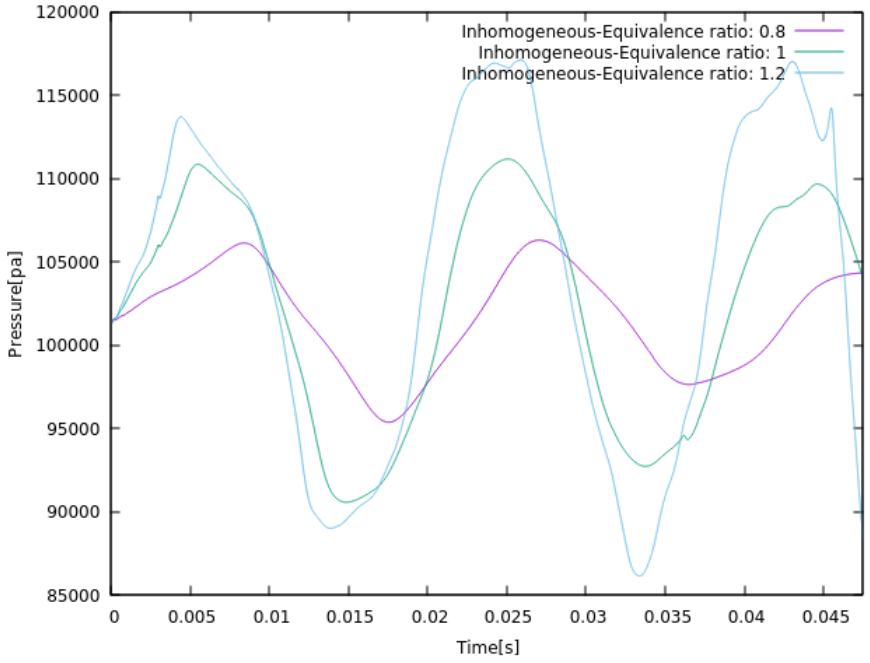

Figure 5.6. Pressure of probe1 in inhomogeneous H_2-air mixture with different equivalence ratio

5.3 Homogeneity and inhomogeneity of H_2-air mixture

In this section, effect of homogeneity and inhomogeneity of H_2-air mixture is investigated by having similar H_2 concentration.

In fuel-lean condition ($\phi = 0.8$), as observed in figures 5.7-5.9 homogeneous H_2-air mixture shows faster acceleration with higher velocity and pressure. This behavior is due higher flame

elongation in homogeneous than inhomogeneous one which is prevented by oscillation. In figure 5.7 it can be observed that after 38 milliseconds flame reaches nearly end of channel in homogeneous case while in inhomogeneous condition after this time, it just reached less than 1/3 of geometry. Further observation in figure 5.8 shows higher velocity of 175 m/s for homogeneous case while for inhomogeneous condition, it has maximum value of 17 m/s with fluctuation. Finally in figure 5.9 by comparison near ignition point in probe1, it shows higher pressure in homogenous case with maximum amount of 130 kpa while in inhomogeneous condition it reaches to maximum 106 kpa and reduces oscillatory during simulation.

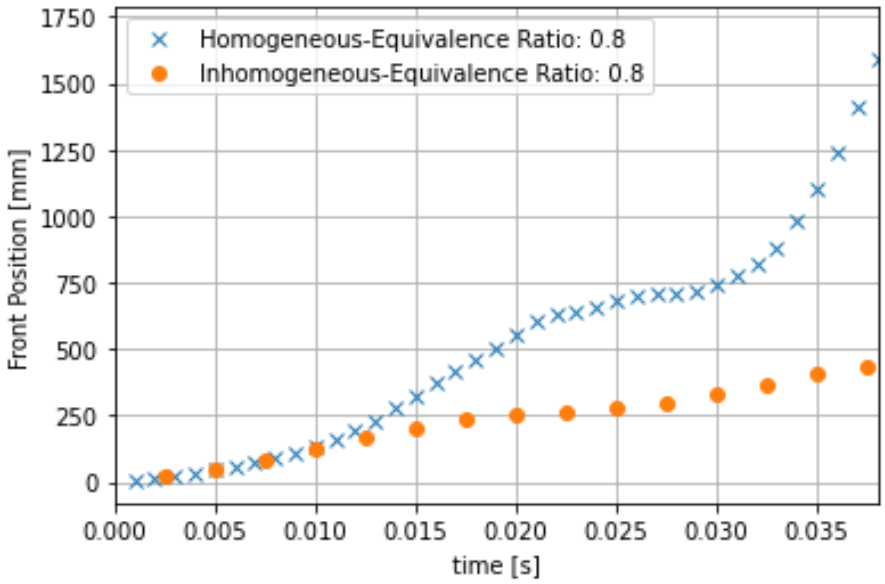

Figure 5.7. Flame front position in homogeneous and inhomogeneous H_2-air mixture-equivalence ratio 0.8

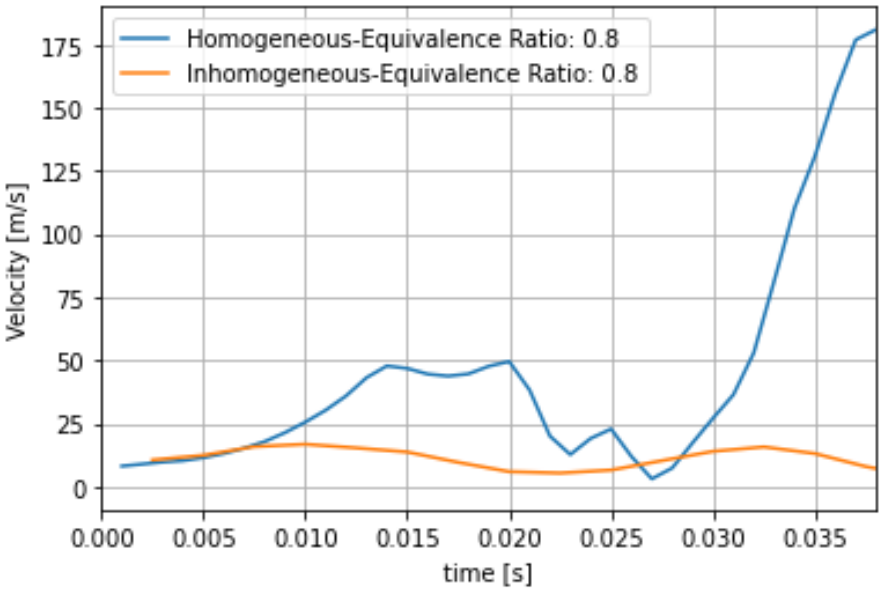

Figure 5.8. Flame front velocity in homogeneous and inhomogeneous H_2-air mixture-equivalence ratio 0.8

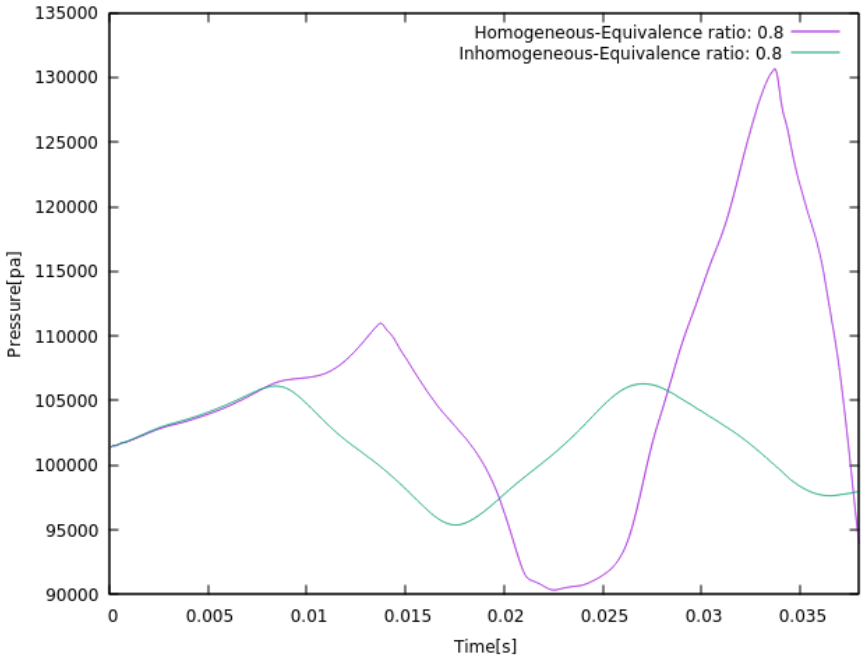

Figure 5.9. Pressure of probe1 in homogeneous and inhomogeneous H_2-air mixture-equivalence ratio 0.8

In stoichiometric condition ($\phi = 1$), as observed in figures 5.10-5.12 homogeneous H_2-air mixture shows faster acceleration with higher velocity and pressure. Flame in homogeneous case reached nearly end of channel after 24 milliseconds while in inhomogeneous condition it is much slower in propagation as seen in figure 5.10. Furthermore, homogeneous mixture shows higher velocity of 225 m/s while for inhomogeneous one, it is less than 50 m/s with fluctuation as observed in figure 5.11. Finally in figure 5.12 by comparison near ignition point in probe1, it shows higher pressure in homogenous case with maximum amount of 175 kpa while in inhomogeneous condition it oscillates around 110 kpa.

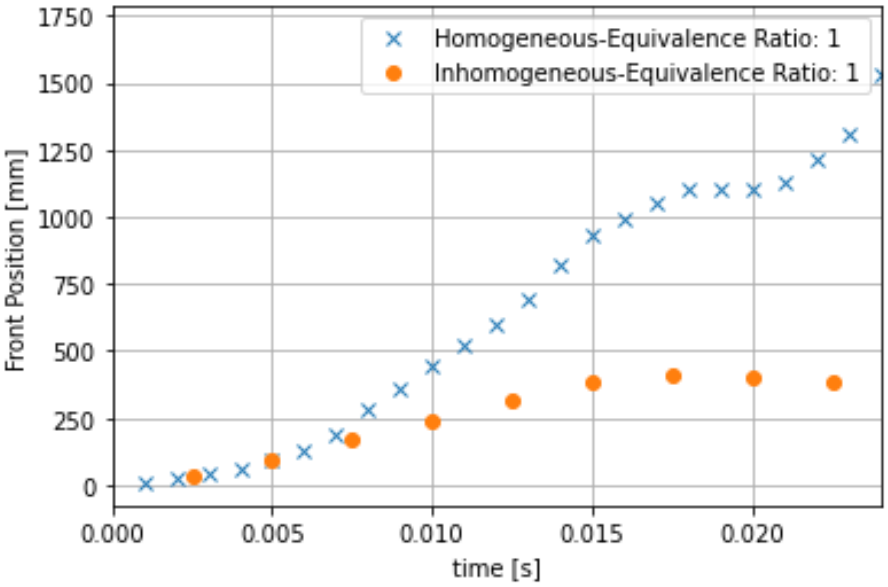

Figure 5.10. Flame front position in homogeneous and inhomogeneous H_2-air mixture-equivalence ratio 1

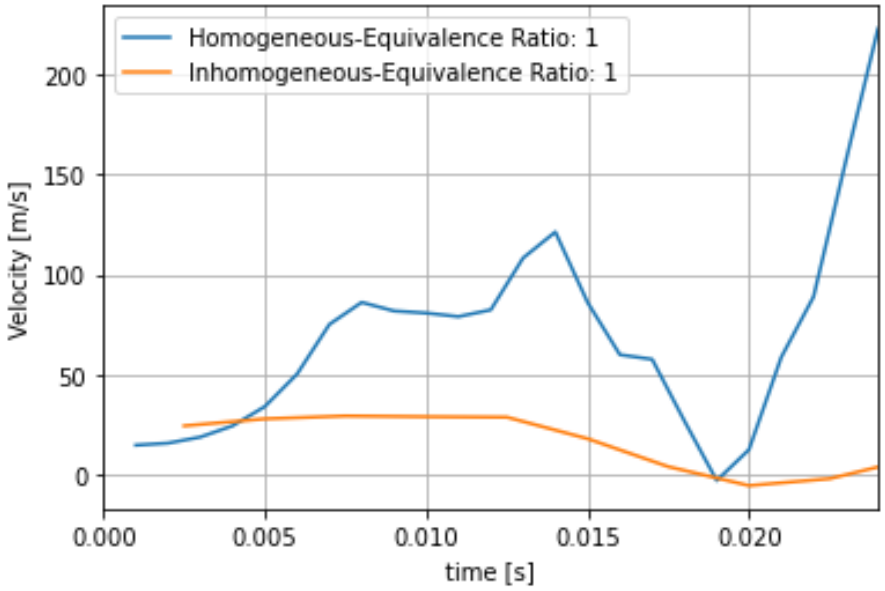

Figure 5.11. Flame front velocity in homogeneous and inhomogeneous H_2-air mixture-equivalence ratio 1

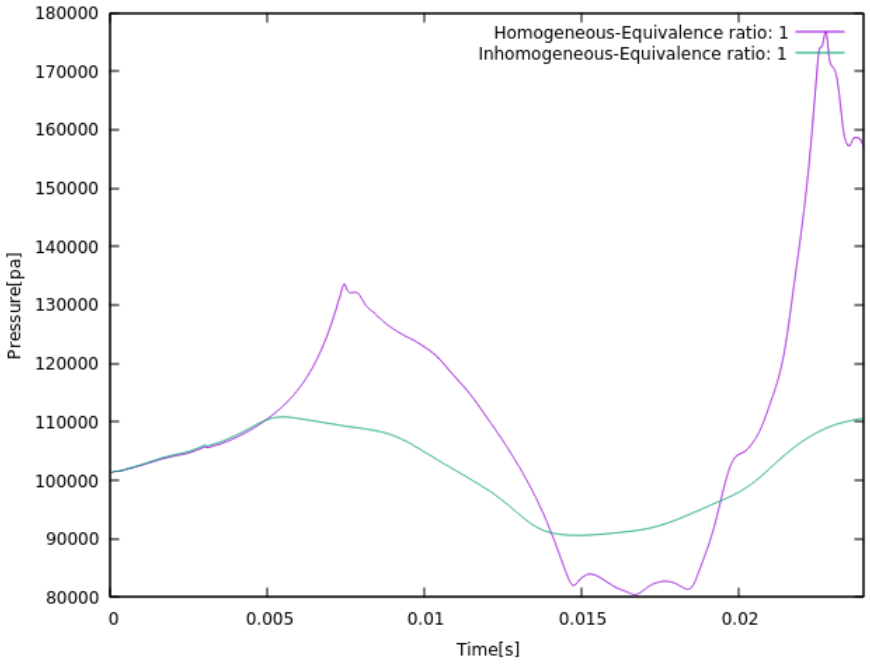

Figure 5.12. Pressure of probe1 in homogeneous and inhomogeneous H_2-air mixture-equivalence ratio1

Finally, for rich condition of H_2 in mixture ($\phi = 1.2$), as presented in figures 5.13-5.15 by comparison between homogeneity and inhomogeneity of H_2-air mixture, similar observation can be seen as two previous cases. Flame in homogeneous case reached nearly end of channel after 21 milliseconds while in inhomogeneous condition it passed just 500 mm of channel from ignition point as observed in figure 5.13. Also, homogeneous mixture shows higher velocity of 150 m/s while for inhomogeneous one, it is around 40 m/s with fluctuation as observed in figure 5.14. Finally in figure 5.15 by comparison in probe1 near ignition point, it shows higher

pressure in homogenous case with maximum amount of 145 kpa while in inhomogeneous condition it oscillates around 117 kpa.

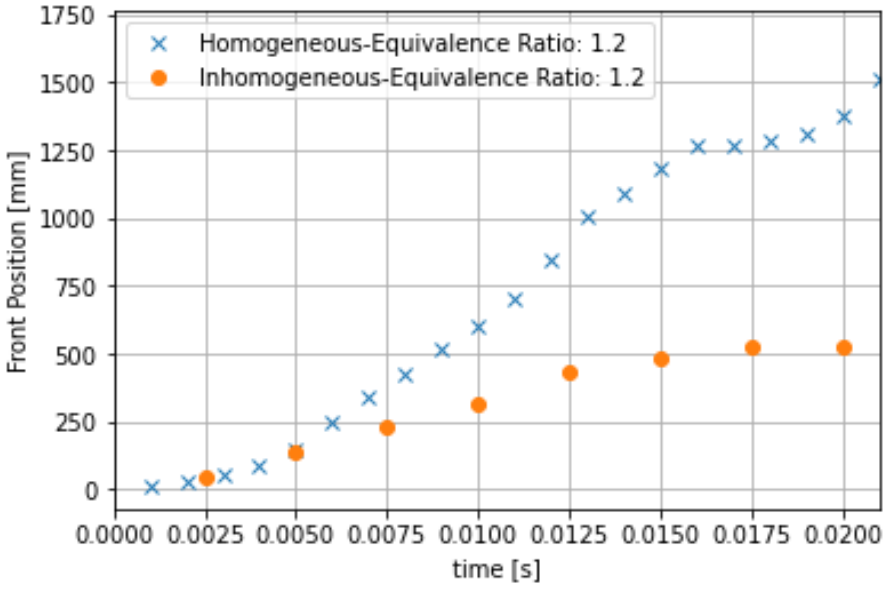

Figure 5.13. Flame front position in homogeneous and inhomogeneous H_2-air mixture-equivalence ratio 1.2

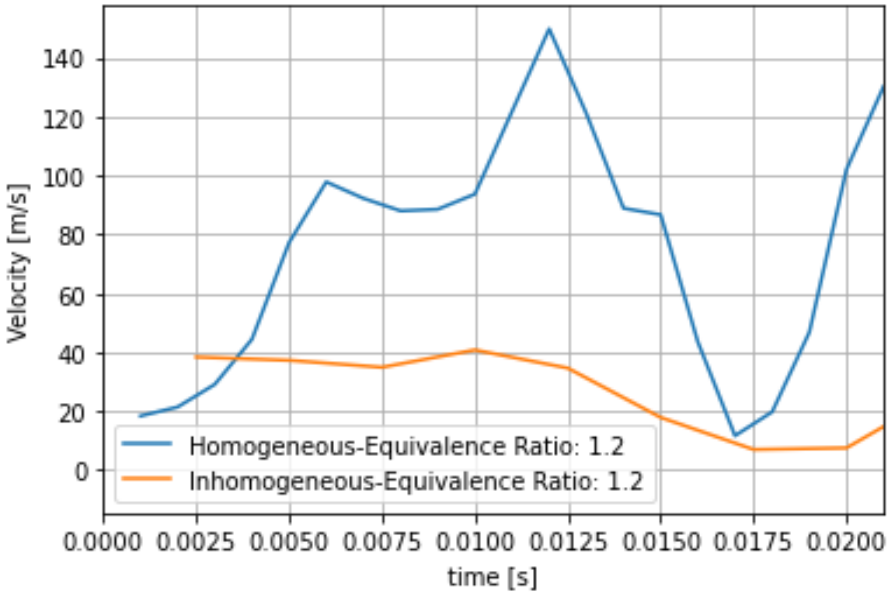

Figure 5.14. Flame front velocity in homogeneous and inhomogeneous H_2-air mixture-equivalence ratio 1.2

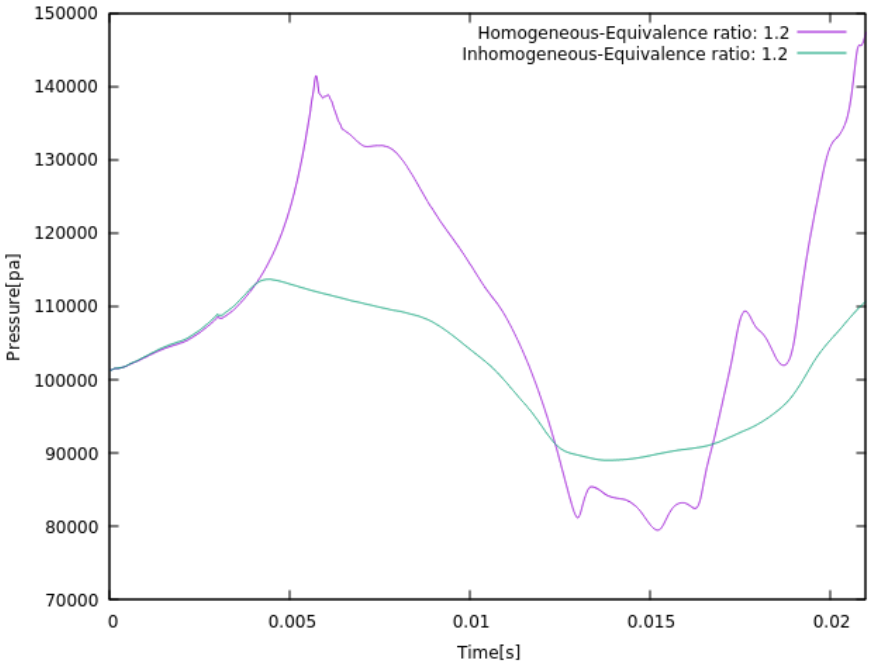

Figure 5.15. Pressure of probe1 in homogeneous and inhomogeneous H_2-air mixture-equivalence ratio 1.2

As observed in lean condition, instabilities happen and there can be observed separated flames with local quenching. This behavior is specifically obvious in inhomogeneous mixture as shown in figure 4.13 rather than homogeneous one. By increasing concentration of hydrogen, stability of flame increases as shown in figures 4.17 and 4.21 which has been described in cellular propagation in section 2.2.2. Also as mentioned in this section, because of high species diffusion of hydrogen, flame tends to be unstable and cellular propagation mostly occur.

6 Conclusion

Six simulation cases have been studied in this project based on homogeneous and inhomogeneous H_2-air mixture with further consideration of fuel-lean, stoichiometric, and fuel-rich conditions for each mixture. First homogeneous H_2-air mixture has been implemented in whole domain of channel and flame propagation and acceleration has been investigated. Then inhomogeneous H_2-air mixture has been implemented by defining two homogeneous layers in the channel as H_2-air mixture in half top of channel and air in half bottom of it as an inert layer. This inhomogeneity definition made a two-step concentration of H_2 in channel instead of concentration gradients that was performed in experiments. In this condition also flame propagation and acceleration has been investigated and compared with homogeneous case.

First in homogeneous H_2-air explosions, it was observed that flame elongation and enlargement of flame surface area results to increase in reaction rate and show higher flame acceleration with an almost symmetric shape in flame front. Also, homogeneous H_2-air cloud showed that by increasing H_2 concentration and having rich condition, flame propagates faster and reveals much higher velocity and pressure within the geometry. Pressure probes located in channel recorded same trend of pressure during the simulation period and by going far from ignition point, pressure reduced subsequently.

Second in inhomogeneous H_2-air explosions, it was observed that flame propagates irregularly, and oscillation prevent flame elongation. Flame propagates faster in top of channel rather than in bottom due to higher H_2 concentration in this region and it is inclined with a finger shape in front. It also showed that in lean mixture, flame cannot propagate near the lower wall while for stoichiometric and fuel-rich mixture, flame can propagate downward through whole of domain. Inhomogeneous cases also exhibit oscillation in velocity and consequently in pressure during simulation which can be as result of oscillation in wave of explosion. Furthermore, by increasing H_2 concentration, it was observed that flame propagates faster and reveals much higher pressure and velocity. Pressure probes also showed that by going far from ignition point, pressure value and its fluctuation reduce subsequently. Strong pressure oscillation of inhomogeneous mixture shows that they may cause structural damage to channel, tubes or buildings and facilities in them.

Finally by making comparison between homogeneous and inhomogeneous H_2-air explosions with similar H_2 concentration, it was observed that due to free elongation of flame and enlargement of flame surface area in homogeneous explosions by having flammable H_2-air mixture within the whole domain of geometry, higher reaction rates occur that result in flame propagation and acceleration with higher pressure and velocity, while for inhomogeneous explosions inert layer hinder flame elongation and prevent enlargement of flame surface area that results in reduction of flame propagation and acceleration. This observation is similar in stoichiometric and non-stoichiometric conditions.

Observations in this work shows that XiFoam solver in openFOAM CFD toolbox is a useful solver to model combustion of premixed and partially premixed turbulent flames that can exhibit flame acceleration process during explosions. Despite of high aspect ratio in objective geometry in this work to reach high explosion effects, this solver shows that it cannot consider DDT and Detonation effects on explosion as results of velocity and pressure revealed here. In

contrast, some numerical simulation works in openFOAM have been executed with density-based solvers , such as combination of rhoCentralFoam and reactingFoam [23] or implementing ExplosionFoam [24] in order to simulate FA and DDT processes for inhomogeneous H_2-air mixtures with concentration gradients. These numerical simulations observed good agreement with results in experiment works [19, 20, 22].

6.1 Suggestions for further work

In this work, CFD-simulations in openFOAM for inhomogeneous condition was implemented by two homogeneous layers of H_2-air and inert air. As a suggestion for further work, inhomogeneity can be defined by multi layers of H_2-air mixture within channel with different concentration to reach situation as concentration gradients in experiments. So, some developments need to be applied in codes to make it closer to this situation. Also, confined geometry and existence of obstacles in geometry can be investigated in further works to observe effect of them on flame propagation and strength of explosions for inhomogeneous mixtures. Since XiFoam solver in this work shows only flame acceleration of mixtures and cannot simulate DDT and detonation regimes, as a suggestion, some other solvers or combination of them can be studied to observe propagation regimes rather than FA.

References

[1] S. R. Turns, *Introduction to combustion*. McGraw-Hill Companies, 1996.

[2] H. K. Versteeg and W. Malalasekera, *An introduction to computational fluid dynamics: the finite volume method*. Pearson education, 2007.

[3] D. Bjerketvedt, J. R. Bakke, and K. Van Wingerden, "Gas explosion handbook," *Journal of hazardous materials,* vol. 52, no. 1, pp. 1-150, 1997.

[4] L. Böck, "Deflagration-to-detonation transition and detonation propagation in H2-air mixtures with transverse concentration gradients," Technische Universität München, 2015.

[5] A. Kumamoto, H. Iseki, R. Ono, and T. Oda, "Measurement of minimum ignition energy in hydrogen-oxygen-nitrogen premixed gas by spark discharge," in *Journal of Physics: Conference Series*, 2011, vol. 301, no. 1: IOP Publishing, p. 012039.

[6] B. Lewis and G. Von Elbe, *Combustion, flames and explosions of gases*. Elsevier, 2012.

[7] D. Lee and S. Hochgreb, "Hydrogen autoignition at pressures above the second explosion limit (0.6–4.0 MPa)," *International journal of chemical kinetics,* vol. 30, no. 6, pp. 385-406, 1998.

[8] A. Borisov, S. Khomik, V. Mikhalkin, and E. Saneev, "Critical energy of direct detonation initiation in gaseous mixtures," *Prog. Astronaut. Aeronaut,* vol. 133, pp. 142-155, 1991.

[9] I. Moen, J. Lee, B. Hjertager, K. Fuhre, and R. Eckhoff, "Pressure development due to turbulent flame propagation in large-scale methane□ air explosions," *Combustion and Flame,* vol. 47, pp. 31-52, 1982.

[10] R. Eckhoff, K. Fuhre, C. Guirao, and J. Lee, "Venting of turbulent gas explosions in a 50 m3 chamber," *Fire safety journal,* vol. 7, no. 2, pp. 191-197, 1984.

[11] B. Hjertager, K. Fuhre, S. Parker, and J. Bakke, "Flame acceleration of propane-air in a large-scale obstructed tube," *Progress in astronautics and aeronautics,* vol. 94, pp. 504-522, 1984.

[12] B. Hjertager, K. Fuhre, and M. Bjørkhaug, "Concentration effects on flame acceleration by obstacles in large-scale methane-air and propane-air vented explosions," *Combustion science and technology,* vol. 62, no. 4-6, pp. 239-256, 1988.

[13] B. Hjertager, M. Bjørkhaug, and K. Fuhre, "Explosion propagation of non-homogeneous methane—air clouds inside an obstructed 50 m3 vented vessel," *Journal of hazardous materials,* vol. 19, no. 2, pp. 139-153, 1988.

[14] C. Wang, J. Li, Z. Tang, Y. Zhuang, and J. Guo, "Flame propagation in methane-air mixtures with transverse concentration gradients in horizontal duct," *Fuel,* vol. 265, p. 116926, 2020.

[15] K. Vollmer, F. Ettner, and T. Sattelmayer, "Deflagration-to-detonation transition in hydrogen/air mixtures with a concentration gradient," *Combustion Science and Technology,* vol. 184, no. 10-11, pp. 1903-1915, 2012.

[16] K. G. Vollmer, F. Ettner, and T. Sattelmayer, "Influence of concentration gradients on flame acceleration in tubes," *Science and Technology of Energetic Materials,* vol. 72, no. 3-4, pp. 74-77, 2011.

[17] M. Kuznetsov, T. Jordan, and J. Grune, "Combustion regimes in a stratified layer of hydrogen-air mixture," 2011.

[18] M. Kuznetsov, J. Yanez, J. Grune, A. Friedrich, and T. Jordan, "Hydrogen combustion in a flat semi-confined layer with respect to the Fukushima Daiichi accident," *Nuclear Engineering and Design,* vol. 286, pp. 36-48, 2015.

[19] L. Boeck, M. Msalmi, F. Koehler, J. Hasslberger, and T. Sattelmayer, "Criteria for DDT in hydrogen-air mixtures with concentration gradients," in *10th International Symposium on Hazards, Prevention and Mitigation of Industrial Explosions*, 2014.

[20] L. R. Boeck, J. Hasslberger, and T. Sattelmayer, "Flame acceleration in hydrogen/air mixtures with concentration gradients," *Combustion Science and Technology,* vol. 186, no. 10-11, pp. 1650-1661, 2014.

[21] O. K. Sommersel, "Hydrogen leaks in partially confined spaces-dispersion and explosions," 2017.

[22] F. Ettner, K. G. Vollmer, and T. Sattelmayer, "Numerical simulation of the deflagration-to-detonation transition in inhomogeneous mixtures," *Journal of Combustion,* vol. 2014, 2014.

[23] R. K. Azadboni, J. X. Wen, A. Heidari, and C. Wang, "Numerical modeling of deflagration to detonation transition in inhomogeneous hydrogen/air mixtures," *Journal of Loss Prevention in the Process Industries,* vol. 49, pp. 722-730, 2017.

[24] C. Wang and J. X. Wen, "Numerical simulation of flame acceleration and deflagration-to-detonation transition in hydrogen-air mixtures with concentration gradients," *International Journal of Hydrogen Energy,* vol. 42, no. 11, pp. 7657-7663, 2017.

[25] C. K. Law, *Combustion physics*. Cambridge university press, 2010.

[26] R. Amirante, E. Distaso, P. Tamburrano, and R. D. Reitz, "Laminar flame speed correlations for methane, ethane, propane and their mixtures, and natural gas and gasoline for spark-ignition engine simulations," *International Journal of Engine Research,* vol. 18, no. 9, pp. 951-970, 2017.

[27] Ö. L. Gülder, "Correlations of laminar combustion data for alternative SI engine fuels," SAE Technical Paper, 0148-7191, 1984.

[28] P. Dirrenberger *et al.*, "Measurements of laminar flame velocity for components of natural gas," *Energy & fuels,* vol. 25, no. 9, pp. 3875-3884, 2011.

[29] O. Gülder, "Burning velocities of ethanol–air and ethanol–water–air mixtures," *AIAA Progr Astronaut Aeronaut,* vol. 95, pp. 181-197, 1984.

[30] S. Liao, D. Jiang, and Q. Cheng, "Determination of laminar burning velocities for natural gas," *Fuel,* vol. 83, no. 9, pp. 1247-1250, 2004.

[31] M. Metghalchi and J. C. Keck, "Laminar burning velocity of propane-air mixtures at high temperature and pressure," *Combustion and flame,* vol. 38, pp. 143-154, 1980.

[32] A. A. Konnov, "Remaining uncertainties in the kinetic mechanism of hydrogen combustion," *Combustion and flame,* vol. 152, no. 4, pp. 507-528, 2008.

[33] P. Clavin, "Dynamic behavior of premixed flame fronts in laminar and turbulent flows," *Progress in energy and combustion science,* vol. 11, no. 1, pp. 1-59, 1985.

[34] M. Hertzberg, "Selective diffusional demixing: occurrence and size of cellular flames," *Progress in Energy and Combustion Science,* vol. 15, no. 3, pp. 203-239, 1989.

[35] C. Law, "Dynamics of stretched flames," in *Symposium (international) on Combustion*, 1989, vol. 22, no. 1: Elsevier, pp. 1381-1402.

[36] D. Bradley and C. Harper, "The development of instabilities in laminar explosion flames," *Combustion and Flame,* vol. 99, no. 3-4, pp. 562-572, 1994.

[37] D. Bradley, C. Sheppart, R. Woolley, D. Greenhalgh, and R. Lockett, "The development and structure of flame instabilities and cellularity at low Markstein numbers in explosions," *Combustion and flame,* vol. 122, no. 1-2, pp. 195-209, 2000.

[38] G. Darrieus, "Propagation d'un front de flamme. Essai de théorie des vitesses anormales de déflagration par développement spontané de la turbulence," in *Unpublished works presented at la technique moderne*, 1938.

[39] L. Landau, "0n the Theory of Slow Combustion," *Dynamics of Curved Fronts,* vol. 19, no. 0, p. 403, 2012.

[40] C. Sun, C.-J. Sung, L. He, and C. K. Law, "Dynamics of weakly stretched flames: quantitative description and extraction of global flame parameters," *Combustion and flame,* vol. 118, no. 1-2, pp. 108-128, 1999.

[41] G. H. Markstein, "Experimental and theoretical studies of flame-front stability," *Journal of the Aeronautical Sciences,* vol. 18, no. 3, pp. 199-209, 1951.

[42] B. Karlovitz, D. Denniston Jr, D. Knapschaefer, and F. Wells, "Studies on Turbulent flames: A. Flame Propagation Across velocity gradients B. turbulence Measurement in flames," in *Symposium (international) on combustion*, 1953, vol. 4, no. 1: Elsevier, pp. 613-620.

[43] M. J. Brown, I. C. McLean, D. B. Smith, and S. C. Taylor, "Markstein lengths of CO/H2/air flames, using expanding spherical flames," in *Symposium (International) on Combustion*, 1996, vol. 26, no. 1: Elsevier, pp. 875-881.

[44] G. Dixon-Lewis, "Kinetic mechanism, structure and properties of premixed flames in hydrogen—oxygen—nitrogen mixtures," *Philosophical Transactions of the Royal Society of London. Series A, Mathematical and Physical Sciences,* vol. 292, no. 1388, pp. 45-99, 1979.

[45] O. Reynolds, "On the dynamical theory of incompressible viscous fluids andthe determination of the criterion," *Proceedings of the Royal Society of London,* vol. 56, no. 336-339, pp. 40-45, 1894.

[46] A. N. Kolmogorov, "The local structure of turbulence in incompressible viscous fluid for very large Reynolds numbers," *Cr Acad. Sci. URSS,* vol. 30, pp. 301-305, 1941.

[47] A. N. Kolmogorov, "A refinement of previous hypotheses concerning the local structure of turbulence in a viscous incompressible fluid at high Reynolds number," *Journal of Fluid Mechanics,* vol. 13, no. 1, pp. 82-85, 1962.

[48] H. Tennekes and J. L. Lumley, *A first course in turbulence*. MIT press, 2018.

[49] G. Damköhler, "Der einfluss der turbulenz auf die flammengeschwindigkeit in gasgemischen," *Zeitschrift für Elektrochemie und angewandte physikalische Chemie,* vol. 46, no. 11, pp. 601-626, 1940.

[50] P. Clavin and F. Williams, "Theory of premixed-flame propagation in large-scale turbulence," *Journal of fluid mechanics,* vol. 90, no. 3, pp. 589-604, 1979.

[51] S. Pope and M. Anand, "Flamelet and distributed combustion in premixed turbulent flames," in *Symposium (International) on Combustion,* 1985, vol. 20, no. 1: Elsevier, pp. 403-410.

[52] Ö. L. Gülder, "Turbulent premixed flame propagation models for different combustion regimes," in *Symposium (International) on Combustion,* 1991, vol. 23, no. 1: Elsevier, pp. 743-750.

[53] R. Borghi, "On the structure and morphology of turbulent premixed flames," in *Recent advances in the Aerospace Sciences*: Springer, 1985, pp. 117-138.

[54] N. Peters, "The turbulent burning velocity for large-scale and small-scale turbulence," *Journal of Fluid mechanics,* vol. 384, pp. 107-132, 1999.

[55] N. Peters, "Turbulent combustion," ed: IOP Publishing, 2001.

[56] F. Williams, "Turbulent combustion," in *The mathematics of combustion*: SIAM, 1985, pp. 97-131.

[57] B. Karlovitz, D. Denniston Jr, and F. E. Wells, "Investigation of turbulent flames," *The Journal of Chemical Physics,* vol. 19, no. 5, pp. 541-547, 1951.

[58] G. Ciccarelli and S. Dorofeev, "Flame acceleration and transition to detonation in ducts," *Progress in energy and combustion science,* vol. 34, no. 4, pp. 499-550, 2008.

[59] G. Ciccarelli, C. T. Johansen, and M. Parravani, "The role of shock–flame interactions on flame acceleration in an obstacle laden channel," *Combustion and Flame,* vol. 157, no. 11, pp. 2125-2136, 2010.

[60] C. T. Johansen, *Experimental and numerical investigation of flame acceleration in an obstructed channel*. Queen's University (Canada), 2009.

[61] M. Brouillette, "The richtmyer-meshkov instability," *Annual Review of Fluid Mechanics,* vol. 34, no. 1, pp. 445-468, 2002.

[62] R. D. Richtmyer, "Taylor instability in shock acceleration of compressible fluids," Los Alamos Scientific Lab., N. Mex., 1954.

[63] G. Thomas, R. Bambrey, and C. Brown, "Experimental observations of transition to detonation," *Combustion Theory and Modelling,* vol. 5, pp. 573-594, 2001.

[64] A. Khokhlov, E. Oran, and G. Thomas, "Numerical simulation of deflagration-to-detonation transition: the role of shock–flame interactions in turbulent flames," *Combustion and flame,* vol. 117, no. 1-2, pp. 323-339, 1999.

[65] H. F. Coward and G. W. Jones, *Limits of flammability of gases and vapors*. US Government Printing Office, 1952.

[66] M. Jordan, *Zündung und Verbrennung in vorgemischten turbulenten Freistrahlen*. na, 1999.

[67] S. Dorofeev, M. Kuznetsov, V. Alekseev, A. Efimenko, and W. Breitung, "Evaluation of limits for effective flame acceleration in hydrogen mixtures," *Journal of loss prevention in the process industries,* vol. 14, no. 6, pp. 583-589, 2001.

[68] E. S. Oran and V. N. Gamezo, "Origins of the deflagration-to-detonation transition in gas-phase combustion," *Combustion and Flame,* vol. 148, no. 1-2, pp. 4-47, 2007.

[69] P. Urtiew and A. Oppenheim, "Experimental observations of the transition to detonation in an explosive gas," *Proceedings of the Royal Society of London. Series A. Mathematical and Physical Sciences,* vol. 295, no. 1440, pp. 13-28, 1966.

[70] E. Dziemińska and A. K. Hayashi, "Auto-ignition and DDT driven by shock wave–boundary layer interaction in oxyhydrogen mixture," *International Journal of hydrogen energy,* vol. 38, no. 10, pp. 4185-4193, 2013.

[71] G. Thomas, S. Ward, R. L. Williams, and R. Bambrey, "On critical conditions for detonation initiation by shock reflection from obstacles," *Shock Waves,* vol. 12, no. 2, pp. 111-119, 2002.

[72] M. Kellenberger and G. Ciccarelli, "Propagation mechanisms of supersonic combustion waves," *Proceedings of the Combustion Institute,* vol. 35, no. 2, pp. 2109-2116, 2015.

[73] J. Grune, K. Sempert, H. Haberstroh, M. Kuznetsov, and T. Jordan, "Experimental investigation of hydrogen–air deflagrations and detonations in semi-confined flat layers," *Journal of Loss Prevention in the Process Industries,* vol. 26, no. 2, pp. 317-323, 2013.

[74] J. C. Krok, "One-dimensional flame propagation mechanisms," *Unpublished notes on the solution of ideal steady high-speed flames. RPI, Troy, NY,* 1991.

[75] D. L. Chapman, "VI. On the rate of explosion in gases," *The London, Edinburgh, and Dublin Philosophical Magazine and Journal of Science,* vol. 47, no. 284, pp. 90-104, 1899.

[76] E. Jouguet, "Sur la propagation des réactions chimiques dans les gaz," *J. Maths. Pure Appl.,* vol. 7, p. 347, 1905.

[77] J. D. Anderson, *Modern compressible flow*. Tata McGraw-Hill Education, 2003.

[78] J. H. Lee, *The detonation phenomenon*. 2008.

[79] Y. B. Zeldovich, "On the theory of the propagation of detonation in gaseous systems," 1950.

[80] J. Von Neuman, "Theory of detonation waves," Institute for Advanced Study Princeton NJ, 1942.

[81] W. Döring, "Über den detonationsvorgang in gasen," *Annalen der Physik,* vol. 435, no. 6-7, pp. 421-436, 1943.

[82] J. Shepherd, "Chemical kinetics of hydrogen-air-diluent detonations.[Kinetic Models to Predict Detonation Cell Size]," Sandia National Labs., Albuquerque, NM (USA), 1985.

[83] J. M. Austin, "The role of instability in gaseous detonation," 2004.

[84] A. Gavrikov, A. Efimenko, and S. Dorofeev, "A model for detonation cell size prediction from chemical kinetics," *Combustion and flame,* vol. 120, no. 1-2, pp. 19-33, 2000.

[85] A. Vasiliev and Y. Nikolaev, "Closed theoretical model of a detonation cell," in *Gasdynamics of Explosions and Reactive Systems*: Elsevier, 1980, pp. 983-996.

[86] M. Kaneshige and J. E. Shepherd, "Detonation database," 1997.

[87] W. Rudy, M. Kuznetsov, R. Porowski, A. Teodorczyk, J. Grune, and K. Sempert, "Critical conditions of hydrogen-air detonation in partially confined geometry," *Proceedings of the Combustion Institute,* vol. 34, no. 2, pp. 1965-1972, 2013.

[88] A. Gaathaug, K. Vaagsaether, and D. Bjerketvedt, "Detonation propagation in a reactive layer: the role of detonation front stability," in *Proceedings of the 10th International Symposium on Hazards, Prevention and Mitigation of Industrial Explosions, Bergen, Norway*, 2014.

[89] D. Bjerketvedt, O. Sonju, and I. Moen, "The influence of experimental condition on the reinitiation of detonation across an inert region," *Progress in Astronautics and Aeronautics,* vol. 106, pp. 109-130, 1986.

[90] Y. Wang, C. Huang, R. Deiterding, H. Chen, and Z. Chen, "Propagation of gaseous detonation across inert layers," *Proceedings of the Combustion Institute,* vol. 38, no. 3, pp. 3555-3563, 2021.

[91] W. Calhoon and N. Sinha, "Detonation wave propagation in concentration gradients," in *43rd AIAA Aerospace Sciences Meeting and Exhibit*, 2005, p. 1167.

[92] D. Kessler, V. Gamezo, and E. Oran, "Gas-phase detonation propagation in mixture composition gradients," *Philosophical Transactions of the Royal Society A: Mathematical, Physical and Engineering Sciences,* vol. 370, no. 1960, pp. 567-596, 2012.

[93] E. K. Dabora, J. Nicholls, and R. Morrison, "The influence of a compressible boundary on the propagation of gaseous detonations," in *Symposium (International) on Combustion*, 1965, vol. 10, no. 1: Elsevier, pp. 817-830.

[94] A. Clarke, "Calculation and consideration of the Lewis number for explosion studies," *Process Safety and Environmental Protection,* vol. 80, no. 3, pp. 135-140, 2002.

[95] R. J. Kee, "A fortran chemical kinetics package for the analysis of gasphase chemical and plasma kinetics," *Sandia National Laboratories,* 1996.

[96] A. Favre, "Statistical Equations of Turbulent Gases, in Problems of Hydrodynamics and Continuum Mechanics (Sedov 60th Birthday Volume)," ed: SIAM Philadelphia, 1969.

[97] W. Jones and J. Whitelaw, "Calculation methods for reacting turbulent flows: a review," *Combustion and flame,* vol. 48, pp. 1-26, 1982.

[98] H. Weller, "The development of a new flame area combustion model using conditional averaging," *Thermo-fluids section report TF,* vol. 9307, 1993.

[99] H. Weller, G. Tabor, A. Gosman, and C. Fureby, "Application of a flame-wrinkling LES combustion model to a turbulent mixing layer," in *Symposium (International) on Combustion*, 1998, vol. 27, no. 1: Elsevier, pp. 899-907.

[100] B. Launder, C. Priddin, and B. Sharma, "The calculation of turbulent boundary layers on spinning and curved surfaces," 1977.

[101] "openFOAM user guide." [Online]. Available: https://cfd.direct/openfoam/user-guide/v8-thermophysical/#x36-2680007.1.

[102] W. S. LII, "The viscosity of gases and molecular force," *Lond. Edinb. Dublin Philos. Mag. J. Sci*, vol. 36, pp. 507-531, 1893.

[103] D. R. Stull, *JANAF Thermochemical Tables*. Clearinghouse, 1965.

[104] B. J. McBride, *Coefficients for calculating thermodynamic and transport properties of individual species*. NASA Langley Research Center, 1993.

[105] E. Yasari, J. Runsten, and J. Andric, "Tutorial XiFoam," ed: Sweeden, 2010.

[106] M. Bratland, D. Bjerketvedt, and K. Vaagsaether, "Structural response analysis of explosions in hydrogen-air mixtures in tunnel-like geometries," *Engineering Structures*, vol. 231, p. 111844, 2021.

Appendices

Apendix A: Task description

University of South-Eastern Norway

Faculty of Technology, Natural Sciences and Maritime Sciences, Campus Porsgrunn

FMH606 Master's Thesis

Title: CFD-simulations of inhomogenous H_2-air explosions

USN supervisor: Prof. Dag Bjerketvedt, Stip. Mathias Henriksen, and Prof. Knut Vaagsaether

External partner: MoZEES

Task background:

In the next decades, we expect hydrogen to make a significant contribution to clean energy transitions. However, hydrogen's success will depend on factors such as the economy, technology, and safety. All safety aspects regarding hydrogen are not fully understood. Flame propagation in inhomogenous H_2-air clouds is one of these areas.

Task description:

- Make a literature review on flame propagation in inhomogenous fuel-air clouds focusing on flame acceleration in H_2-air and transition to detonation.
- OpenFOAM simulations on flame acceleration in inhomogeneous H_2-air

Student category: EET and PT students with the CFD course

The task is suitable for online students (not present at the campus): Yes

Practical arrangements:

Supervision:

As a general rule, the student is entitled to 15-20 hours of supervision. This includes the necessary time for the supervisor to prepare for supervision meetings (reading material to be discussed, etc.).

Signatures:

Supervisor (date and signature):

Student (write clearly in all capitalized letters): **OMID AGHAABBASI**

Student (date and signature): **31.01.2021**